

**DESIGN AND DEVELOPMENT OF A
PHYSIOTHERAPY ROBOT FOR
REHABILITATION OF
STROKE PATIENTS**

Thesis

Submitted in partial fulfilment of the requirements for the degree of

DOCTOR OF PHILOSOPHY

by

ANTONIO DYLAN DO ROSARIO CARVALHO



DEPARTMENT OF MECHANICAL ENGINEERING
NATIONAL INSTITUTE OF TECHNOLOGY KARNATAKA,
SURATHKAL, MANGALORE – 575025

MAY, 2023

DECLARATION

I hereby *declare* that the Research Thesis entitled “**DESIGN AND DEVELOPMENT OF A PHYSIOTHERAPY ROBOT FOR REHABILITATION OF STROKE PATIENTS**”, which is being submitted to the **National Institute of Technology Karnataka, Surathkal** in partial fulfilment of the requirements for the award of the Degree of **Doctor of Philosophy in Department of Mechanical Engineering** is a *bonafide report of the research work carried out by me*. The material contained in this Research Thesis has not been submitted to any University or Institution for the award of any degree.

Register Number : 177041ME002

Name of the Research Scholar : **ANTONIO DYLAN DO ROSARIO
CARVALHO**

Signature of the Research Scholar: 

Department of Mechanical Engineering

Place : NITK, Surathkal

Date : 02/05/2023

C E R T I F I C A T E

This is to *certify* that the Research Thesis entitled “**DESIGN AND DEVELOPMENT OF A PHYSIOTHERAPY ROBOT FOR REHABILITATION OF STROKE PATIENTS**” submitted by Mr. **ANTONIO DYLAN DO ROSARIO CARVALHO** (Register Number: **177041ME002**) as the record of the research work carried out by him, is *accepted as the Research Thesis submission* in partial fulfilment of the requirements for the award of degree of **Doctor of Philosophy**.

Research Guide

AM Karanth
2/5/2023

Dr. Navin Karanth P

Associate Professor

Department of Mechanical Engineering

&

V Desai
2/5/2023

Dr. Vijay Desai

Professor

Department of Mechanical Engineering

Dr. H. H. H.

Chairman - DRPC

Date: 3.5.2023



ACKNOWLEDGEMENT

First, I would like to thank God for my good health and strength and for blessing me with a good team whose constant encouragement helped me complete my research successfully. I would like to extend my sincere gratitude to Dr. Navin Karanth P (Associate Professor), and Dr. Vijay Desai (Professor), Department of Mechanical Engineering, National Institute of Technology Karnataka, Surathkal, for their invaluable constructive guidance and encouragement extended throughout my Ph.D. tenure.

I thank my Research Progress Assessment Committee Members, Dr. Hemantha Kumar, and Dr. Prasanna B.D, for their valuable inputs, useful discussions, suggestions, and constant encouragement.

I would like to thank the former heads of the department, Prof. Narendranath S., Prof. Shrikantha S Rao, Prof. S. M. Kulkarni, and Prof. Ravikiran Kadoli Head of the Mechanical Engineering Department, and all the faculty members and support staff at Mechanical Engineering Department for their support throughout this research work. I would also like to extend my gratitude to the CSD and DIC labs of the Mechanical Engineering Dept.

I thank my family for their constant encouragement and immeasurable support during my research. I sincerely thank my colleagues Dr. Mohith S, Mr. J Vamsi, Mr. Kalyan P, Dr. Roopa, Mr. Ajay Chourasia, Mr. Suraj Patil, and all my friends for their constant support and help. I would also like to thank Mr. Yashas M in a special way for all his assistance and support. I also extend my sincere gratitude to Dr. Charu Eapen (HOD Physiotherapy) and her team at KMC Mangalore for their constant support and insight.

(Antonio Dylan Do Rosario Carvalho)

ABSTRACT

The motivation for this research is the huge disparity between the number of patients and available physiotherapists in developing countries like India. The study of literature on prior research and consultation with physiotherapists showed the requirement of an exoskeleton device to impart repetitive therapy to the elbow joint. The elbow joint required a device that allowed its movement through two degrees of freedom, flexion/extension, and pronation/supination. Initially, a modular exoskeleton is built to impart a one-degree of-freedom flexion/extension motion to the elbow joint. The literature and preliminary study showed that pneumatic actuators or McKibben muscles best suit this application.

The drawbacks of the commercial muscle, such as smaller contraction and longer formfactor(length), led to the development of an inhouse designed muscle actuator. The inhouse developed muscle has been designed with a unique pair of end-fittings that facilitated its easy assembly/disassembly. As the muscle is developed for a critical medical application, the muscle must be tested and characterized. The characterization process led to the design and development of two test rigs to conduct all tests with minor adjustments to the setup. The test results revealed the influence of the size and material of the bladder and braided sleeve used in the muscle's construction, on the behaviour of the muscle. The tests also showed a lower hysteresis error in the developed muscle compared to the commercial muscle. The lifecycle test on the developed pneumatic muscle successfully endured a life of over 200000 cycles at maximum pressure and loading conditions. The 12 mm styrene-based muscle with a larger braided sleeve is most effective in space-constraint applications requiring large contraction and compliance characteristics. On the other hand, the 12 mm latex-based muscle with a larger braided sleeve is most effective in applications requiring a balance of accuracy, high load capacity and compliance. The research also involves the comparison of three mathematical models to find a model that best represents the behaviour of the developed muscle.

The initial design of the exoskeleton has a direct actuator-mounted arrangement. The drawbacks of the direct actuator-mounted exoskeleton such as smaller range of motion

(ROM) led to the development of the EXPHYSIO. EXPHYSIO is short for exoskeleton for physiotherapy, which is an indirectly actuated exoskeleton system designed to impart repetitive motion to the elbow joint through two degrees of freedom. The indirectly actuated EXPHYSIO is tested for performance using the 12 mm latex muscles. The EXPHYSIO shows a 20% increase in flexion in comparison to the direct actuator mounted arrangement. It is observed that the exoskeleton executed repetitive tasks with ease, allowing the control of the elbow joint through its two degrees of freedom motion. Therefore, this research accomplished a safe, easy-to-teach, and compliant exoskeleton system for the repetitive therapy of the elbow joint through two degrees of freedom.

Keywords: Pneumatic Muscle Actuator (PMA), McKibben Muscle, Novel Pneumatic Muscle End-Fittings, Soft Actuator, Pneumatic Muscle Simulation, Elbow Exoskeleton, Physiotherapy, Repetitive Therapy

CONTENTS

ACKNOWLEDGEMENT	i
ABSTRACT	iii
LIST OF FIGURES	vii
LIST OF TABLES	xi
ABBREVIATIONS	xiii
1 INTRODUCTION	1
1.1 Anatomy of the Upper Extremity.....	2
1.1.1 Elbow Joint Anatomy.....	7
1.1.2 Elbow Joint Injuries Requiring Physiotherapy Intervention.....	8
1.2 Assistive Devices for Physiotherapy.....	12
2 LITERATURE REVIEW	15
2.1 End-Effector Assistive Device.....	15
2.2 Exoskeleton Type Assistive Device.....	18
2.3 Robotic Devices in Physical Rehabilitation.....	21
2.4 Actuator Selection.....	28
2.4.1 Pneumatic Muscle Actuator.....	29
2.5 Summary and Motivation.....	33
2.6 Objectives.....	35
2.7 Desired Attributes.....	36
3 METHODOLOGY	37
4 DEVELOPMENT OF PNEUMATIC MUSCLE ACTUATOR	45
4.1 Design and Fabrication of the PMA.....	47
4.2 PMA Characterization.....	54
4.2.1 PMA Test Rig Development for Displacement Measurement.....	55
4.2.2 PMA Test Rig Development for Force Measurement.....	57
4.2.3 Force Versus Contraction Characteristics.....	58
4.2.4 Pressure vs Deflection Characteristics.....	64
4.2.5 Pressure vs Force Characteristics.....	66
4.2.6 Comparing Displacement and Force Characteristics of The Developed PMA with a Commercial PMA.....	67

4.2.7	Life Cycle Test.....	69
4.3	Mathematical Model of a Pneumatic Muscle Actuator (PMA)	71
4.3.1	Mathematical Models of PMA.....	71
4.3.2	Comparing Experimental and Simulated Results	75
4.4	PMA Characterization for Varying Bladder and Braided Sleeve Configurations.....	77
4.5	PMA Displacement Characteristics	79
4.6	PMA Force Characteristics	92
4.7	Conclusion.....	93
5	EXOSKELETON.....	97
5.1	Design and Development of an Exoskeleton for the Actuation of the Elbow Joint 97	
5.1.1	Testing the PMA on the Designed Elbow Exoskeleton.....	107
5.2	Improved Exoskeleton Design	109
5.2.1	The Exoskeleton of the EXPHYSIO.....	111
5.2.2	The Actuator Block (AB) of the EXPHYSIO.....	120
5.2.3	The Control Unit of the EXPHYSIO	129
5.2.4	Programming and Using the EXPHYSIO.....	136
5.2.5	Testing the EXPHYSIO using the Developed PMA	141
5.3	Conclusion.....	143
6	SUMMARY AND CONCLUSIONS.....	147
6.1	Summary	148
7	FUTURE SCOPE	149
	REFERENCES.....	151
	ANNEXURE.....	163
	LIST OF PUBLICATIONS	167
	BIO-DATA.....	169

LIST OF FIGURES

Fig No	Title	Pg No
Fig 1.1	Anatomy of Upper Extremity	3
Fig 1.2	Muscle Anatomy of the Upper Extremity	4
Fig 1.3	Elbow Joint Anatomy	7
Fig 1.4	Classification of stroke	10
Fig 1.5	Classification of Assistive device for upper extremity	13
Fig 1.6	Schematic of end-effector and exoskeleton-type rehabilitation devices	14
Fig 2.1	RUPERT	23
Fig 2.2	MEDARM	23
Fig 2.3	4-DOF rehabilitation robot	24
Fig 2.4	University of Salford Rehabilitation Exoskeleton (SRE)	24
Fig 2.5	ARMin	26
Fig 2.6	ARMin 3	26
Fig 2.7	CABexo	28
Fig 2.8	MULOS	28
Fig 2.9	Pair of muscles used to counter the antagonistic nature of PMAs	32
Fig 3.1	Flow diagram of the procedure used in the development of the exoskeleton	40
Fig 4.1	FBD to calculate motor torque for forearm-exoskeleton pair	45
Fig 4.2	FBD of the forearm	45

Fig 4.3	Simplified FBD of the forearm	46
Fig 4.4	FBD of exoskeleton support for the forearm	46
Fig 4.5	Simplified FBD of exoskeleton support for the forearm	46
Fig 4.6	The Developed PMA with the Novel End-Fittings and Clamps	48
Fig 4.7	10x14 PMA of weight 90 gms vs the commercial PMA of 150 gms	50
Fig 4.8a	Test Rig for PMA Displacement	56
Fig 4.8b	Test Rig for PMA Force	57
Fig 4.9	Force vs Contraction Ratio of Developed PMA	60
Fig 4.10	Force vs Contraction Ratio of Developed and Commercial PMA of identical diameter and actuation length	61
Fig 4.11	Deflection vs Pressure of 10 X 14 PMA	66
Fig 4.12	Force vs Pressure of 10 X 14 and 12x17 PMA	67
Fig 4.13	Deflection and Force Characteristics of the commercial PMA tested	68
Fig 4.14	Lifecycle Test Flowchart	70
Fig 4.15	Schematic of PMA with braid fibre	71
Fig 4.16	Force vs Contraction (where 'M1', 'M2', 'M3', are mathematical models & 'Exp' is obtained experimentally)	76
Fig 4.17	Categories of PMA fabricated based on material and dimensional characteristics	78
Fig 4.18	Displacement vs Pressure of 6mm and 8mm ID Muscles	84
Fig 4.19	Displacement vs Pressure of 12mm ID Muscles	87
Fig 4.20	Volume Ratio and Braid Angle of PMA	89

Fig 4.21	Force vs Pressure for 12mm ID PMA	92
Fig 5.1	Aluminium T-slot (Isometric View)	98
Fig 5.2	Aluminium T-slot (Cross-section)	98
	Designed Exoskeleton Assembly with direct actuator mounting	
Fig 5.3	arrangement	99
Fig 5.4	C-Bracket manufacturing process	100
Fig 5.5	PMA Mounts	101
Fig 5.6	Commercial Hinge	102
Fig 5.7	Hinge Design with shaft type potentiometer	102
Fig 5.8	Elbow Flexion greater than 90deg	104
Fig 5.9	Elbow Flexion less than 90deg	104
	FBD of forearm-exoskeleton pair for calculation of required spring	
Fig 5.10	torque	104
Fig 5.11	FBD of the forearm	105
Fig 5.12	Simplified FBD of the forearm	105
Fig 5.13	FBD of exoskeleton support for the forearm	105
Fig 5.14	FBD of the exoskeleton support for the forearm	106
Fig 5.15	Pressure vs Deflection with no load	107
Fig 5.16	Pressure vs Deflection with an attached load	107
	Experimental setup for determining pressure vs angular deflection	
Fig 5.17	characteristics of the exoskeleton	108
Fig 5.18	EXPHYSIO System	110
Fig 5.19	Exoskeleton with Direct vs Indirect actuation	110

Fig 5.20	Exoskeleton of the EXPHYSIO	111
Fig 5.21	New design of 3D Printed Clamps	112
Fig 5.22	New 3D printed hinge	114
Fig 5.23	Novel Pronation/Supination Mechanism	116
Fig 5.24	Method to record real-time Pronation Angle Measurement	119
Fig 5.25	Actuator Block Design	120
Fig 5.26	FBD for forearm actuated indirectly by PMA via cable mechanism	123
	Pneumatic Circuit using two proportional pressure regulators	
Fig 5.27	(PPR)	124
Fig 5.28	Pneumatic Circuit using a single proportional pressure regulator	125
Fig 5.29	Photos of Actuator Block (AB)	128
Fig 5.30	Control Unit Development process for the EXPHYSIO	131
	Program Flowchart Developed for Efficient and Safe Operation of	
Fig 5.31	EXPHYSIO	135
Fig 5.32	F/E Angle vs Pressure for the exoskeleton of the EXPHYSIO	141
Fig 5.33	P/S Angle vs Pressure for the exoskeleton of the EXPHYSIO	142

LIST OF TABLES

Table No	Title	Pg No
Table 3.1	Flowchart of the training and usage of the proposed robot exoskeleton for two degrees of freedom therapy of the elbow joint	37
Table 3.2	Methodology	39
Table 4.1	Comparison of the Length of Developed PMA with the Commercial PMA	52
Table 4.2	Dimensions of bladder and braided sleeve used in the developed PMA	54
Table 4.3	Ratio of bladder volume to actuator volume for different PMA sizes	62
Table 4.4	Details of tested PMAs	79
Table 5.1	Anthropometric data of upper extremity	100
Table 5.2	Sizes of C-Brackets	100
Table 5.3	Torsion Spring Design parameters	106

ABBREVIATIONS

ADL	Activities Of Daily Living
AFO	Ankle-Foot Orthosis
AFR	Air Filter Regulator
ASTM	American Society for Testing and Materials
BCI	Brain Control Interface
BIC	Biceps Brachii
CI	Co-Contraction Index
CR	Center Of Rotation
DAC	Digital-To-Analog Converter
DAQ	Data Acquisition
DC	Direct Current
DCV	Directional Control Valve
DOF	Degree Of Freedom
ECR	Extensor Carpiradialis
EMG	Electromyography
EXHYSIO	Exoskeleton For Physiotherapy
FBD	Free Body Diagram
FCR	Flexor Carpiradialis
FMA	Fugl-Meyer Assessment
FRL	Filter-Regulator-Lubricator
HMI	Human Machine Interface
IO	Input Output
IP	Interphalangeal
L	Large Size
LB	Large Braided-Sleeve
LCD	Liquid Crystal Display
M	Medium Size
MAS	Modified Ashworth Score
MAV	Micro-Air Vehicle
MCP	Metacarpophalangeal

NI	National Instruments
NL	No Load
PAM	Pneumatic Artificial Muscle
PC	Personal Computer
PCB	Printed Circuit Board
PET	Polyethylene Terephthalate
PLA	Polylactic Acid/Polylactide
PMA	Pneumatic Muscle Actuator
PNF	Proprioceptive Neuromuscular Facilitation
POT	Potentiometer
PPR	Proportional Pressure Regulator
REPS	Repetitions
ROM	Range Of Motion
S	Small Size
SB	Small Braided -Sleeve
SCS	Screw And Cable Transmission
SMPS	Switched Mode Power Supply
SRE	Salford Rehabilitation Exoskeleton
TRI	Triceps Brachii
UA	Unactuated
UDL	Uniformly Distributed Load
UE	Upper Extremity
USB	Universal Serial Bus
WHO	World Health Organization
XL	Extra Large Size
XS	Extra Small Size
OECD	Organization for Economic Cooperation and Development

1 INTRODUCTION

The OCED Observer (Triviron Healthcare 2019) stated that a sound healthcare system ensures a healthy economy; their analysis found that a simple 10% increase in life expectancy resulted in 0.4% annual economic growth. Developing economies have realized the significance of healthcare and life expectancy in their economic progress. The rising population of the Indian sub-continent has left the healthcare system handicapped. The current statistics have shown an availability of less than one doctor for every thousand citizens, which is less than the standard (of 1:1000) prescribed by the world health organization (WHO).

A solution to this problem could include introducing automation in the healthcare system. Physical activities in highly controlled and predictable situations, as well as data gathering and processing, are the most susceptible to automation. Currently, automation is found in robotic surgery, patient monitoring, and medical scans and imaging analysis to detect cancer, tumors, and other irregularities(Ghergich 2021). Automation does not mean that machines would start prescribing medication; instead, machines could assist doctors in making quicker and more accurate diagnoses. The current benefits of automation in the medical field are as follows (Byrd n.d.):

1. To schedule appointments and treatment processes by maintaining a patient database.
2. Reduced the cost of treatment.
3. Ease of transfer and access to data between various departments of a system (e.g., easy access to patient data between doctors and the pathology lab of the same hospital).
4. It reduced errors due to human factors.
5. The use of machine learning helps in better handling of emergencies and adaption to changes in the number of patients.
6. Automation also increased patient privacy and satisfaction due to reduced human intervention.

Physical therapy or physiotherapy is one field in the healthcare industry where automation has a good potential to provide good effective services to patients.

Physiotherapy is a therapeutic strategy that focuses on the science of movement. Physiotherapy assists people in restoring, maintaining, and optimizing their physical strength, function, mobility, and general well-being by treating underlying physical difficulties (S. Vancouver Physio Clinic n.d.). Physiotherapy is a personalized treatment method, with the therapist catering to each patient. The requirement of physiotherapy is widespread for various medical ailments such as orthopaedic treatments, stroke patients, occupational therapy, and any patient undergoing a surgical procedure. The shortage of physiotherapists is one of the reasons why many patients remain disabled on not receiving timely care(Gadgil 2022). This research attempts to assist physiotherapists by developing a robotic assistive device for the upper extremity. This robotic device would work alongside a physiotherapist to provide repetitive upper extremity therapy with minimal supervision.

1.1 Anatomy of the Upper Extremity

Humans are naturally biped and only use their lower limbs/extremities to transmit bodyweight and locomotion. The upper limbs were designed for higher human functions, such as prehension and manipulation ("Chapter 2. Prehension" 1994). Apart from the power grip and hook grip seen in primates, humans exhibit precision grip, which allows the performance of precision activities such as holding a pen or needle or gripping small instruments. The classification of the upper limb included four main components:

1. The Shoulder
2. The Arm/Upper Arm
3. The forearm
4. The hand

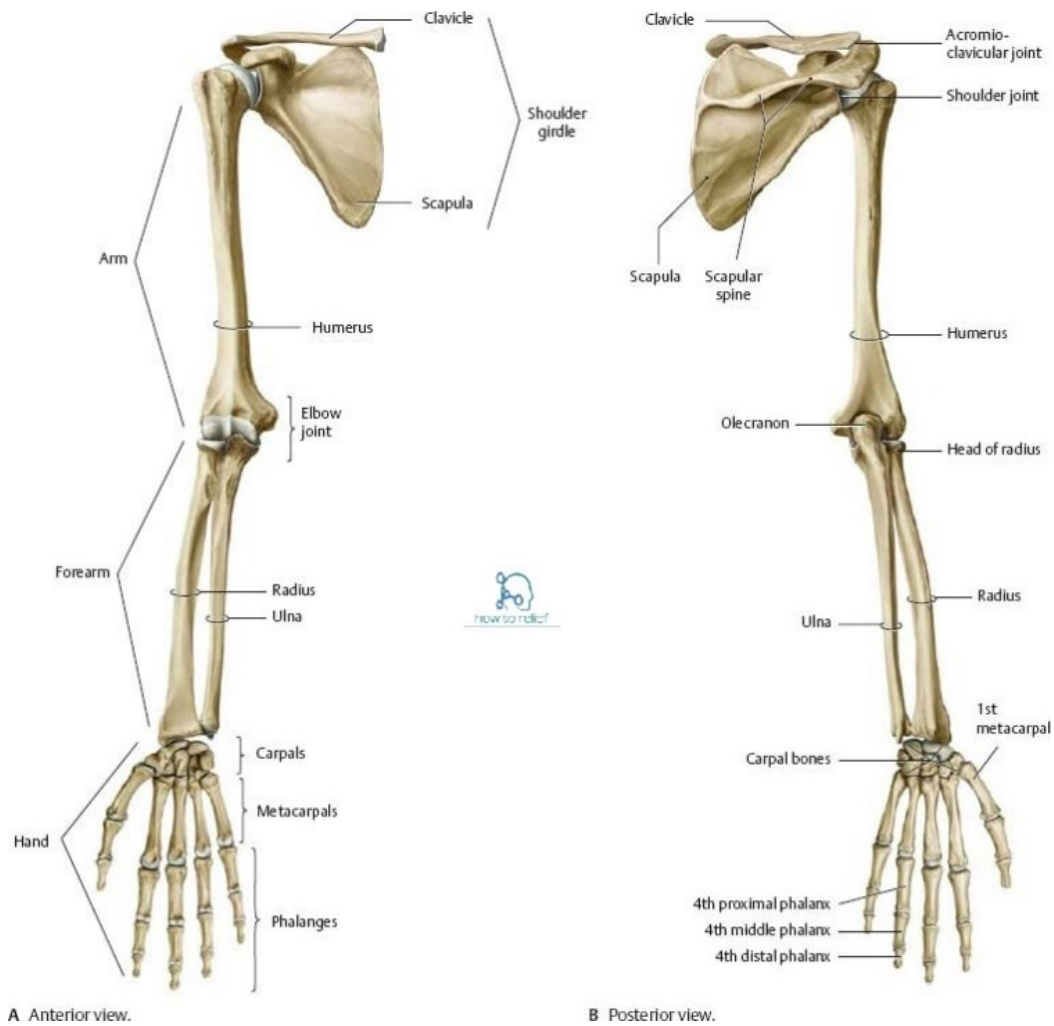


Fig 1.1: Anatomy of Upper Extremity ("Joints of the Upper Limb: Anatomy" 2017)(A: Anterior View, and B: Posterior View)

Fig 1.1 A & B shows the various bones and joints of the upper extremity. The shoulder assembly consists of the clavicle, and the scapula articulates with each other at the acromioclavicular joint forming the shoulder girdle. The sternoclavicular joint articulates the shoulder girdle with the rest of the body. The arm is the part of the upper limb between the shoulder and elbow joints. The humerus bone articulates with the scapula at the shoulder joint and the upper ends of the radius and ulna at the elbow joint to form the arm. The forearm is the upper limb region between the elbow and wrist joints. The forearm consists of the radius and ulna bones, which articulate with the humerus at the elbow joint. The radius and ulna articulate with each other to form the radio-ulna joint. The last component of the upper limb is the hand which consists of the

wrist, hand proper, and digits (thumb and fingers). The wrist consists of the carpal bones, the metacarpal bones at the hand proper, and the phalanges at the digits.

The brachial plexus is a network of nerves that supplies nerves to the upper limb. The five main branches of the brachial plexus are:

1. The auxiliary nerve supplies the deltoid and the teres minor muscles.
2. Three nerves supply the anterior compartments of the arm and forearm: musculocutaneous, median, and ulnar.
3. The radial nerve supplies the posterior (extensor) compartments of the arm and forearm.

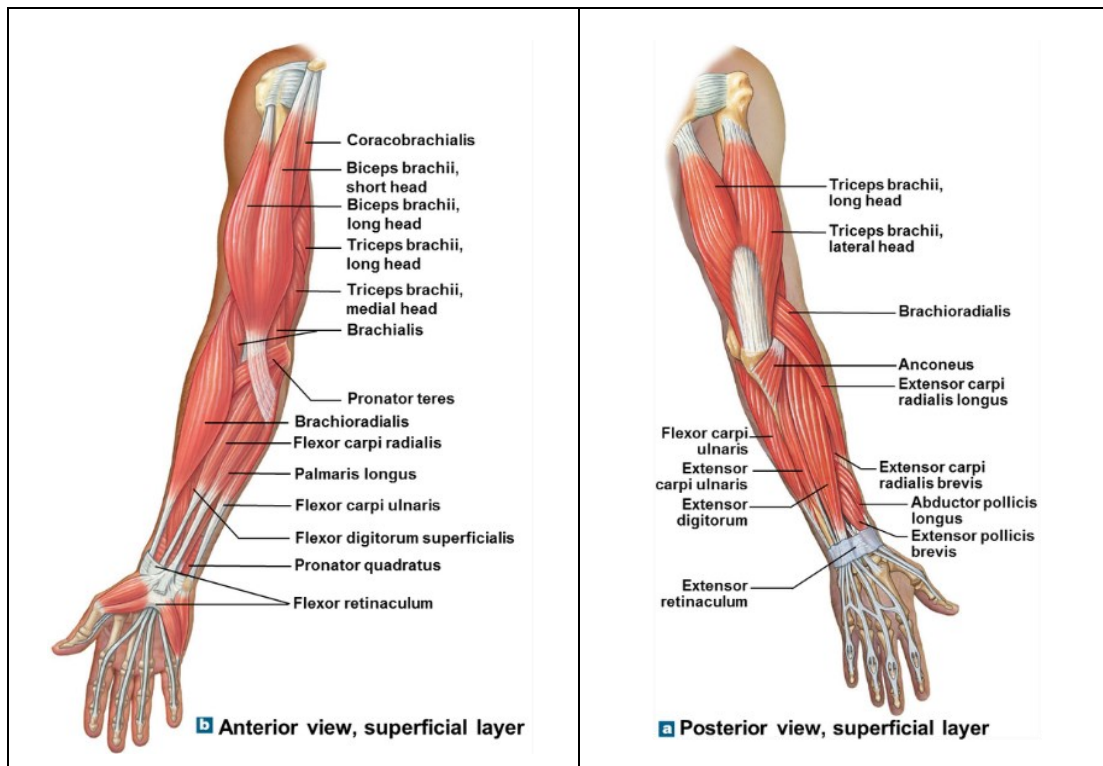


Fig 1.2: Muscle Anatomy of the Upper Extremity ("Anatomy Quiz: Upper Limb - Anatomy and Physiology" n.d.) (Left: Anterior View and Right: Posterior View)

As shown in Fig 1.2, the four main muscles responsible for motion in the arm include:

1. Biceps brachii: is responsible for flexion and supination of the forearm when the elbow is flexed. Flexion is defined as the motion of the elbow joint that results in the movement of the forearm towards the body, while supination is the clockwise rotation of the forearm about the long axis of the forearm.

2. Coracobrachialis: helps in flexion and adduction of the arm. Adduction is the limb's motion toward the body's midline
3. Brachialis: facilitates the flexion of the elbow joint.
4. Triceps-brachii: is positioned in the arm's posterior compartment and responsible for the elbow joint extension.

The classification of muscles in the anterior compartment of the forearm includes three layers (Fig 1.2):

1. Superficial Compartment:
 - a. Flexor Carpi Ulnaris: is responsible for the flexion and adduction of the wrist.
 - b. Palmaris longus: produces flexion of the wrist joint.
 - c. Flexor Carpi Radialis: this muscle is responsible for the flexion and abduction at the wrist. Abduction is a limb's motion away from the body's midline
 - d. Pronator Teres: helps in the pronation of the forearm.
2. Intermediate Compartment:
 - a. Flexor Digitorum is the only muscle in the intermediate compartment responsible for flexing the metacarpophalangeal joints. It helps flex the proximal interphalangeal joints at the four fingers and the wrist.
3. Deep Compartment:
 - a. Flexor Digitorum Profundus: this is the only muscle that flexes the distal interphalangeal joints of the fingers. This muscle also produces flexion at the metacarpophalangeal joints and the wrist.
 - b. Flexor Pollicis Longus: flexes the interphalangeal joint and the metacarpophalangeal joint of the thumb.
 - c. Pronator Quadratus: is responsible for the pronation of the forearm. Pronation is the forearm's counter-clockwise rotation about the forearm's long axis.

Muscles in the posterior compartment of the forearm:

The muscles in the posterior compartment of the forearm are commonly known as the extensor muscles. These muscles are divided into deep and superficial layers, as seen in Fig 1.2:

1. Superficial Muscles:

- a. Brachioradialis is a paradoxical muscle (similar to an extensor but a flexor). This muscle produces flexion in the elbow joint.
- b. Extensor Carpi Radialis Longus and Brevis: are responsible for the extension and abduction of the elbow joint.
- c. Extensor Digitorum Communis: helps extend the medial four fingers at the interphalangeal (IP) and metacarpophalangeal (MCP) joints.
- d. Extensor Digiti Minimi: produces extension in the little finger and contributes to the wrist extension.
- e. Extensor Carpi Ulnaris: is responsible for the extension and adduction of the wrist.
- f. Anconeus: this muscle stabilizes and extends the elbow joint. It also abducts the ulna during pronation of the forearm.

2. Deep Muscles

- a. Supinator: located on the floor of the cubital fossa and helps in the supination of the forearm.
- b. Abductor Pollicis Longus: is located distal to the supinator muscle and responsible for the thumb's abduction.
- c. Extensor Pollicis Brevis: extends the metacarpophalangeal and carpometacarpal joints of the thumb.
- d. Extensor Pollicis Longus: produces extension in all the thumb joints (carpometacarpal, metacarpophalangeal, and interphalangeal).
- e. Extensor Indicis Proprius: extends the index finger and allows the index finger to move independently of the other fingers during extension.

1.1.1 Elbow Joint Anatomy

The present research attempts to develop, build, and characterize a robotic assistive device to impart physiotherapy to the elbow joint. As shown in Fig1.3, the elbow joint is a synovial joint connecting the arm to the forearm.

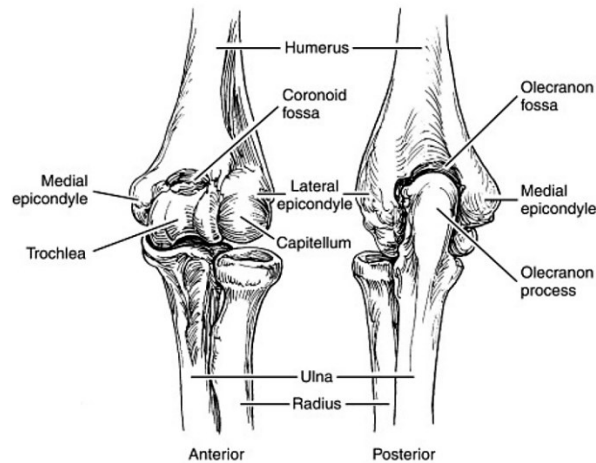


Fig 1.3: Elbow Joint Anatomy ("ELBOW JOINT - SAMARPAN PHYSIOTHERAPY CLINIC AHMEDABAD" n.d.)

As shown in the Fig1.3, the elbow joint is a combination of three joints formed by the articulation between the humerus, radius, and ulna(Morrey et al. 2018; "The Elbow Joint - Structure - Movement - TeachMeAnatomy" n.d.):

1. The humero-ulnar joint connects the humerus with the ulna, allowing the arm to flex and extend.
2. The radius and humerus form the humero-radial (radio-capitellar) joint, which allows for flexion, extension, supination, and pronation.
3. The ulna and radius bones form the proximal radio-ulnar joint and facilitate the rotation of the forearm.

Ligaments of the Elbow Joint:

1. The radial collateral ligament is located on the lateral side of the joint, extending from the lateral epicondyle and merging with the radius annular ligament.
2. The ulnar collateral ligament arises from the medial epicondyle and is connected to the ulnar coronoid process and olecranon.

The ulnar, radial, and median nerves are the primary nerves of the elbow joint. These nerves carry impulses from the brain to the muscles that help elbow motions. They also relay sensory information such as touch, pain, and temperature to the brain. Any damage or injury to these nerves or ligaments could result in discomfort, weakness, or joint instability.

Movement of the Elbow Joint:

The elbow joint is a hinge-like joint with two degrees of freedom (DOF), including Flexion/Extension (F/E) and Pronation/Supination (P/S) motions. The set of muscles that produce the different movements of the elbow joint are listed below:

1. Flexion: Brachialis, Biceps Brachii, and Brachioradialis
2. Extension: Triceps, and Anconeus
3. Supination: Supinator, Biceps Brachii (when the elbow is flexed), and Brachioradialis (supinates the pronated forearm to mid position)
4. Pronation: Pronator-Teres, Pronator-Quadratus, and Brachioradialis (pronated the supinated forearm to the middle position).

Elbow Carrying Angle:

The carrying angle is the acute angle formed by the median axis of the arm and the forearm in full extension and supination. This position allowed the forearm to clear the hip during swinging movements while walking. The carrying angle is more significant in females than males and is also greater in the non-dominant arm (Sharma et al. 2013).

1.1.2 Elbow Joint Injuries Requiring Physiotherapy Intervention

The injuries to the elbow joint are classified into the following categories (Alahmari and Kakaraparthi 2015):

1. Injury to soft tissue: These include ligament sprains, tendinitis, and nerve traumas
2. Injury to the bone: The primary injuries are fractures, dislocations, avulsion injury, and osteophyte formation.
3. Epicondylitis: This is a pathological change in the muscle-tendon origin at the epicondyle.

- a. Medial Epicondylitis: This causes Golfers elbow or Pitchers elbow
 - b. Lateral Epicondylitis: This causes Tennis elbow condition.
 - c. Role of physiotherapy exercise to treat epicondylitis:
 - i. Wrist range of motion
 - ii. Wrist stretches
 - iii. Pronation and supination of the forearm
 - iv. Elbow range of motion
 - v. Radial-ulna deviation exercise
4. Distal Bicep Tendon Rupture: A decreased strength in the bicep tendon may cause this injury. Tendon ruptures usually occur at the bone attachment or the junction of the tendon and labrum. This injury is more prominent in the dominant arm, and a surgical correction is recommended. Role of physiotherapy exercise to treat distal bicep tendon rupture:
- a. Physiotherapy is used to improve strength and range of motion (ROM).
 - b. As recovery progresses, the patient is given resistance exercises.
5. Elbow Dislocations: This is considered a more severe type of injury, and a large force is required to cause such an injury. Fractures, muscle or ligament tears, cartilage, or nerve damage usually result from such an injury. The role of physiotherapy exercise in treating elbow dislocation includes:
- a. After sufficient rest to the affected elbow joint, an exercise protocol is started to improve the range of motion and strength of muscles around the affected elbow and forearm.
 - b. Active and passive ROM exercises: The elbow treatment is started with elbow flexion/extension exercises, followed by pronation/supination motion. Isometric exercises and proprioceptive neuromuscular facilitation (PNF) techniques help decrease the pain and increase the ROM in the elbow joint. As the elbow improves, strength and endurance exercises such as squeezing a ball can begin after the patient can perform pain-free activities. Stretching exercises help to reduce tightness in the elbow joint.

6. Stroke is a condition that occurs due to interruption of blood flow to the brain resulting in a sudden loss of neurological functions (Susan B. O'Sullivan 2007).

Fig 1.4 shows the classification of stroke, which includes:

- a. Ischemic stroke: This is caused by a clot or impeded blood flow, obstructing oxygen supply and other vital nutrients to the brain.
- b. Hemorrhagic stroke: Occurs when blood vessels rupture, causing blood leakage in and around the brain.

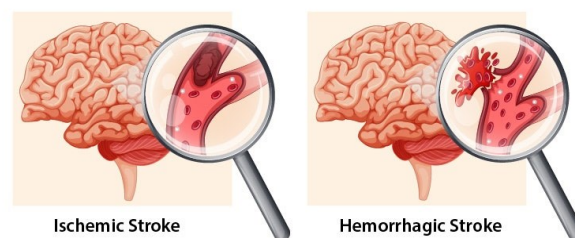


Fig 1.4: Classification of stroke ("Classification of Stroke" 2018)

The stages of motor recovery in stroke patients include:

- a. Firstly, flaccid paralysis is seen, which is followed by spasticity, hyperreflexia, and mass patterns of movement known as obligatory synergies.
- b. In the second stage, the facilitatory stimuli would evoke synergies with no or limited voluntary movement, also known as early synergy.
- c. Spasticity and strong obligatory synergy mark the progression of recovery.
- d. As some movements diverge from synergy, synergy's influence starts to wane at this stage.
- e. Synergy and spasticity become more independent as recovery progresses, and isolated joint movements become more pronounced.
- f. The final stage results in nearly normal movement patterns.

The first few weeks post-stroke is the period where the fastest recovery is possible, with measurable neurological and functional recovery occurring within the first month. This recovery is attributed to the resolution of transient inhibition of function that accompanies an acute stroke.

The existence of neuroplasticity (Alia et al. 2017) gives hope to patients for complete recovery from stroke and other neuromuscular deficiencies. Robot-based rehabilitation has promoted network plasticity and functional recovery. It is also reported that there are no significant differences in the capability of motor recovery between stroke type (hemorrhagic/ischemic) and location (brainstem/hemispheric).

An exercise plan has to be designed keeping in mind that stroke patients have a high incidence of hypertension and cardiac disease. Stroke rehabilitation methods are built on task-oriented repetitious training to achieve a satisfactory functional outcome (Oujamaa et al. 2009). Unlike other localized injuries, the limb affected by stroke receives negligible control input from the brain; therefore, interventions for stroke are primarily based on retraining the brain. The role of Physiotherapy exercise for stroke recovery (Pollock et al. 2014) is given as follows:

1. Bilateral arm training: Here, identical movements are given to both arms simultaneously. This exercise is believed to activate the affected hemisphere in the brain, thus improving motor control of the affected limb.
2. Electrical stimulation using electrical impulses is used to activate the muscles of the affected arm to strengthen and improve voluntary control.
3. In the manual therapy technique, the therapist gives partial or complete assistance to the patient through various upper limb movements.
4. The method of mirror therapy uses a mirror in the sagittal plane to reflect the healthy arm movement giving an illusion of movement of the unhealthy arm resulting in the gradual restoration of motion in the affected limb.
5. Repetitive task training involves repeated movement of the affected limb, strengthening the affected limb and helping in motor relearning.
6. Robotic intervention is used to move the affected limb through assistive or resistive motion. Robotic devices are very efficient in providing repetitive motion training and could also be used to impart physiotherapy to localized injuries.

7. Assistive/resistive movements are given by a therapist or physiotherapy equipment to improve the strength of the affected arm in the strength training method of physiotherapy.
8. In task-specific training, the patient is encouraged to use the affected hand to perform certain activities of daily living (ADL).
9. Virtual reality is a more modern technique that uses interactive simulation. Virtual reality uses computer hardware and software to provide a simulated environment to perform task-based activities in a virtual space.

1.2 Assistive Devices for Physiotherapy

In a populous country like India, with a population of almost 139 crores, there are only 0.59 physiotherapists for every 10000 people("India - Physiopedia" n.d.), which is approximately one physiotherapist for every 20000 people. This disparity between the number of patients and available physiotherapists results in a handicapped medical rehabilitation system. The use of technology and robotic devices to reduce the burden on physiotherapists could be a boon to the medical system. Still, the exorbitant cost (Turchetti et al. 2014) made them a disadvantage to an economically developing country like India. Robotics in rehabilitation has gained importance in recent years, focusing on exoskeletons. Assistive devices for the upper extremity (Rasedul Islam 2017) are classified and depicted in fig 1.5.

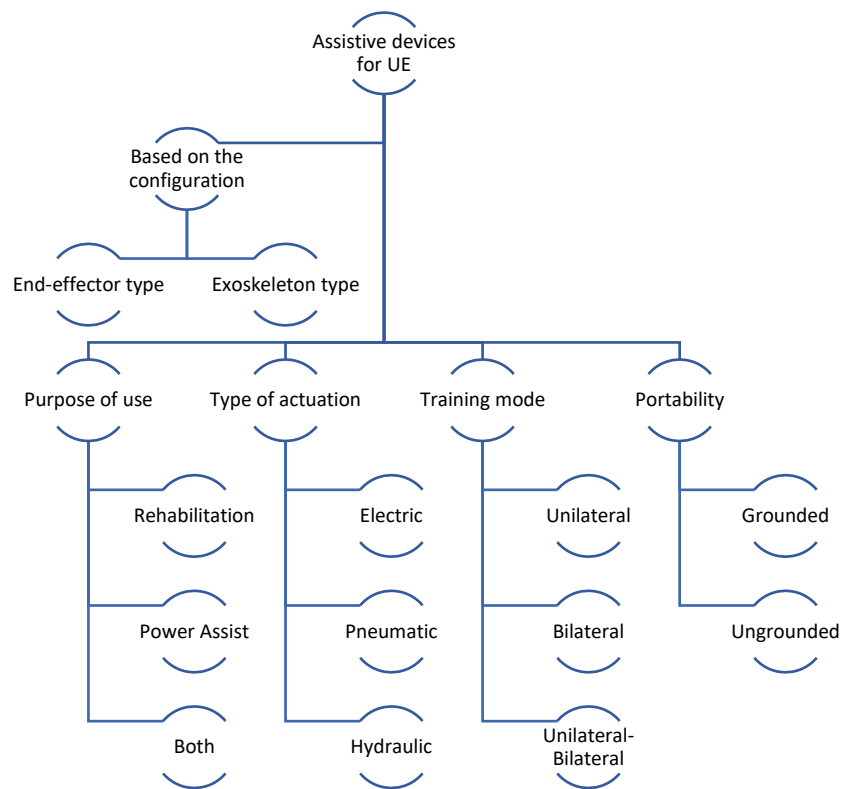


Fig 1.5: Classification of Assistive device for upper extremity (Rasedul Islam 2017)

In a broader sense, an upper extremity (UE) assistive device can be used either for rehabilitation, power assist (for force multiplication), or to serve both purposes. The classification is based mainly on the end-effector and exoskeleton configuration specific to physical rehabilitation, as shown in Fig 1.6(a & b). The end-effector type assistive device consists of a robotic arm whose end-effector is attached to the patient's hand. The end-effector's motion is translated to the movement of the patient's arm. The exoskeleton-type device involves a support structure attached to the patient's limb and imparts the torque necessary for movement directly to the joints. The end-effector type device does not support the whole arm during physical therapy. Therefore, end-effectors are preferred much less compared to the exoskeleton-type device. The motion to these devices is achieved using either an electric (e.g., motor), pneumatic (cylinder, air-motor, or muscle), or hydraulic actuation system. The classification can also be based on the training modes as unilateral, which involves one arm, bilateral (e.g., MIME) involving both arms, or a combination of both. The last but essential

classification is based on portability, which is either grounded (fixed base) or ungrounded (the device is fixed to the arm and is portable).

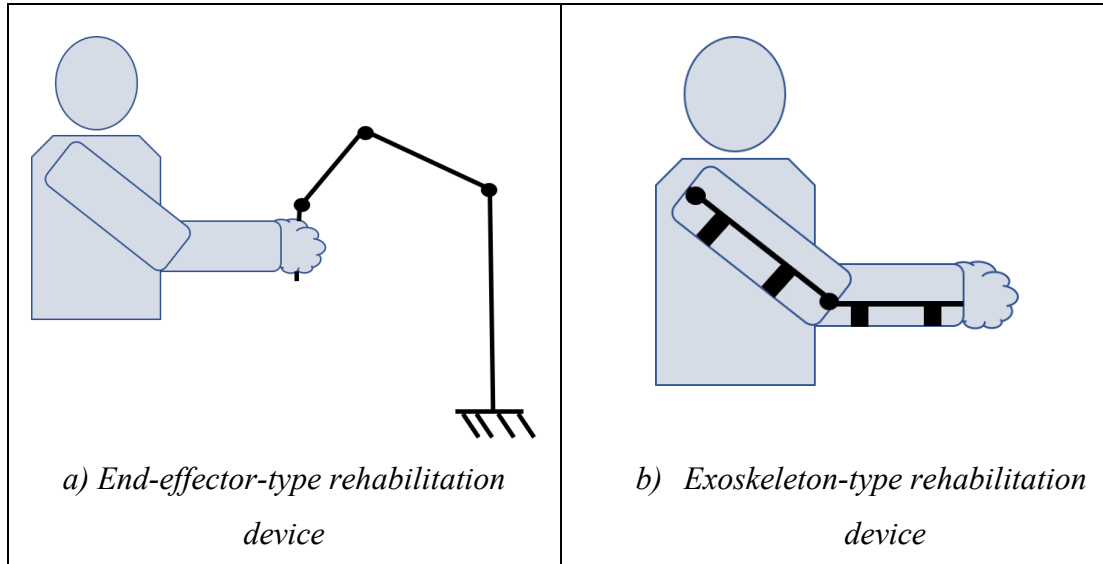


Fig 1.6: Schematic of end-effector and exoskeleton-type rehabilitation devices

The high power-to-weight ratio and compliance of pneumatic muscles (Robinson et al. 2012) have made it an ideal choice to be used in assistive exoskeletons for both upper and lower limb applications. In this thesis, pneumatic muscles of varying dimensional and material characteristics are developed and fabricated. As the exoskeleton is designed to be directly in contact with the user, the forces exerted by the actuators must be adequate to perform the motion and, at the same time, should not harm the user. The criticality of this application demands several tests on the developed pneumatic muscles to check their feasibility for this application. This thesis also presents a comparative analysis between the developed and commercially available muscles. A mathematical model is developed and used to simulate the displacement of the muscle actuator, and the results are compared with experimental findings. The final objective of this research involves testing the performance of the pneumatic muscle in a real-world scenario for which an exoskeleton is designed and fabricated. This report presents the design of the pneumatic muscle actuator and its implementation on the newly designed exoskeleton.

2 LITERATURE REVIEW

Machines impart repetitive motions, unlike humans, who get fatigued, thus compromising the quality of treatment with time. In physical therapy, a similar issue is observed where the therapist has to give repetitive exercises to patients. Still, as a human, the therapist is bound to get tired, thus compromising the accuracy and quality of therapy. The low quality of repetitive therapy became the prime reason for developing a robotic assistive device for imparting physical therapy. In countries like India, with a vast population, the problem is even worse as there are too few physiotherapists to cater to many patients. Therefore, it has become mandatory to have more automated devices to assist in fields such as physiotherapy. Lo et al. (Lo and Xie 2012) conducted a comparative study on robotic and normal therapy. In this study, 49 patients received intensive robot-assisted treatment, 50 received intensive comparative treatment, and 28 received usual care. After 12 weeks, robotic therapy's FMA (Fugl-Meyer Assessment) ratings were reported to be higher than the standard therapy. As previously discussed, assistive devices are broadly classified as end-effector and exoskeleton-type devices based on their configuration. In the preceding sections, the various works on upper limb assistive devices have been discussed.

2.1 End-Effector Assistive Device

The MIT-MANUS (Krebs et al., 2007) developed by the Massachusetts Institute of Technology is reported to be the most approved and well-known end effector device. The MIT-MANUS has a two-degrees-of-freedom (DOF) robot manipulator that assists the shoulder and elbow movement by moving the patient's hand in the horizontal plane. It uses a novel impedance control mode allowing it to be compliant when interacting with the patient's arm, thus closely matching the human therapist-patient interaction. The study conducted with the MIT-MANUS revealed a more significant improvement in shoulder and elbow motor function and strength compared to conventional therapy (Hidler et al. 2015). Another well-known end-effector type configuration is the Mirror Image Movement Enabler (MIME) (Lum et al. 2002), a robotic device for shoulder and elbow neuro-rehabilitation in subacute stroke patients. The MIME incorporates a PUMA 560 robot in three dimensions to apply forces to the paretic limb during

unilateral and bilateral movements. The 6 degrees of freedom of the robot allows the forearm to move in an extensive range of positions and orientations in three-dimensional space. Hesse et al. (Hesse et al. 2003) developed a robot-assisted arm trainer called, Bi-Manu-Track to impart passive and active bilateral forearm and wrist movements in hemiparetic subjects. Bi-Manu-Track is a portable reconfigurable device with one active and one passive DOF between wrist flexion/extension and forearm pronation/supination. The authors reported that most patients treated on the Bi-Manu-Track had favourable outcomes, with the extremity feeling more vivid; subjects also noticed a reduction in spasticity, ease of hand hygiene, and pain relief. The arm trainer enabled seriously impaired stroke patients to get extensive bilateral elbow and wrist rehabilitation. Sukal et al. (Sukal et al. 2005) used a 6 DOF robot arm called the arm coordination training 3-D (ACT 3D) and a novel method for recording movement patterns to generate a varying amount of shoulder abduction torque. The ACT 3D robotic system records movement patterns as subjects develop different degrees of shoulder abduction torque. This technique was adopted to produce preliminary data demonstrating how higher shoulder abduction forces limited a stroke subject's effective work area in a manner consistent with flexion synergy. The REHAROB (Fazekas et al., 2007) is another unique therapeutic device to impart passive robot-mediated physiotherapy to patients with spastic hemiparesis. This device uses two industrial robots which support the patient's arm and delivers the therapy taught to it by the physiotherapist. The end-effector type configuration, a single point of contact device, does not support the patient's arm during treatment which could cause pain, discomfort, or harm the patient's limb.

Liu et al. (Liu et al. 2017) developed a unique end-effector upper limb rehabilitation robot with two active degrees of freedom. The device designed by Liu et al. is based on the interaction force and displacement of the end-effector in order to assist patients in training for point-to-point line and circle-tracking jobs. Their research looked into the kinematics and dynamics of the robot system, the control system, and the implementation of various rehabilitation methods. They also investigated the effect of constraint on contact force and muscle activation in rehabilitation therapy. Song et al. (Song et al. 2015) created an adaptive motion control technique for a 4-DOF end-

effector upper limb robot based on impedance identification. They proved their control strategy could achieve system adaptation in five experiments involving healthy individuals. Intelligent control algorithms were proposed as a viable method for improving the adaptation of rehabilitation robot systems during clinical trials.

The iPAM (Jackson et al. 2007) used a twin robotic system to deliver therapeutic upper-limb exercise for post-stroke rehabilitation. The iPAM includes two coordinated, pneumatically-actuated robotic arms attached to the patient's forearm and upper arm to provide assistance and simulate a physiotherapy intervention. The controller was developed and 'tuned' to enable gravity adjustment for robots, reducing potentially harmful stresses on the patient's arm. Two small-scale trials were conducted to test the system's mechanical design for allowing normal arm mobility and its capacity to deliver varying levels of lift to the patient's arm to increase the range of motion. The first of these tests were found to be comparable to free arm movement in healthy subjects and stroke patients with the iPAM attached. The authors reported that the robot has no discernible effect on movement patterns. In the second series of experiments, patients with significant upper-limb disability improved their reach but changed their movement pattern when subjected to higher values of 'lift.'

End-effector robots are attached to patients at a single distal point, and their joints do not correspond to human joints(Lo and Xie 2012; Maciejasz et al. 2014). The forces exerted at the distal contact simultaneously alter the location of adjacent joints, making the independent movement of a single joint difficult. Although end-effector robots are proven to be effective in rehabilitation, and several devices have been commercially successful, they suffered from several critical limitations(Shen et al. 2020) listed below:

1. Compared to the human arm, end-effector robots typically have a much-limited range of motion.
2. For an end-effector robot's workspace to match the workspace of a human arm, the robot needs to be large since the base needs to extend beyond the arm's reach to avoid collisions.
3. Furthermore, the robot has to reach every region of the human arm's workspace without physically overlapping with the user.

4. As the end-effectors move specific sites of the human arm, it is difficult for an end-effector rehabilitation robot to target a single joint motion for therapy.

A large variety of upper limb exoskeleton robots have been developed to overcome the limitations of end-effector-type devices. Unlike end-effector robots, exoskeleton-type devices are similar to human limbs that attach directly to the patient at several locations, and their joint axes correspond to the human joint axes. Therefore, exoskeleton devices make it feasible to train individual muscles by controlling joint motions at predetermined torques.

2.2 Exoskeleton Type Assistive Device

Nowadays, research is focussed more on the development of exoskeleton devices, as they are found to offer better support to the patient's paretic limb. Exoskeletons could also be made portable and greatly enhance recovery by applying torques directly to the affected joints. Kaiguchi et al. (Kiguchi et al. 2003) designed a two-degree-of-freedom (DOF) exoskeleton robot for shoulder joint assistance control using wires, links, and a sliding mechanism. A moving mechanism for the centre of rotation (CR) of the exoskeletal robot's shoulder joint was proposed to adapt the CR of the robot shoulder joint with that of the physiological human shoulder joint during shoulder motion. An efficient fuzzy-neuro controller was also devised to operate the robot using EMG signals from the human shoulder muscles. SUEFUL-7 (Gopura et al. 2009) is another exoskeleton robot with a muscle model-oriented and EMG-controlled system. This device offers vertical and horizontal flexion/extension of the shoulder, shoulder internal/external rotation, elbow flexion/extension, forearm supination/pronation, wrist flexion/extension, and wrist radial/ulnar deviation for physically weak individuals. The SUEFUL-7 uses pulleys and cable mechanisms alongside gears for power transmission while using EMG and force sensors (forearm and hand) as feedback for control. Biomimetic Orthosis for the Neurorehabilitation of the Elbow and Shoulder (BONES) is a very innovative design involving pneumatic actuators to move the user's arm (Klein et al. 2008). BONES is a 4 DOF pneumatically actuated upper extremity rehabilitation device that uses a simple parallel mechanism with mechanically grounded actuators. Four mechanically grounded pneumatic actuators were installed below the main

structural frame to regulate shoulder motion through sliding rods. The elbow flexion/extension was controlled using a fifth cylinder installed on the structure. The apparatus allowed the full range of motion to the arm while achieving low inertia and direct-drive force production capability at the shoulder.

Moubarak et al. (Moubarak et al. 2009) developed a 3 DOF wheelchair-mounted exoskeleton device for the rehabilitation training of weak and injured people without the continuous presence of a therapist. Using their device, they achieved three degrees of freedom (DOF) at the shoulder and one at the elbow (flexion/extension). The primary goal of this device was to assist people with disabled upper limbs in performing activities of daily living (ADL) by providing various levels of training and therapeutic modalities. The device was developed to help post-stroke situations, spinal cord injury patients, accident victims, and aged people to improve muscle strength and heal faster. This device allowed the patient to receive consistent training without the constant support of the therapist; as a result, the latter could work on multiple patients simultaneously, lowering the total cost of the therapy. The L-EXOS (Frisoli et al. 2009) is a 5 DOF motor actuated exoskeleton designed as a wearable haptic interface, capable of providing a controllable force at the centre of the user's right-hand palm, regardless of its orientation. The L-EXOS allowed the rehabilitation of the right upper limb combined with a virtual reality tool. The L-EXOS showed significant improvements in Fugl-Meyer scores, the Ashworth scale, and increments of active and passive ranges of motion on the impaired limb's shoulder, elbow, and wrist joints. The Fugl-Meyer Assessment (FMA) and the Modified Ashworth Scale (MAS) are frequently used in clinical practice to assess motor dysfunction and resistance to passive movement (i.e., spasticity)(Rech et al. 2020). L-EXOS also demonstrated an improvement in quantitative indexes, such as task time and error, synergies, and smoothness of movement. The MGA Exoskeleton (Carignan et al. 2007) is another device that supports the shoulder and acts as a haptic interface for virtual task training. The MGA Exoskeleton had five actuated joints and one unpowered joint, with four shoulder DOF and two elbow DOF. A single pitch joint controlled the elbow flexion/extension, and a passive forearm roller handle permitted free forearm supination/pronation. The MGA

was actuated using brushless DC motors and harmonic drives and had applications in orthopaedic and neuro-rehabilitation.

Ren et al. (Ren et al. 2009) developed a 10 DOF whole-arm exoskeleton robot with a hand opening and closing mechanism for upper limb stroke rehabilitation. They observed that, in robot assistive training, patients were frequently instructed to hold a handle firmly, which could cause intense hand muscle contractions with the hand in an abnormal posture. Whenever the muscular tension in the subject's hand was not managed correctly, the flexibility of the hand/fingers could deteriorate, and the robot training could result in aberrant muscle tone. However, because the patient's fingers were already in an aberrant position, properly aligning the joints and making the robot easy to be attached became critical. Ren et al. focused on a patient-friendly mechanism driven by a single motor attached to the whole arm rehabilitation robot for the opening and closing function of the fingers and hand. They designed exercise routines for intensive stretching of the MCP-thumb joints and other spastic upper extremity joints and active assistive exercise using robot-computer games with a gripping task to improve voluntary neuromuscular control. Their work also included an outcome evaluation, including cross-coupling torques between the fingers/thumb and other joints during hand opening/closing and other upper limb movements. A cable-driven mechanism for the upper extremity designed by Perry et al. (Perry and Rosen n.d.) had 7 DOF exoskeleton having low inertias, high-stiffness links, and back-drivable transmissions without backlash. The design considered the upper limb's kinematics and dynamics during everyday living tasks, as well as joint physiological and anatomical considerations, workspace studies, and joint ranges of motion. Proximal motor placement and distal pulley reductions resulted in high-stiffness links, low inertias, and back-drivable transmission with negligible backlash. The design applications included physiotherapy, assistive, haptic, or as a master for teleoperation. Kung et al. (Kung et al. 2007) designed an exoskeleton for patients with neuromuscular disorders. This device mainly assists the patient in pronation and supination of the forearm. The robot is designed to guide the user's forearm to pronate/supinate in a predefined seesaw-like or ramp-and-hold trajectory in active or passive mode. Preliminary testing on normal participants demonstrated that the robot could lead the relaxed forearms of subjects in

the planned trajectory in passive mode and apply a specific torque to the forearm during voluntary movement in the active mode.

2.3 Robotic Devices in Physical Rehabilitation

The robotic devices and rehabilitation, attracted researchers to do extensive research as these devices were known for their excellent repeatability and performance. The human upper limb has seven DOF, including three DOF at the shoulder, two at the elbow, and two DOF at the wrist joint. Tsai et al. (Tsai et al. 2010) found that designing a seven DOF exo-device resulted in unfavourable singularities in the range of motion. Therefore, they developed a nine-DOF articulated rehabilitation robot for upper limb physiotherapy and training, including six DOF at the shoulder, one at the elbow, and two at the wrist. They determined the desired posture by mapping the kinematics of the human arm with that of the robot. They also used EMG and force sensors to detect the patient's volition, and a circle drawing was set as a testing criterion to measure the patient's progress. Looned et al. (Looned et al. 2014) designed a two DOF elbow exoskeleton (extension/flexion and pronation/supination). The device was designed for individuals with neurological disorders and hemiparetic stroke. They used a brain control interface (BCI) alongside electric stimulation to assist patients in independently drinking using a glass. The study was conducted on healthy individuals who were asked to impersonate stroke motion behaviour. The system produced motion of the impaired arm when it received brain signals from the individuals intending to move their arm. All subjects completed the task of drinking a glass of liquid at an average speed of 127 seconds. The incremental elbow extension and flexion motions were the key limiting factors for accomplishing this activity quickly. ABLE (Garrec et al. 2008) is another upper extremity device with a lightweight form factor that assists disabled people in performing certain basic tasks. It had four degrees of freedom, involving three DOF at the shoulder and one at the elbow (Flexion / Extension). The ABLE used a new mechanical transmission called the screw and cable transmission or SCS for high-fidelity force feedback. The ABLE was back-drivable, highly efficient, low inertia actuator with high force capacity and supported hybrid force-position control without force sensors. Rocon et al. (Rocon et al. 2007) developed a wearable orthosis for tremor assessment and suppression (or WOTAS). WOTAS was a 3 DOF exoskeleton mainly

used to detect and suppress tremors in the user's limb. WOTAS had 2 DOF at the elbow (extension/flexion) and 1 DOF at the wrist (extension/flexion).

The process of rehabilitation, especially repetitive tasks, can be very cumbersome for patients. As a result, Colombo et al. (Colombo et al. 2007) focused on motivating patients during physical therapy to improve involvement and recovery. They used gaming feedback and developed an evaluation metric to see the patient's progress. The study involved two groups of patients, one involving wrist movements, while the other was shoulder-elbow movements and both groups showed improvement in motor function. Another indirectly actuated device was the NeReBot (Rosati et al. 2007), which had an innovative design involving a 3 DOF wire-driven robot for poststroke treatment. Physical therapy was taught by the teach-by-show method, while using strings which resulted in a safe and cost-effective design. Results showed that patients treated with this method alongside conventional treatment had improved functional ability. Tsagarakis et al. (Tsagarakis and Caldwell 2003) developed a 7 DOF upper arm training/rehabilitation system powered by pneumatic muscles (PMA). The authors reported that using PMAs had the advantage of being lightweight, having an excellent power-to-weight ratio, inherently safe, naturally compliant, ease of fabrication, and low cost. The study demonstrated how the system used the inherent controlled compliance to create an incredibly powerful unit, delivering a wide variety of functionality (motion and forces) while still being safe for patients.

Exoskeletons are very effective in medical rehabilitation and stroke recovery. Evidence of brain plasticity is seen in robot-assisted upper extremity repetitive therapy (or RUPERT) (Sugar et al. 2007), which showed hope for the motor recovery of stroke patients. Sugar et al. stated that intensive, repetitive physical rehabilitation was found to help reverse upper extremity deficiencies. Still, the therapy was time-consuming, costly, and difficult to quantify and objectively evaluate. RUPERT, shown in Fig 2.1, was a non-gravity compensated five DOF pneumatically actuated exoskeleton. It aided with shoulder elevation, humeral external rotation, forearm supination, elbow extension, and wrist/hand extension. RUPERT was designed to provide patients and therapists with a low-cost, safe, and simple-to-use robotic device to assist them in achieving more systematic therapy at home or in a clinical setting. The authors believed

that practising tasks in the natural environment improved the recovery rate. Another research that emphasized the importance of repetitive robotic therapy was the MEDARM (Ball et al. 2007). MEDARM is a rehabilitation robot primarily focused on the shoulder complex, thus providing 5 DOF to the shoulder. Fig 2.2 shows the MEDARM with 6 DOF, of which 5 DOF are at the shoulder complex and 1 DOF at the elbow. It used cables and belts to transmit the motion of the motors to the exoskeleton, with the joint axes aligned to replicate the natural workspace of the upper extremity while limiting singular configurations. The main advantage of MEDARM was its ability to independently monitor and control all five of the main DOFs of the shoulder complex.



Fig 2.1: RUPERT (Sugar et al. 2007)



Fig 2.2: MEDARM (Ball et al. 2007)

Anan et al. (Sutapun and Sangveraphunsiri 2015) designed a four-DOF upper extremity exoskeleton with three DOF at the shoulder and one at the elbow joints, as shown in Fig 2.3. This exoskeleton is powered by electric motors and uses two control strategies, active-resistive and resistive, for patients in different stages of recovery. A unique feature of the exoskeleton was the use of input current to estimate the torque at each joint. Kousidou et al. (Kousidou et al. 2007) developed a multi-modal environment called Rehab-Lab. Rehab-Lab used a seven DOF upper-limb exoskeleton called Salford Rehabilitation Exoskeleton (SRE), as shown in Fig 2.4. The SRE was a pneumatic muscle-actuated and gravity-compensated upper extremity exoskeleton. It had three DOF at the shoulder joint, two at the wrist, and two at the elbow joint, which permitted

the elbow flexion/extension and pronation/supination motions. The main aim of this work was to make an easy-to-use software environment that physiotherapists could easily use. The method used protocols that were small basic tasks such as elbow extension or flexion. The therapist had to select the required protocol or create a new one and arrange them in the required sequence to create a task. The other attributes of a protocol included the number of repetitions, resting periods between tasks, speed, and range of motion. Kousidou et al. designed a system with three modes of operation. A fully assistive mode in which the exoskeleton provided 100% support to the patient to perform the desired motion, and a partial assistive mode, where a force/torque sensor was used to sense the user's volition and provide only the required amount of force to complete the task. The last mode was the non-assistive mode, wherein the exoskeleton offered resistance to the motion to improve the strength of the user's limbs.

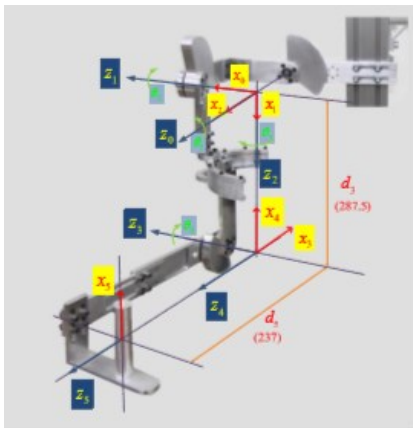


Fig 2.3: 4-DOF rehabilitation robot (Sutapun and Sangveraphunsiri 2015)

Fig 2.4: University of Salford Rehabilitation Exoskeleton (SRE) (Kousidou et al. 2007)

Hu et al. (Hu et al. 2009) studied the motor functional recovery process in chronic stroke patients during robot-assisted training using EMG and co-contraction index (CI). They focused on EMG activation in the following four muscles:

1. Biceps Brachii (BIC)
2. Triceps Brachii (TRI)
3. Flexor Carpiradialis (FCR)

4. Extensor Carpiradialis (ECR)

The results showed that the EMG values for FCR, BIC, and ECR dropped during training, which was reported to be associated with the MAS (Modified Ashworth Score) for the wrist and elbow joints. They also observed a decrease in CI scores for muscle pairs BIC & TRI, FCR & BIC, and ECR & BIC. They concluded that the drop in CI for BIC was mainly due to reduced BIC EMG activation, thus suggesting better isolation of wrist movements from elbow movements. The study (Cheng et al. 2003) aimed to improve elbow torque capability without compromising movement performance. In their research, they developed a controller to provide assistive torque to the elbow, proportional to the difference between the weighted biceps and triceps EMG signals.

Fig 2.5 shows a functional rehabilitation robot, the ARMin (Nef et al. 200), for patient-cooperative arm therapy. Mobilization therapy was based on repetitive human arm movements while the patient remained passive on a patient-specific trajectory. Execution of mobilization therapy involved the following two steps:

1. The therapist moved the patient's arm with the robot onto the desired trajectory. The therapist could set the exact shape of the movement (ranges, speed) by considering the individual impairment of the patient.
2. The second step involved the robot repeating the trajectory with an adjustable velocity.

Patients with unstable shoulder joints, resulting in shoulder subluxations, could not be treated by the ARMin. Thus, their shoulder actuation approach was acceptable for healthy subjects but problematic for patients with shoulder problems. As many stroke patients suffered from shoulder problems, they modified their design and developed the ARMin 3 (Nef et al. 2009). The ARMin 3, as shown in Fig 2.6, had a new ergonomic shoulder actuation principle that provided the motion to the humerus head. It involved a 7 DOF motor-harmonic drive actuated system with an additional module for pronation and supination of the forearm. The pronation/supination of the elbow was another attachment that used a motorized rotating bar that had to be grasped by the user.

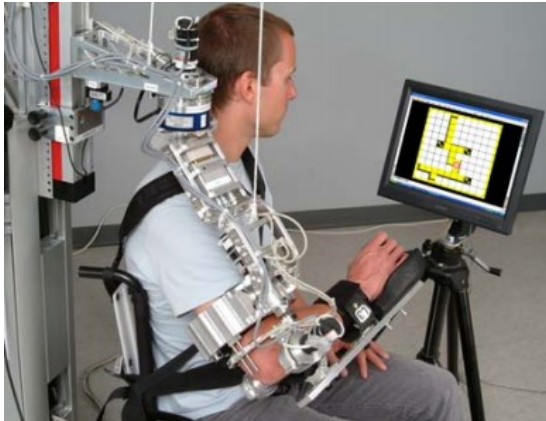


Fig 2.5: ARMin (Nef et al. 2007)

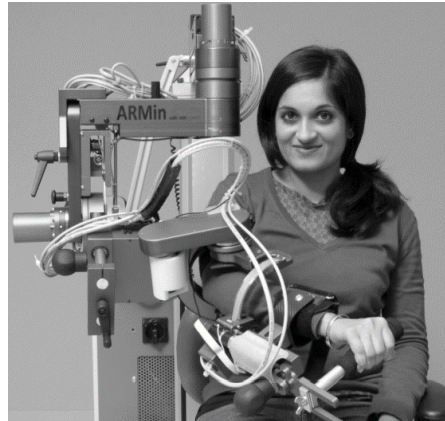


Fig 2.6: ARMin 3 (Nef et al. 2009)

MULOS (motorized upper-limb orthotic system) (Johnson et al. 2001) was an electrically powered device with three degrees of flexibility at the shoulder, one at the elbow, and one to facilitate pronation/supination, as shown in Fig 2.8. The shoulder mechanism comprised a serial linkage with an equivalent centre of rotation close to the anatomical shoulder; this was a self-contained module with tensioned cables for power transfer. Additionally, the elbow and pronation/supination modules were also self-contained. The system had been designed to perform the following three modes of control:

1. An assistive robot connected to the arm provided a controlled motion for individuals with severe disabilities.
2. Continuous passive motion was used to treat injured joints. The joint trajectory was determined by 'walk-through' programming and could be replayed for a set number of cycles at a set speed.
3. As strengthening exercise equipment, for the elderly and those recuperating from surgery or an injury.

Mao et al. (Mao and Agrawal 2012) listed a few of the shortfalls of the existing exoskeleton designs as listed below:

1. They required precise alignment of exoskeletal and human joints.
2. Due to the nature of the bony segments that created the joints, precise alignment of exoskeletal joint axes with arm joint axes was difficult.

3. The shoulder joint was highly complex, as the placement of the glenohumeral joint centre shifted throughout the motion.

Researchers have tried to address the shortfalls of existing exoskeletons by adding additional DOF at the shoulder complex, but all these resulted in a heavy and bulky design. Mao et al. presented a cable-driven upper arm exoskeleton or CAREX, a five DOF upper extremity exoskeleton. Compared to previous cable-driven exoskeletons, the CAREX ensured a controlled tension in all cables and used seven cables to control five DOF. The main objective of their study was to control the force at the end-effector. This control was achieved using the motors in torque mode and load cells to measure and control the tension in the cables. The CAREX used a method of assist as needed control for rehabilitation, in which assistive force is provided when the user has a strength deficit in completing a particular task.

The CABexo (or cable-driven wearable exoskeleton) (Xiao et al. 2017) is a six DOF cable-driven exoskeleton shown in Fig 2.7. The cable transmission system operated on the same principles as the gear transmission structure. However, instead of employing the meshing force between gears to transmit torque, it used cables on wheel faces, resulting in a quieter process, improved precision, and smoother transmission. As per the authors, cable drives were lightweight but difficult to control; therefore, they used them alongside epicyclic gears. The main body of the exoskeleton was hard, making it easier to manage compared to the parallel mechanism with flexible linkages. Another advantage over the ARMin and RUPERT was the mounting of the actuators on the backboard, thus making it lightweight and easy to be used by stroke patients. Xiao et al. reported that even while the CAREX was cable driven, it was more challenging to manoeuvre compared to the CABexo with a parallel mechanism.

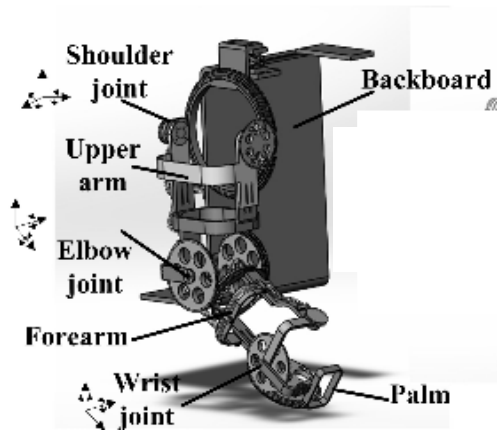


Fig 2.7: CABexo (Xiao et al. 2017)

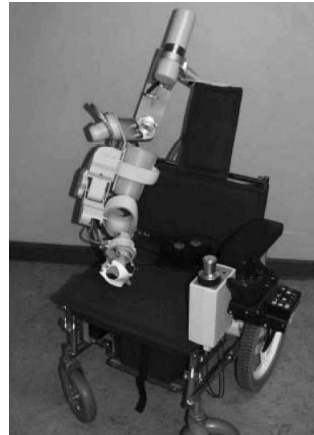


Fig 2.8: MULOS(Johnson et al. 2001)

2.4 Actuator Selection

An actuator is a component used to drive the motion of the various joints of the exoskeleton. These actuators can be electric (e.g., motors), pneumatic (e.g., pneumatic cylinders), or hydraulic (e.g., hydraulic cylinders). The main requirements of an actuator used to power a rehabilitation exoskeleton includes a high power-to-weight ratio, high compliance, and ease of control. Previous research in the field of rehabilitation exoskeletons have mainly used electric actuation. It is also evident from the literature that electric actuators were predominantly used to power exoskeletons built for the upper limb, hand, and forearm.

In contrast, only a small number are powered using pneumatics or hydraulics (Tiboni et al. 2022). Electric actuators are easy to control, but high torque motors are bulky and have a low power-to-weight ratio. Hydraulic actuators have an excellent power-to-weight ratio, but as they use hydraulic oil, they can contaminate the sterile medical environment in case of an accidental leak. The pneumatic actuators are safe to operate in medically sterile working environments as they use air as the actuation media. The exoskeleton designed in this research is powered using braided pneumatic muscles due to their high power-to-weight ratio, safe nature, and inherent compliance.

2.4.1 Pneumatic Muscle Actuator

The pneumatic muscle actuator (PMA) consists of three essential components: a hyper-elastic bladder, a braided sleeve enclosing the bladder, and two end fittings clamped on either end. The history of pneumatic muscles reveals two significant events. The first was its invention by Richard Gaylord in 1958 (Gaylord 1958). The inability of the muscle actuator to produce high force and the requirement of a power pack (compressor) led to it being side-lined by the electric motor (Snelson et al. 1961). Joseph L McKibben reintroduced the PMA in the year 1960; as a result, the PMA is also known as the McKibben Muscle. The principle of operation of the PMA involves the supply of pressurized air resulting in the radial expansion of the bladder, which in turn is restricted by the enveloping braided sleeve, thus converting the radial expansion into axial contraction (Tondu and Lopez 2000). The PMA's contraction ratio is defined as the ratio of displacement to the original length of the muscle, given in equation 2.1.

$$\text{Contraction Ratio} = \frac{\text{Displacement produced by actuated PMA}}{\text{Initial Length of PMA}} \quad (2.1)$$

The two output parameters associated with the PMA included:

1. Maximum axial contraction
2. and Blocked force

The maximum axial contraction is realized by allowing the actuator to actuate freely with unconstrained ends. In contrast, the force generated by an actuated muscle with constrained ends is known as blocked force. The PMA's high power-to-weight ratio (Caldwell et al. 2000) and inherent compliance make it very favourable for assistive applications such as medical exoskeletons. Daerden et al. (Daerden and Lefeber 2002) defined compliance as the inverse of stiffness on account of the compressible nature of the fluid (air) filled within the bladder (Xiang et al. 2016) and the hyperelastic nature of the bladder.

Several researchers have developed compact and efficient designs of the PMA. Kothera et al. (Kothera et al. 2009) aimed to present the experimental characterization of McKibben muscles of varying lengths and diameters and compared the results obtained using a mathematical formulation of the muscle. A muscle of diameter 12.7 mm and

length 203 mm was developed and found to generate a maximum blocked force of 60 N and maximum contraction of 4.43% at an actuation pressure of 4 bar. The improved mathematical model given by Kothera et al. could predict the muscle's static behaviour more accurately. Hocking et al. (Hocking and Wereley 2012) developed a miniature pneumatic muscle for robotics and Aerospace applications. They designed, fabricated, and experimentally characterized a miniature-sized pneumatic muscle actuator with a mean diameter of 4 mm and a length of 40 mm. This small muscle showed to achieve a blocked force of 140 N and a maximum contraction ratio of 8% at 5.5 bar. They also presented an improved version of the force block model and found it to predict the behaviour of the miniature PMA with reasonable accuracy.

A study on miniature PMAs was also conducted by De et al. (de Volder et al. 2011), who developed a control strategy for accurately positioning their developed PMA and compared the results with a model simulation. The developed actuator had a diameter of 1.5 mm and length of 22 mm, which achieved 15% contraction and 6 N of blocked force at 10 bar pressure. Vocke et al. (Vocke et al. 2012) designed and tested a small-scale pneumatic muscle for micro-air vehicle (MAV) applications. They also compared PMA and conventional electric servo actuators for MAV applications. Koizumi et al. (Koizumi et al. 2018) developed a soft actuator by braiding several McKibben muscles together. The study showed an increase of up to 37% in the contraction percentage. The main drawback of the multi-braided actuator is its decreased contraction force (by almost 10%). Oliver et al. (Oliver-Salazar et al. 2017) developed and characterized a braided pneumatic muscle and used it to actuate a four-degree-of-freedom mechatronic finger. The study involved the fabrication of three muscle lengths (60 mm, 100 mm, and 140 mm) with a constant diameter of 6 mm, which were tested up to a pressure of 4 bar and a payload of 10 kg. The author reported a life of 260000 cycles with 14% contraction per cycle, after which perforation of the silicon bladder was observed. Chakravarthy et al. (Chakravarthy et al. 2014) developed a small braided pneumatic muscle of 1.2 mm diameter to actuate an endoscopic surgical tool. The muscle was experimentally characterized and showed a contraction percentage and blocked force of 18% and 4 N at 8 bars, respectively.

Meller et al. (Meller et al. 2014) experimentally analyzed the energy conversion capability of the McKibben muscle. They found that the inelastic bladder improved the performance of the muscle but resulted in an increase in hysteresis error. The authors reported a higher efficiency in traditional latex bladders when these were actuated at higher actuation pressures and a stroke closer to the initial unactuated length of the muscle. The muscles showed greater than 60% efficiency when actuated at 5.2 bar in one cycle. They also reported a greater than 80% efficiency if the stroke range was limited. Ball et al. (Ball and Garcia 2016a) presented a mathematical model and experimental validation to explain the effect of pre-strain and bladder thickness on the behaviour of the pneumatic muscle. The authors stated that modelling the bladder as a thin-walled tube provided a better fit for experimental results on the wall thickness. They also reported that a thick-walled bladder model was required to explain pre-strain effects better. Sangian et al. (Sangian et al. 2015) developed a cost-effective hydraulic muscle and studied its performance. They investigated the effect of actuator length on reaction time and isotonic strain and determined that muscles with shorter lengths responded faster owing to their reduced bladder volume. They also found the stiffness of the bladder influenced the increase in maximum strain with increasing pressure. Pillsbury et al. (Pillsbury et al. 2015) investigated the influence of bladder thickness on the static actuation performance of miniature pneumatic muscles. According to their findings, increasing bladder thickness reduced blocked force and muscular contraction while widening the pressure deadband. Wang et al. (Wang et al. 2015) developed a mathematical model based on Gaylord's formulation for the McKibben muscle to evaluate the contraction and the force generated by the muscle. Coyle et al. (Coyle et al. 2018) reviewed the actuation, materials selection, and design of soft robots. Several soft viscoelastic materials were used and compared. They concluded that stiffer materials had higher energy densities, but were less compliant. Wakimoto et al. (Wakimoto et al. 2011) created a flexible actuator by combining smaller McKibben muscles. They also compared the experimental and results obtained from a finite element model. Gordon et al. (Gordon et al. 2006) created an ankle-foot orthosis (AFO) that used a pneumatic muscle actuator. The study also examined the performance when two muscles were used to activate the AFO. The dual muscle arrangement showed greater plantar flexion but shorter muscle length and decreased force. Tondu et al.

(Tondu et al. 2016) built a robot arm with seven degrees of freedom operated by pneumatic muscle actuators. The study demonstrated the compliant nature of the pneumatic muscles, which gave a soft touch to the robot arm, but at the same time introduced hysteresis error in the motion of the arm.

The pneumatic muscle actuator is antagonistic in nature, which results in its inability to apply force in the extension stroke. This characteristic of the PMA poses difficulty when used to actuate a single degree of freedom (DOF) joint in both directions. Several researchers (Ariga et al. 2012; Das et al. 2016; Robinson et al. 2014; Ulutas et al. 2008) used a pair of muscles in a series to actuate a single rotary joint, as shown in Fig 2.9. This series arrangement of muscles, known as an agonistic pair, allows countering the muscle's antagonistic nature. The agonistic configuration depicted in Fig 2.9 uses the second muscle to extend the first muscle when the air from the first muscle is released. This agonistic arrangement allows the soft-compliant muscle to be used to actuate robots and exoskeletons with ease but results in a pricier system.

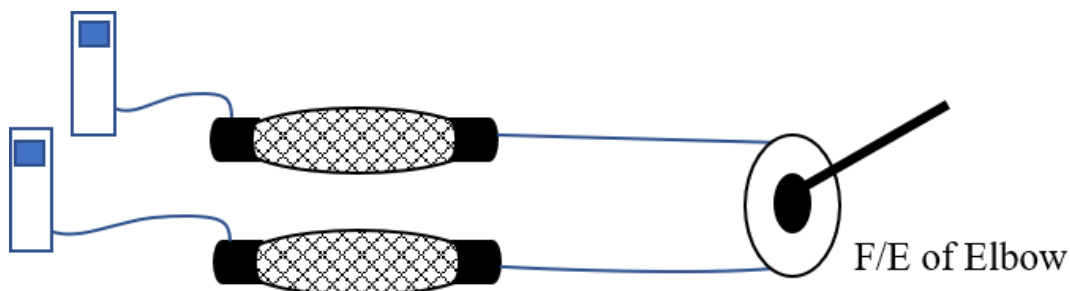


Fig 2.9: Pair of muscles used to counter the antagonistic nature of PMAs

The literature is seen to focus on miniature pneumatic muscles for micro-actuation applications. As per the literature, these miniature pneumatic muscles demonstrate a lower level of contraction percentage and blocked force. In larger applications such as assistive exoskeletons, the miniature muscle failed to achieve the required contraction percentage and load handling capability. The bladder and braided sleeve configuration (size and material) influence the behaviour of the pneumatic muscle. As the bladder occupies a large volume percentage of the PMA, the material and geometric properties greatly influence its behaviour (Ball and Garcia 2016b; Hocking and Wereley 2012; Kothera et al. 2009; Pillsbury et al. 2015). The other drawback of the existing pneumatic muscles is the lack of flexibility and difficulty in assembly/disassembly, which

significantly affects the experimentation with new bladder and braided sleeve materials and the maintenance process. Several researchers have attempted to ease the process of assembly of the PMA. Using metal end-fittings increases the weight of the overall muscle and the risk of damaging the delicate bladder. This research aimed at solving the drawbacks of existing PMAs by presenting a novel end-fitting arrangement that is easy to assemble and maintain.

A mathematical model can optimize the process of finding the right size and material of the bladder and braided sleeve, which suits the intended application (e.g., upper limb exoskeleton). The PMA is a soft actuator that uses a hyperelastic bladder. The hyperelastic bladder posed challenges in modelling it mathematically. The literature revealed several researchers who attempted to model the PMA using techniques such as energy or force balance (Caldwell et al. 2000; Ferraresi et al. 2001; Gaylord 1958; Hal F Schulte 1961; Kothera et al. 2009; Tondu and Lopez 2000; Tsagarakis and Caldwell 2003). These models were later improved by considering additional factors, such as the effect of the braided sleeve (e.g., friction between braids) and bladder (e.g., Hyperelastic nature) on the force or contraction developed by the PMA (Caldwell et al. 2000; Ferraresi et al. 2001; Hal F Schulte 1961; Kothera et al. 2009; Tondu and Lopez 2000; Tsagarakis and Caldwell 2003). In this thesis, three mathematical models are presented and compared to find a model that closely resembles the behaviour of the developed PMA. A summary of various PMAs described in the literature is compiled in a tabular format in annexure A.

2.5 Summary and Motivation

Several end-effector, exoskeleton, and cable-driven robotic assistive devices are presented in the literature review. End-effector-type devices are observed to be easily adjustable due to a single point of contact. The single contact point of end-effector-type devices does not support the entire arm and limits the angular feedback at the joints (Rasedul Islam 2017). Cable drives such as NeReBot are lightweight, low-cost, and simple to maintain. Still, a significant drawback of the cable drive is its ability only to pull but not push, thus limiting its function to one direction (Sicuri et al. 2014).

The actuators used by most researchers are either electric, pneumatic, or hydraulic. Two main parameters that are considered while selecting an actuator for rehabilitation application include compliance, ease of control, safety, and power-to-weight ratio. Most of the previous research shows the use of electric motors as they offer excellent controllability, but their heavy weight is a significant drawback. Hydraulic actuators provide an outstanding power-to-weight ratio, but accidental fluid leakage is of substantial concern in medical applications. On the other hand, Pneumatics provided an excellent power-to-weight ratio and has no risk of medical contamination, but inaccuracies have been projected as a problem.

The ARMin has a unique method of teaching or Mobilization therapy, which involves a lead through programming of the exoskeleton. Mobilization therapy enables the device to be programmed quickly and easily by therapists. Like most other research, the ARMin also used the typical pronation/supination mechanism with the patient's hand made to grasp a handle, thus hindering hand and finger freedom during therapy. Activities of daily living (ADLs), such as picking objects requires the hand and fingers to be kept free to function independently of the assistive structure. Kousidou et al. also presented a unique method of teaching the exoskeleton the required exercises using protocols selected and sequenced by the therapist.

The above discussions based on the literature led to certain conclusions. Firstly the pneumatic actuator, especially the pneumatic muscle actuator (PMA), would best suit medical assistive applications. Secondly, devices for physiotherapy applications require a lightweight and modular structure to be a universal fit for most Indian anthropometric dimensions. Thirdly, an innovative mechanism has to be designed to perform the pronation/supination of the elbow joint, while keeping the patient's hand and fingers free for other therapy exercises (strength training or ADLs). As the cable mechanism and pneumatic muscles suffered from being antagonistic, a suitable mechanism needs to be developed to use them in the exoskeleton application efficiently. The PMA and cable mechanisms have a considerable advantage in the rehabilitation application as they offer compliance and make the overall system lightweight, less bulky, and safer for patients. The design needs to be made user-friendly and safe. Therefore, it is necessary to make the system easy to be programmed and operated by physiotherapists

with little training (shallow learning curve). The system should also be autonomous, with safety features inbuilt to facilitate the unsupervised performance of repetitive therapy.

The motivation for this work is the current healthcare situation in developing countries like India, which suffers from a shortage of medical facilities to cater to the mass population. Stroke rehabilitation, physiotherapy, and other forms of therapy involve a personal approach. The expert has to administer such treatment methods directly to the patient by manually moving the limbs through the required trajectory. This disparity between the number of patients and therapists led to many stroke patients ending up disabled as they did not receive timely and quality care. The literature indicates that physiotherapy should be administered to the patient no sooner than the stroke patient is medically stabilized. Another problem with the current therapy is neglecting the upper extremity treatment while spending most of the time on lower limb therapy. Thus, many stroke patients who have undergone therapy have regained lower extremity function but end up disabled due to delays in treating the upper extremity. Lowering the cost of exoskeletons was also a factor to be considered, especially in developing countries. Due to the high cost of development combined with a relatively low benefit for patients and clinics, the price/performance ratio is rather dissatisfactory (Qian and Bi 2015). This research aims at designing a compliant, easy-to-use, safe, and modular robot assistive rehabilitation device for physiotherapy applications.

2.6 Objectives

The following are the objectives of this research work:

1. Design and fabrication of an appropriate actuator for the rehabilitation exoskeleton.
2. To design a compliant assistive robotic device and an optimal system for the physiotherapy application.
3. To demonstrate the realization of the developed exoskeleton using the newly developed actuator.

2.7 Desired Attributes

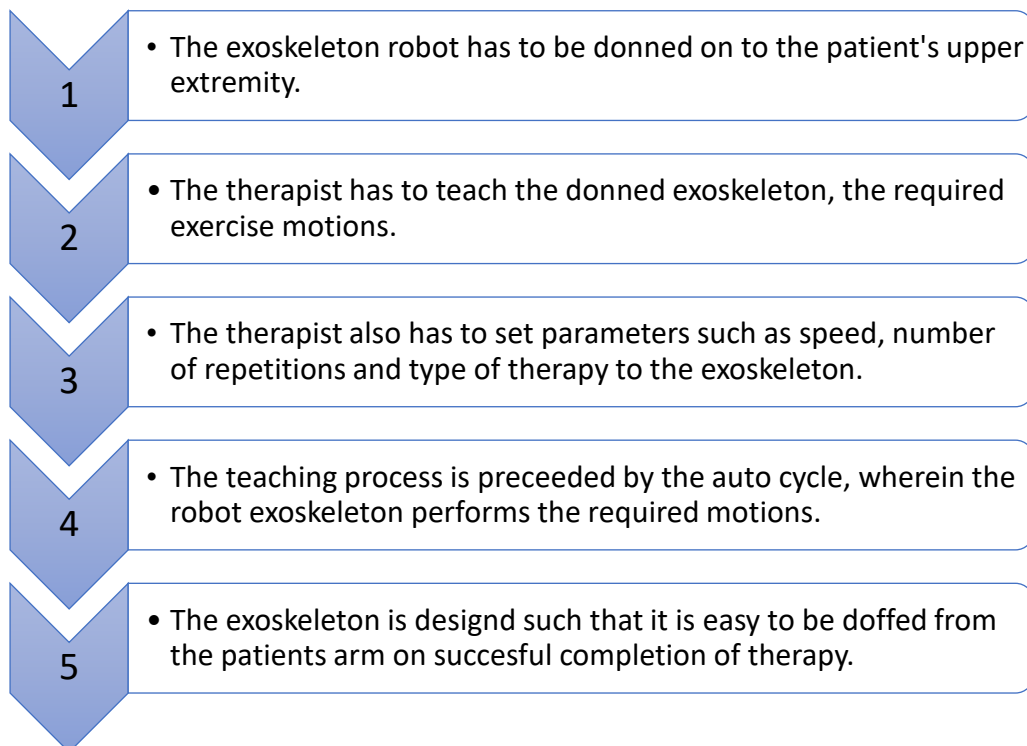
The following are listed the desired attributes of this research work:

1. The first step is to decide the number of DOF through literature review and in consultation with physiotherapists.
2. An important step in the design involves selection of an appropriate actuator to make the device compliant, lightweight, and safe for a medically sterile environment.
3. The actuator suitable for the exoskeleton application needed to be mathematically modelled, developed and characterization.
4. The next step after the actuator is developed involves testing the performance of an identical commercially available actuator and comparing its performance with the developed actuator.
5. This research also requires the development of a feedback system for the exoskeleton's angle and position to make the system real-time.
6. A control strategy is needed for easy teaching and real-time system control by incorporating the following parameters that define the physiotherapy process.
 - a. Sensor feedback
 - b. Maximum limits of range of motion (ROM) set by the therapist
 - c. Ability to adjust therapy routine
 - d. Ability to stop the system in case of an emergency
7. The final step involves testing the developed actuator on the exoskeleton for various degrees of freedom.

3 METHODOLOGY

As seen in the previous sections, physiotherapy has to be given by the therapist directly to the patient by manually moving the limbs through the required motion trajectories. The manual process is tedious, and repeating such motions is very cumbersome. The literature enumerated in chapter 2 shows a significant disparity between the number of patients and trained physical therapists, thus leading to several patients living the rest of their lives either paralyzed or with motion defects. The other problem a larger developing population (e.g., India) faces is the prioritization in treating the lower limb while the upper limb remains non-functional or with deformities. This research aims to develop a compliant, lightweight, modular, and autonomous upper extremity exoskeleton robot that is used alongside physiotherapists to impart physical therapy to the elbow joint. The flowchart in Table 3.1 gives an overall picture of the procedure of working of the developed exoskeleton robot developed:

Table 3.1: Flowchart of the training and usage of the proposed robot exoskeleton for two degrees of freedom therapy of the elbow joint.



The upper extremity comprises the upper arm, the forearm, and the hand proper. The elbow exoskeleton is mounted on the patient's upper arm and forearm to move the elbow joint through its two degrees of freedom (F/E and P/S). The exoskeleton is designed to be modular to fit most Indian upper extremities easily and makes the process of donning and doffing quick and efficient. Once the exoskeleton is securely fixed to the patient's arm, the next step involves the physiotherapist teaching the exoskeleton the required motion exercises. The exoskeleton is designed to move the elbow joint through two degrees of freedom. Therefore, the exoskeleton can move the elbow joint through individual motion trajectories (F/E or P/S) or a combined motion (F/E, P/S, F/E...) based on the patient's requirement. The physiotherapist trains the exoskeleton in the motion trajectory for various repetitive or functional exercises.

The system records the trained motion exercises and imparts the repetitive motion to the patient's paretic or injured elbow joint when put in auto mode. The designed system also allows the physiotherapist to set parameters such as speed, number of repetitions, and the type of therapy (individual or combined motion therapy) based on the patient's requirements. The controller is then run autonomously through the trained motion trajectory, considering the various set parameters and feedback from multiple sensors. The exoskeleton system's successful working is achieved by many tests and design improvements, whose methodology is discussed in Table 3.2.

Table 3.2: Methodology

Methodology	The physiotherapy motions to be given to the patient by the exoskeleton are decided in consultation with physiotherapists.
	The appropriate number of DOF are decided based on designs suggested in the literature and suggestions received from the physiotherapist.
	A exoskeleton support structure for the upper extremity is designed.
	Once all the design parameters are decided the exoskeleton is fabricated.
	The rehabilitation application required a lightweight, compliant, and safe actuator to actuate the exoskeleton.
	The pneumatic muscle actuator is developed and characterized to suite the exoskeleton application.
	The correct mounting position of the actuators on the exoskeleton is done to ensure effecient force transfer and mechanical advantage.
	The exoskeleton motion is tested using the developed muscle actuators, to study the range of motion, and payload handling capabilities.
	Based on the preliminary testing the exoskeleton structure is modified in order to increase range of motion, safety, and actuator efficiency.
	The controller board hardware and software are designed to increse safety, and usability of the designed exoskeleton system.
	Once the complete system (Exoskeleton + Actuator + Controller + Software) becomes operational it is tested to ensure its efficiency and safety for the intended rehabilitation application.
The test on the exoskeleton are analysed and presented.	

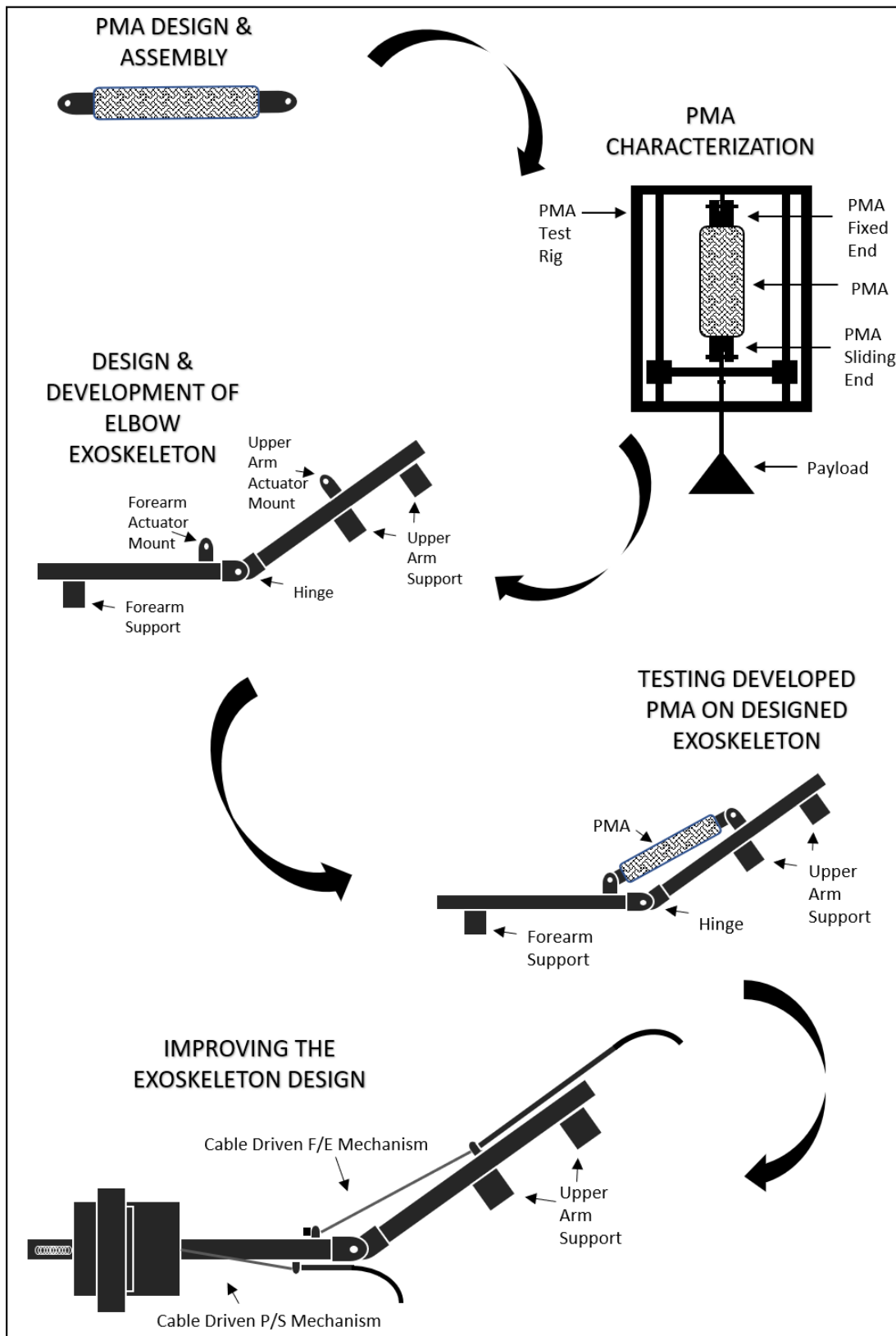


Fig 3.1: Flow diagram of the procedure used in the development of the exoskeleton

The study of the literature gives an understanding of the need for an upper extremity exoskeleton. The consultation with physiotherapists helped to decide the type of exercises needed to be given to the upper extremity. A device that could provide a repetitive motion to the upper limb, more specifically the elbow joint, through its two degrees of freedom, with minimal supervision, is considered the need of the hour. The two degrees of freedom of the elbow joint include flexion/extension (F/E) and pronation/supination (P/S). As the elbow joint is being designed for medical rehabilitation, it must be lightweight and compliant. The compliance directly depends on the actuation mechanism; therefore, a correct actuator with good compliance, positional accuracy, and a high power-to-weight ratio is required. As the exoskeleton is designed for the Indian demographic, it has to be made with universal dimensions to fit most upper extremities. The size of the frame also contributes to the structure's weight; therefore, it is built using modular aluminium t-slot sections. The modular t-slots make the exoskeleton easy to adjust to accommodate various sizes of arms and forearms with minimal adjustment to the setup. Once the design is finalized, the exoskeleton is fabricated. The first version of the exoskeleton is fabricated with only flexion/extension elbow motion capability.

The actuator is an essential component of the exoskeleton system as it contributes to its weight, range of motion, payload capacity, and device safety. The exoskeleton being directly mounted to the upper extremity of the user requires a compact, lightweight, and compliant actuator which is safe to be used in a medically sterile environment. The literature has shown that the pneumatic muscle actuator is lightweight and inherently compliant, and using air as the actuation media makes it very safe for rehabilitation applications. Therefore, the pneumatic muscle (PMA) forms the best choice of actuator for the elbow exoskeleton.

Initially, a set of commercially available pneumatic muscles were procured and tested to analyze their feasibility in actuating the elbow exoskeleton. The results show that the commercially available muscle is designed for a length much greater than its actuation length (a percentage of bladder length). The exoskeleton, a space-constrained application, requires a muscle of compact size with a good contraction percentage. Commercial muscles of shorter lengths are available, but as the contraction percentage

is dependent on the length of the bladder, they produce a minimal contraction. The smaller contraction capacity of shorter commercial muscles makes them inadequate for the exoskeleton application. Another major problem of commercial muscles is their long lead time for procurement and maintenance, as they are manufactured outside India. All these drawbacks of the commercial muscle led to the requirement of a new muscle design that can be easily fabricated in-house using raw materials and manufacturing processes available locally.

The pneumatic muscle actuator mainly consists of three components: the elastic bladder, braided sleeve, and the end-fitting clamp assembly. The type of bladder and braided sleeve used in the construction of the muscle plays an essential role in the output behavior achieved by the muscle. Therefore, making the muscle construction modular is crucial to facilitate the easy assembly and disassembly of the bladder and braided sleeve. The modular nature of the designed end-fittings used to construct the muscle also makes the process of maintenance easy and quick. The muscle is designed with a novel set of end-fittings and clamps, which facilitate the easy assembly and disassembly of the bladder-braided sleeve pair. Unlike the commercial muscles, the developed muscles have a compact set of end-fittings wherein the mounting and pneumatic arrangement are combined into a single design, thus making the muscle compact in length. The clamps and the end-fittings are designed to secure the assembled bladder-braided sleeve from dislodging during operation. The clamps were designed to securely maintain the bladder and braided sleeve position over the two end fittings, even at high pressures and loading conditions. The novel end-fittings and clamps thus made the developed muscle modular and compact in length compared with the commercial muscle previously used.

As the muscle is designed to actuate the medical exoskeleton, it had to be subjected to a large number of tests to ensure its safety and performance during operation. The muscle was characterized for parameters such as blocked force, deflection/contraction, and endurance. The characterization process involved the construction of two test rigs, one for analyzing muscle displacement and the other for blocked force.

The displacement setup had a sliding arm fixed to the free/contracting end of the muscle actuator. A laser displacement sensor is used to measure the muscle displacement with

variation in actuation pressure. On the other hand, the force test rig lacked the sliding mechanism and used a load cell instead of the laser displacement sensor. The contracting end of the muscle is attached to the load cell to measure the force developed by the muscle with an increase in actuation pressure. The displacement test rig is also used for the endurance test wherein the muscle to be tested is mounted while a load equivalent to the maximum working load is hung to its free end. The endurance test involves a controller to give cyclical air input to the muscle, which is alternatively contracted and extended, and the number of successful cycles the muscle endured is recorded.

The pneumatic muscle having a flexible bladder and an enclosing braided sleeve is affected by the material and size of the bladder and braided sleeve. The muscle output was also affected by the initial angle of the braided sleeve. As the pneumatic muscle has two separate components, the bladder, and braided sleeve, in contact with each other, it amounts to friction between them and between the individual braids of the braided sleeve, which also affects the contraction and force produced by the muscle. All these factors are studied both through simulation and experimentation. Three mathematical models of the pneumatic muscle are analyzed, simulated, and compared to understand the various inputs and external parameters involved in the muscle's performance and find a model that closely represents the developed muscle. The results obtained from the simulation are compared with the results obtained experimentally.

Several muscles are constructed with varying dimensions and materials of bladders and braided sleeves. These muscles with varying characteristics are tested for force and deflection for various actuation pressures and loading conditions. The commercial muscle is also tested for force and deflection, and its results are compared with developed muscles of identical dimensional characteristics.

The elbow exoskeleton is designed with actuator mounts in order to attach the muscle actuators to drive the exoskeleton. The position of these actuator mounts plays an essential role in achieving a good amount of angular deflection and force transfer from the developed muscle. Though placing the mounts closer to the elbow joint or the fulcrum of the hinge would amount to greater flexion with smaller muscle contraction, this would also result in an increase in the load the muscle should carry to achieve the

motion. Therefore, the free body diagram of the forearm gives the correct position of the mounts to achieve the best mechanical advantage for the muscles to produce greater flexion motion efficiently. After the correct position of the mounts is determined, the exoskeleton is fabricated using the lightweight modular aluminium t-slots. The most critical component of the elbow exoskeleton is the flexion hinge. The hinge is designed with two mechanisms the first to counter the antagonistic nature of the pneumatic muscle actuator, and another is the angle-sensing mechanism that records the elbow flexion in real time.

The muscle characterization is performed to determine an appropriate muscle that suits the exoskeleton application. This includes good positional accuracy, compliance, contraction, and payload capacity. The selected muscle is used on the designed elbow exoskeleton to test it through flexion and extension motion. The angular range of motion and load-handling capability of the elbow exoskeleton is tested when actuated with the selected muscle actuator for various values of actuation pressure.

In continuation of the discussion in the earlier section, the preliminary tests of the muscle have been carried out with the muscle directly attached to the exoskeleton using the actuator mounts. The direct-mounted arrangement had a few drawbacks, such as a lower range of flexion, difficulty in adding pronation/supination capability, and this arrangement also made the exoskeleton bulky. As a result, an improved exoskeleton system was developed. The new exoskeleton system actuated the exoskeleton using pneumatic muscles through an indirect drive mechanism. The system used cables to transmit the force generated by the muscles to the elbow joint via the exoskeleton. The indirect actuator system significantly improved the muscle's performance and the exoskeleton's range of motion. It reduced the overall size and weight of the exoskeleton attached to the user's upper limb and enhanced the system's safety while adding the additional functionality of pronation and supination. The exoskeleton structure of the indirect system was almost similar to the directly actuated exoskeleton, with a few other features such as the pronation/supination mechanism, an improved hinge design, and a forearm length adjustment mechanism.

4 DEVELOPMENT OF PNEUMATIC MUSCLE ACTUATOR

The assistive exoskeleton for rehabilitation applications demands a lightweight, safe, and compliant actuator. The literature shows that pneumatic muscle actuators (PMA) provide the perfect balance of power-to-weight ratio and compliance. As the DC motor offers good controllability, it has been used extensively in exoskeleton applications in the past (Gopura et al. 2016). The free body diagram (FBD) shown in Fig 4.1 and the calculation proved the downside of using the DC motor as an actuator in the designed exoskeleton.

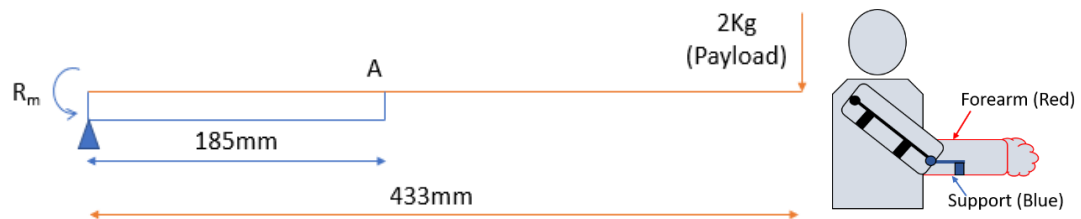


Fig 4.1: FBD to calculate motor torque for forearm-exoskeleton pair

The red-coloured beam represents the patient's forearm with a self-weight represented by a uniformly distributed load (UDL) of 0.0049 N/mm (Chakrabarti Debkumar 1999; Plagenhoef et al. 1983). In contrast, the blue-coloured beam represents the forearm exoskeleton support with a self-weight represented by a UDL of 0.0098 N/mm. The free-body diagram shown in Fig 4.2 is drawn to find the reaction R_A representing the force exerted by the patient's forearm on the exoskeleton support.

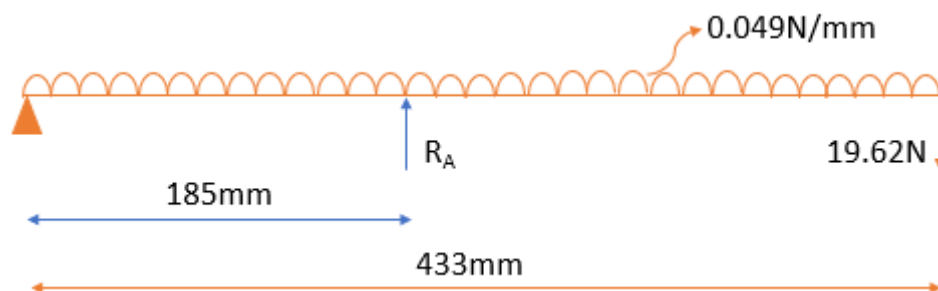


Fig 4.2: FBD of the forearm

Further simplifying the FBD given in Fig 4.2 gives FBD as shown in Fig 4.3:

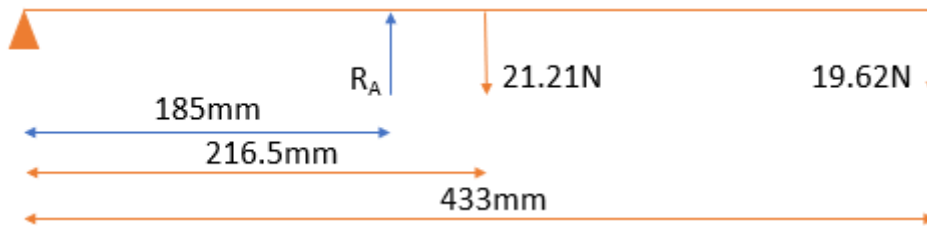


Fig 4.3: Simplified FBD of the forearm

Solving for R_A shown in Fig 4.3 is given by the following:

$$R_A \times 185 = 21.21 \times 216.5 + 19.62 \times 433$$

Therefore, $R_A = 70.74 \text{ N}$

Now, solving for the motor torque R_m in the FBD of the forearm exoskeleton support, as shown in Fig 4.4.

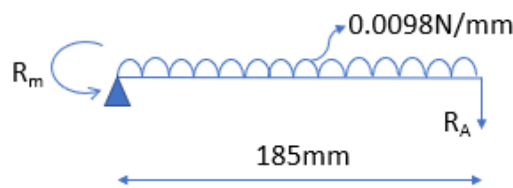


Fig 4.4: FBD of exoskeleton support for the forearm

Where R_m is the required motor torque to lift the forearm

Further simplification of FBD in Fig 4.4 gives FBD in Fig 4.5,

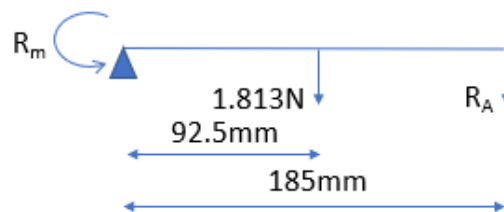


Fig 4.5: Simplified FBD of exoskeleton support for the forearm

Solving for R_m in the FBD shown in Fig 4.5:

$$R_m = 1.813 \times 92.5 + 70.74 \times 185$$

Thus, the required motor torque $R_m = 13254.60 \text{ Nmm}$

A commercially available “worm-gear stepper motor” generating a torque of 14710 Nmm could have been selected based on the required torque calculations of 13254 Nmm. The reason for not using the stepper motor is simplified in two points. Firstly, as the torque necessary increases, so does its weight which for the worm-gear stepper motor is 2.10 Kg. The second point of concern is the volume occupied by the worm-gear stepper motor, which is approximately 324458 mm³, which would result in a bulky exoskeleton support. An important feature required in an actuator for this application is compliance, defined as the inverse of stiffness. Compliance is the property of the PMA that negates the force the actuator applies on the patient, especially when the patient resists its motion. The electric motor being a non-compliant actuator has the tendency to harm the patient who is resisting its motion, therefore making it unfavourable for the exoskeleton application. Several actuators, such as pneumatic and hydraulic actuators (motors or cylinders), could have been considered to actuate the exoskeleton. Hydraulic actuators are known to have a higher power-to-weight ratio, but as it uses hydraulic oil, it poses a higher risk of contaminating the sterile medical environment. Hydraulics also requires a large power pack, therefore making the system bulky. Inherently compliant pneumatic actuators, on the other hand, make use of compressed air, thus making them safe in sterile environments.

4.1 Design and Fabrication of the PMA

The basic structure of the PMA designed in this work consists of three main components, the flexible bladder, the braided sleeve, and the end fittings. The choice of the bladder and braided sleeve significantly influences the behaviour (force and contraction) of the PMA. An application that manipulates large loads (e.g., 5 kg payload to actuate elbow exoskeleton) requires a thicker bladder with a bigger diameter (Ball and Garcia 2016a). The bladder's size and the braided sleeve's initial braid angle are important parameters in determining the maximum contraction percentage achieved by the PMA (Tondu and Lopez 2000). Thus, these parameters allow the user to select and change the same based on the application's requirements. The ease of assembly and disassembly demands the PMA's design to be modular, thus also easing the process of maintenance. In this work, a novel set of end-fittings and clamps, which allow easy assembly and disassembly of the muscle, were designed and incorporated.

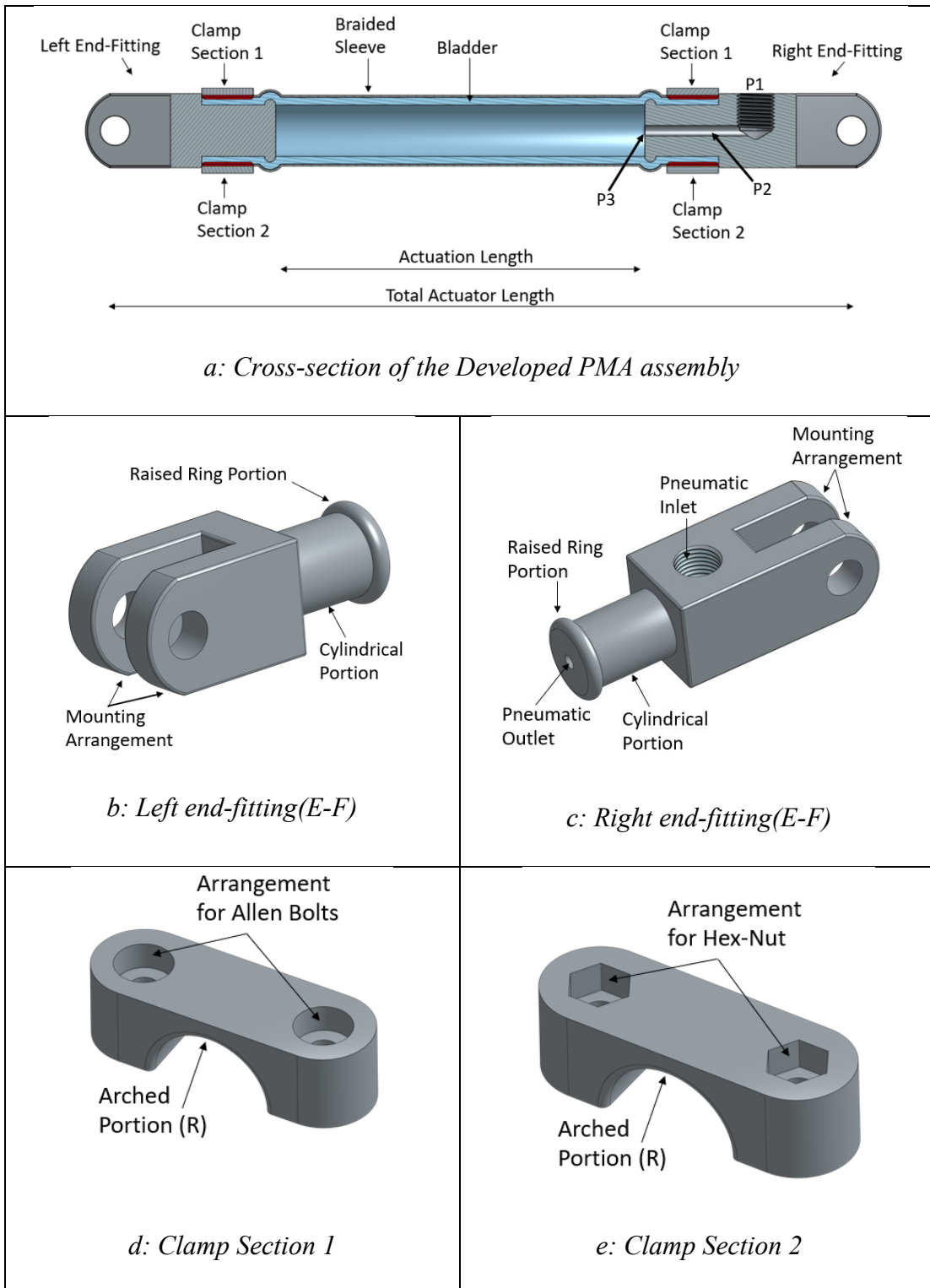
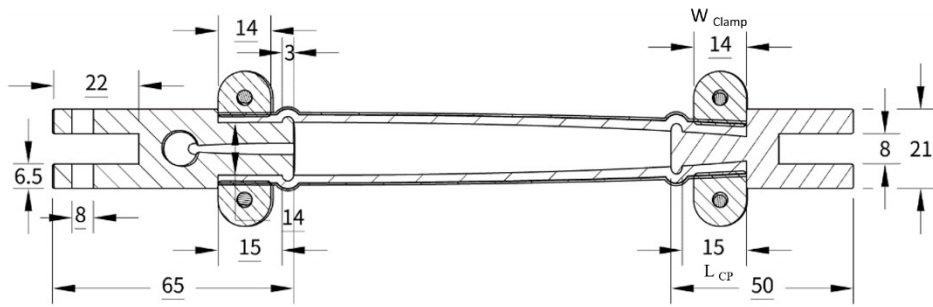
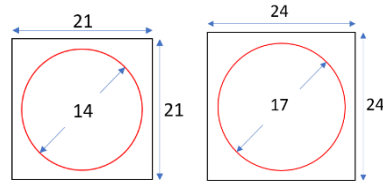


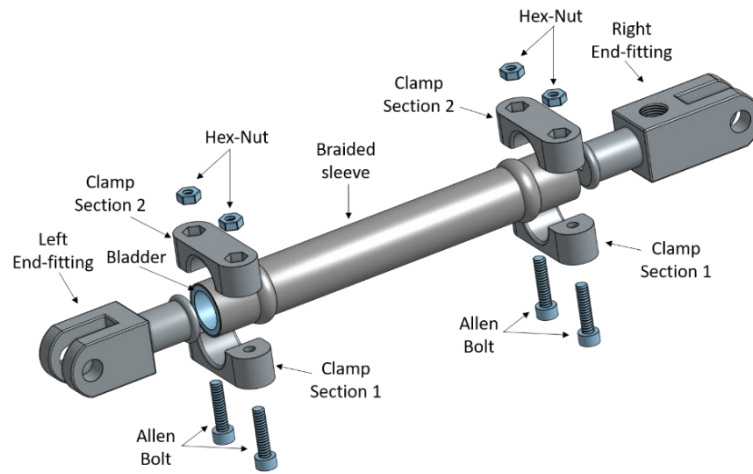
Fig 4.6: The Developed PMA with the Novel End-Fittings and Clamps



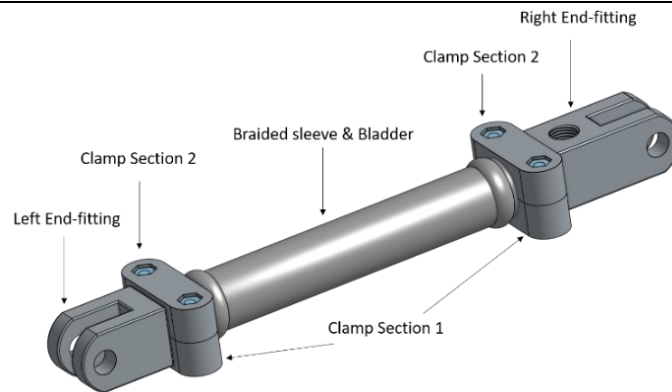
a) 10x14 PMA with dimensions



b) Dimension of cylindrical portion w.r.t E-F body of (10x14 vs. 12x17)



c) Exploded view of PMA



d) Assembled view of PMA

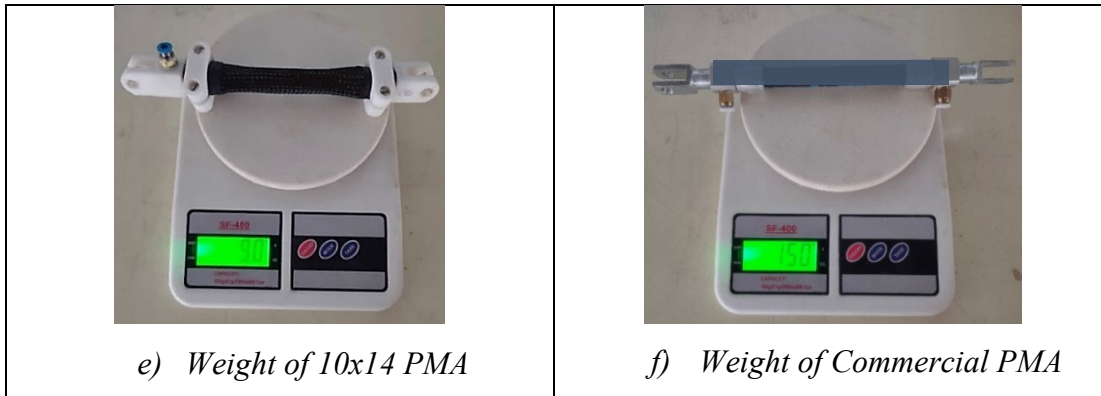


Fig 4.7: 10x14 PMA of weight 90 gms vs the commercial PMA of 150 gms

The PMA design proposed in the current work consists of two novel end-fittings, the left end-fitting and the right end-fitting. Fig 4.6a and 4.7a clearly show that the left end-fitting is shorter and lacks the pneumatic arrangement compared to the right end-fitting. The three primary functions of the end-fitting include; allowing compressed air flow into the PMA, maintaining the air-tight seal, and transferring the force generated by the PMA to the point of actuation in the application. The individual left and right end-fittings are shown in Fig 4.6b and Fig 4.6c, and these show similar design features, including the cylindrical portion, the raised ring portion, and the mounting arrangement. The end-fittings are attached to the two ends of the bladder-braided sleeve pair to form the bladder's air-tight chamber, as shown in Fig 4.6a. The cylindrical portion in all the constructed muscles has a length (L_{CP}) of 15 mm, as shown in 4.7a and varies only in diameter depending on the size of the bladder used (e.g. diameter of 14 mm for the 10x14 muscle). Having the cylindrical portion's diameter equal to the bladder's outer diameter ensures an air-tight fit. Fig 4.7b shows the relation between the diameter of the cylindrical portion and the end-fitting body for the 10x14 and 12x17 muscles. The experimental trials showed that the optimum dimensions of the diameter of the cylindrical section with respect to that of the end effector (E-F) body was achieved when the difference between the two was maintained at 7mm as shown in Fig 4.7b.

The assembled bladder encloses the raised ring and cylindrical portion of the two end fittings. As the bladder envelops the cylindrical portion, the cylindrical portion is made of a diameter slightly larger (3 mm) than the bladder's inner diameter, which ensures that the bladder remains tightly in place and helps form an air-tight seal. The clamps are fixed to the end-fittings at the cylindrical portion keeping the bladder-braided sleeve

pair securely within the PMA. As shown in the Fig 4.7a the length of the cylindrical portion ($L_{CP} = 15\text{mm}$) is slightly larger than the clamp's width ($W_{Clamp} = 14\text{mm}$) to allow the clamps to fit over the end-fittings correctly. The raised ring portion of the end-fittings is another integral part of the clamping assembly. The raised ring portion is designed to have a slightly larger diameter than the arch diameter ($R+R$) formed by the assembled clamp sections 1 and 2 (Fig 4.6d and Fig 4.6e), thus preventing the clamps from slipping off the cylindrical portion of the end-fittings. The significance of the cylindrical and raised ring portion is further highlighted in the clamp design discussion in the following paragraphs. Another common feature of both the end-fittings is the mounting arrangement consisting of two legs with through holes to be attached via a pin connector. The PMA is attached to the mounting bracket (e.g., attached to the exoskeleton) at the gap between the two mounting legs of the end-fittings forming a pin joint with one rotational degree of freedom about the pin axis. This single degree of freedom at the pin joint facilitated an unrestricted actuation of the PMA.

The pneumatic arrangement shown in Fig 4.6c forms the main design difference of the right end-fitting from its left counterpart. The pneumatic arrangement includes a threaded hole (P1 in Fig 4.6a) to attach the pneumatic coupling. The pneumatic coupling connects the PMA to the compressed air supply hose. The compressed air entering the pneumatic coupling is led through a path running axially (P2 in Fig 4.6a) through the cylindrical portion and exiting beyond the raised ring portion (P3 in Fig 4.6a) into the air-tight chamber within the bladder (Fig 4.6a). This novel end-fitting combines the mounting, pneumatic, and bladder fixing arrangement into a single structure, as shown in Fig 4.6c. The provision for connecting the pneumatic coupling at the side face of the end-fitting provides enough room for the mounting arrangement. The second important feature of the novel end-fitting design is the absence of the pneumatic arrangement in the left end-fitting, which reduces the overall length of the PMA without compromising its contraction capability. The maximum contraction percentage achieved by the PMA is observed to be 25-30% (obtained experimentally) of its actuation length (Fig 4.6a & 4.7a). Using a shorter actuation length to accommodate the PMA in a space-constrained application (e.g., exoskeleton) would significantly affect the amount of contraction. This loss of contraction length is seen

mainly in commercial PMAs, which came in standard actuation lengths. A shorter commercial muscle used end-fittings with the pneumatic arrangement at both ends with a shorter actuation length, thus producing a smaller amount of contraction. Unlike most commercial PMAs with the pneumatic arrangement at both ends, the PMA presented in this research has the pneumatic arrangement in only the right end-fitting. This design of having the pneumatic arrangement only at one end significantly reduces the overall length of the PMA without compromising the amount of contraction, which depends on the actuation length, as shown in Table 4.1.

Table 4.1: Comparison of the Length of Developed PMA with the Commercial PMA

Sr. No.	Pneumatic Muscle (PMA)	Actuation Length (mm)	Overall Length of PMA (mm)
1	Commercial PMA	100	260
2	Developed PMA	100	215

The clamps are very crucial elements in the design of the end-fittings. The clamps form an integral part of the end-fittings, which secure the bladder-braided sleeve pair to the cylindrical portion of the end-fitting even at high loads and actuation pressures. The clamps designed in the present work consist of two sections labelled '1' and '2' (Fig 4.6d and Fig 4.6e). The common feature in the design of the clamp sections 1 and 2 is the arch with radius R, which is positioned at the cylindrical portion of the end-fittings over the assembled bladder-braided sleeve pair. The radius R is slightly larger than the end fitting's cylindrical portion to compensate for the thickness added by the enveloping bladder and braided sleeve. The arch radius R is kept marginally smaller than the radius of the raised ring portion of the end-fittings, thus preventing the clamps from slipping off the cylindrical portion of the end-fitting. The two clamp sections, '1' and '2', are positioned diametrically opposite the end fitting's cylindrical portion, thus providing an adequate clamping force that can be increased or decreased with bolts and nuts holding the two sections together securely. The interference fit between the arch portion of the clamps and the raised ring portion of the end-fittings results in a higher clamping force

proportional to the actuation pressure and payload, thus making the PMA design much safer at higher loads. The shape of the counterbore holes is different in the clamp sections 1 and 2, as shown in Fig 4.6d and Fig 4.6e. The clamp section 1 has equally spaced hexagonal-shaped holes on its flat face, which houses the hex-nut. The clamp section 2 has circular-shaped holes on its flat face, allowing the Allen bolt head to fit flush with the clamp face. These Allen nuts and bolts are used to secure the clamps and prevent any accidental disassembly of the PMA.

The assembly of the PMA using the novel end-fittings is a quick and straightforward process which is shown in Fig4.7c and d. The first step in the assembly involves inserting the flexible bladder into the braided sleeve. The next step involves attaching the end fittings at either end of the bladder-braided sleeve assembly, which is done by sliding the bladder and sleeve over the raised ring and cylindrical portion of the end fittings. The last step involves fixing the clamps over the assembled bladder-braided sleeve pair at the cylindrical portion of the end fittings. The clamps are then tightened in place using Allen bolts and nuts. Fig 4.6a and 4.7d clearly show the assembled PMA, wherein the cylindrical portion is enclosed by the bladder-braided sleeve pair and sandwiched between the two clamp sections 1 and 2.

The PMA developed in this study is fabricated using commercially available bladders and braided sleeves. Table 4.2 shows the size and properties of the bladder and braided sleeve used in the muscle construction. A commercially available styrene-based thermoplastic elastomer tube is used as the bladder, which has a tensile modulus of 0.84 MPa for bladder sizes of 4x6 (ID = 4mm, OD = 6mm), 6x9, and 12x17 and 0.89MPa for the 10x14 bladder. These modulus values closely match the properties of the skeletal muscle (Ogneva et al. 2010), which makes them more advantageous in comparison to the Silicon-based rubber bladder (“Materials data sources” 1988). A commercial polyethylene terephthalate expandable cable manager having a tensile strength of 416 MPa is used as the braided sleeve. The length of the PMA considered in this study is 100 mm, to facilitate the comparison with an equivalent commercially available PMA used in this study. The comparative analysis between the developed and commercial PMA is given in section 4.2.6. The end fittings and clamps which held the bladder-sleeve assembly are 3D printed using Polylactide (PLA), which is structurally strong,

lightweight, and biodegradable(Farah et al. 2016). The performance of the PMA is studied for various bladder and braided sleeve sizes, as shown in Table 4.2. The photo of the assembled 10x14 PMA and the test rig are shown in Fig 4.7e and f. The total weight of the developed PMA is 90 gms, making it 50% lighter than the commercial muscle.

Table 4.2: Dimensions of bladder and braided sleeve used in the developed PMA

PMA (size IDxOD (both in mm))	Thickness of Bladder Tube(mm)	Tensile strength of the tube MPa*	Tensile Modulus of tube MPa*	Diameter of braided sleeve (mm)
12x17	2.5	4.54	0.84	19.05
10x14	2	7.75	0.89	19.05
6x9	1.5	4.54	0.84	9.53
4x6	1	4.54	0.84	6.35

*(*experimentally determined values)*

4.2 PMA Characterization

The characteristics of the PMA, such as force, deflection, and endurance for various pressures and loading conditions, are studied to establish its use in the intended application, such as the elbow exoskeleton developed in this research. The four developed PMAs, and one commercially available PMA are experimentally tested and presented in this study. The following subsection details the test setup for characterizing the PMA. The force and contraction characteristics study gives an overall understanding of the inverse relationship between the force generated and the amount of contraction produced with muscles of varying diameters. The pressure vs deflection and pressure vs force tests are more specific tests in order to understand the maximum amount of deflection and force achieved by the developed muscle at different operating pressures. These tests also help understand hysteresis and repeatability errors at various pressures in the developed muscle and a commercially available PMA. The tests of

force vs contraction and pressure vs force and deflection are carried out at quasi-static conditions in which the actuation rate is slow to keep the inertial effect of loading negligible.

4.2.1 PMA Test Rig Development for Displacement Measurement

The developed pneumatic muscle is intended to be used for medical rehabilitation applications. Hence, testing and establishing the performance of the PMA before using it on patients is very important. The exoskeleton for rehabilitation of the upper extremity has a maximum load of 5 kg, as reported by earlier researchers (Chakrabarti Debkumar 1999; Plagenhoef et al. 1983). Hence, the maximum load used for testing is restricted to 10 kg, keeping a factor of safety of 2. The characterization involves testing parameters such as force, deflection, and endurance, which requires a simple but modular test rig that facilitates all tests with minor modifications to the test setup (Yashas et al. 2021). Due to their modular nature, aluminium t-slot sections of size 20 mm x 20 mm are used to fabricate the test setup. The setup for experimental testing of PMA is shown in Fig. 4.8. The outer frame consisted of 12 modular sections, forming a cuboid of dimensions 460 x 235 x 150 (H x W x B in mm). The structure's top face has an aluminium section parallel to the breadth, which housed a clamp to mount the pneumatic muscle actuator's fixed end. A Keyence IL300 laser displacement sensor having a repeatability of 30 microns is used to measure PMA deflection and is mounted on the top face of the test setup. The free end of the PMA is attached to a sliding mechanism of the test rig. The sliding mechanism consists of two linear bearings on either side of the structure, which ensures smooth contraction of the pneumatic muscle. The PMA is tested by suspending dead weights on the sliding mechanism of the test rig. These suspended weights exerted the required force on the free end of the PMA.

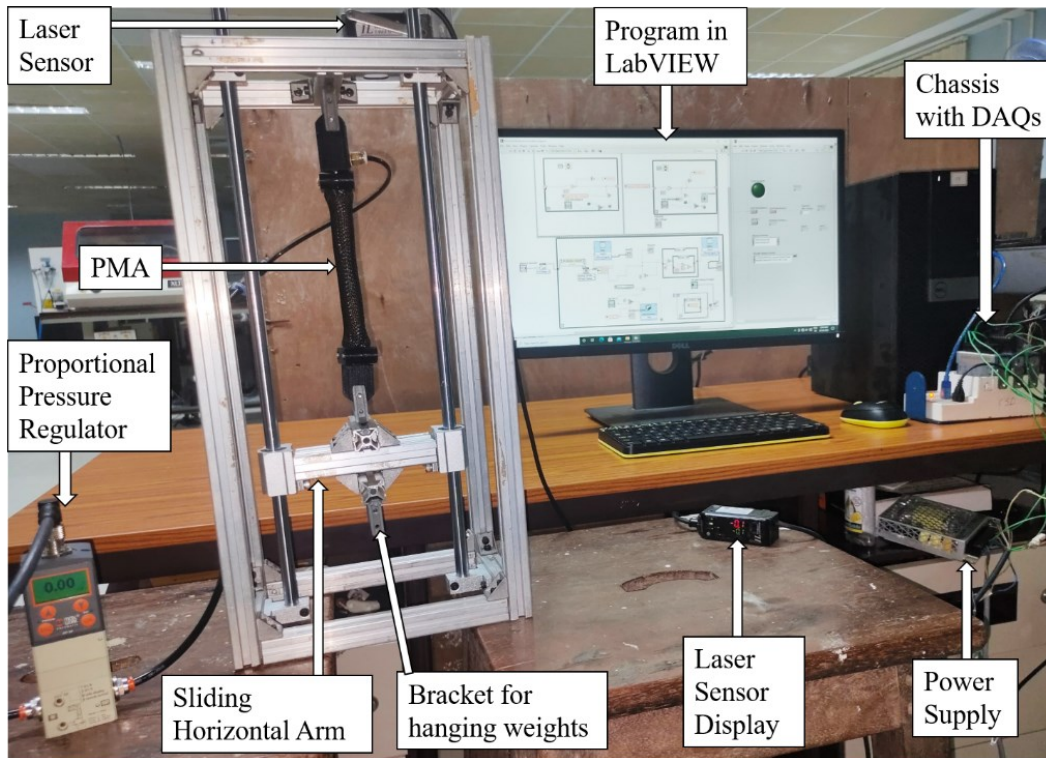


Fig 4.8a: Test Rig for PMA Displacement

The Regtronic $\frac{1}{4}$ (by Metal Works) proportional pressure regulator is an essential part of the test setup that allows the muscle actuator's autonomous actuation. The test setup uses a NI9264 voltage output module (10 V) and a NI9221 analog input module connected to a PC running LabView. The LabView program block diagram for the displacement test setup is shown in Annexure B. The control program runs on the PC that gives an analog voltage signal to the proportional pressure regulator, which is generated by the NI9264. The proportional pressure regulator uses this analog voltage signal to output a proportional pressurized air supply to the pneumatic muscle actuator. The pressurized air causes the pneumatic muscle to contract, thus displacing the horizontal arm of the test setup. This displacement is recorded by the laser displacement sensor, which produces a voltage signal proportional to the displacement value and this is read by the NI9221 analog input module. The voltage value obtained from the NI9221 is converted and stored as displacement or contraction of the PMA with respect to the actuation pressure in the LabVIEW program.

4.2.2 PMA Test Rig Development for Force Measurement

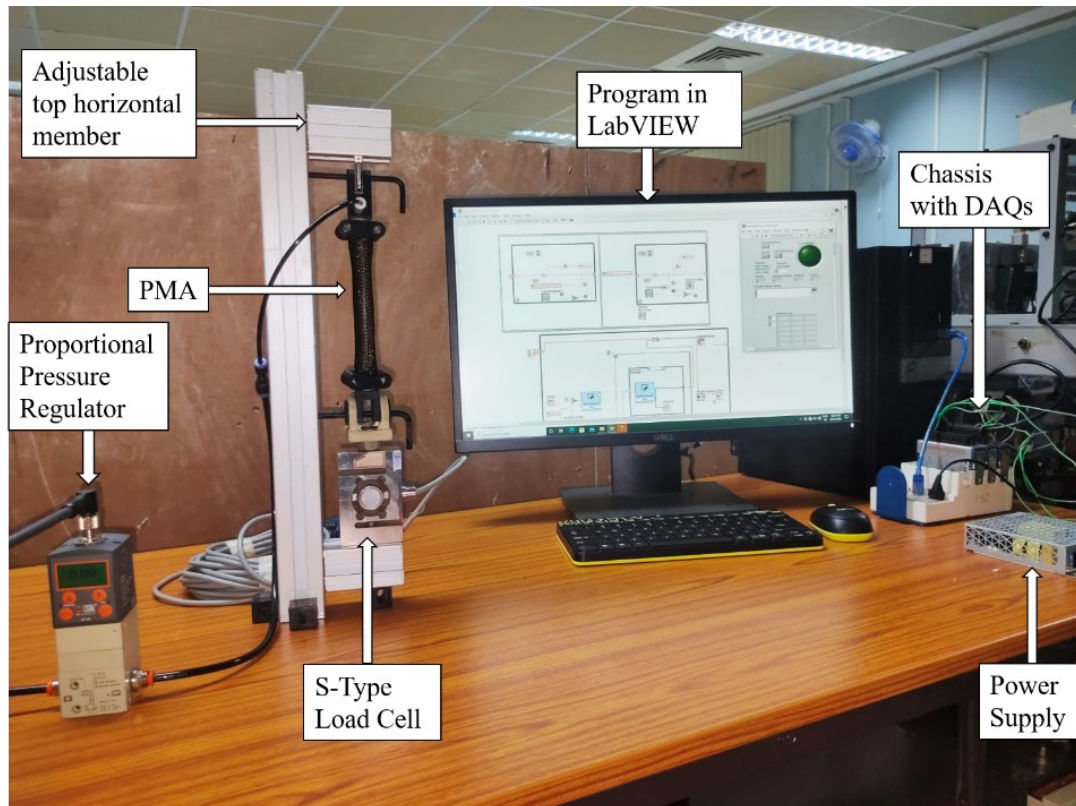


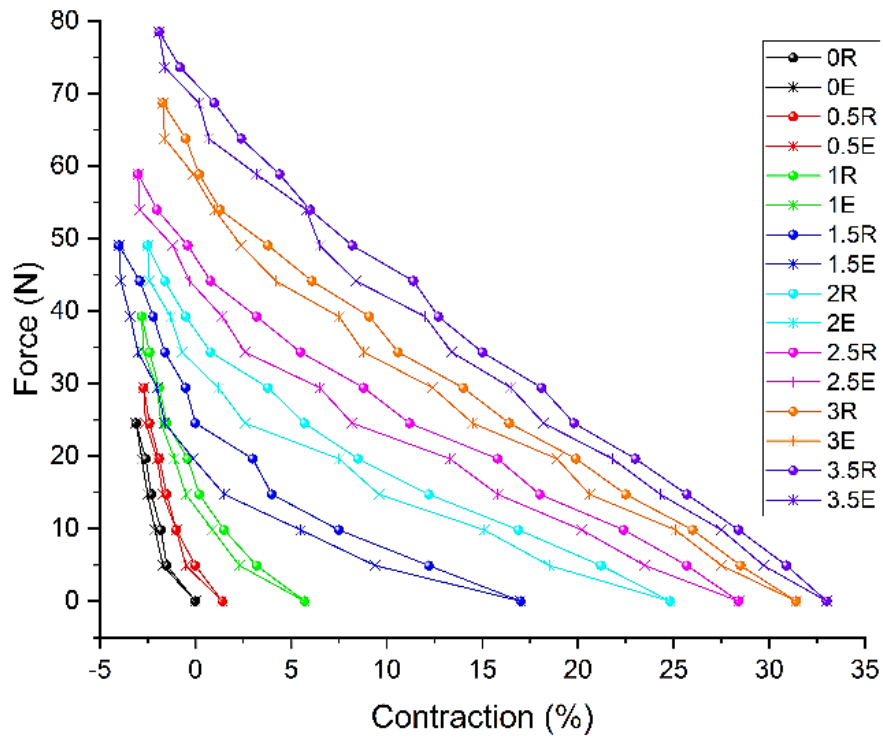
Fig 4.8b: Test Rig for PMA Force

The second test setup shown in Fig 4.8b measures the force generated by the pneumatic muscle actuator. The force setup consists of larger t-slot sections (40 mm x 40 mm), forming a 'C' shaped structure. The advantage of this structure is its ability to test varying muscle lengths by adjusting the position of the top horizontal member of the 'C' shaped structure. The top horizontal member consists of a bracket to mount one end of the pneumatic muscle actuator. The 'S' type load cell (HBM 2 KN) is fixed to the lower horizontal section of the test setup, while the other end of the load cell clamps onto the other end of the PMA. The NI9237 bridge analog input module is used in the force set-up in addition to the other data acquisition module (DAQ, NI9264). The operation of the force setup is similar to the displacement setup. The NI9264 generates a signal for the proportional pressure regulator to actuate the muscle, which results in muscle contraction. The contracting muscle exerts a pulling force measured by the load cell. The measured force value is transmitted to the PC through the bridge analog input

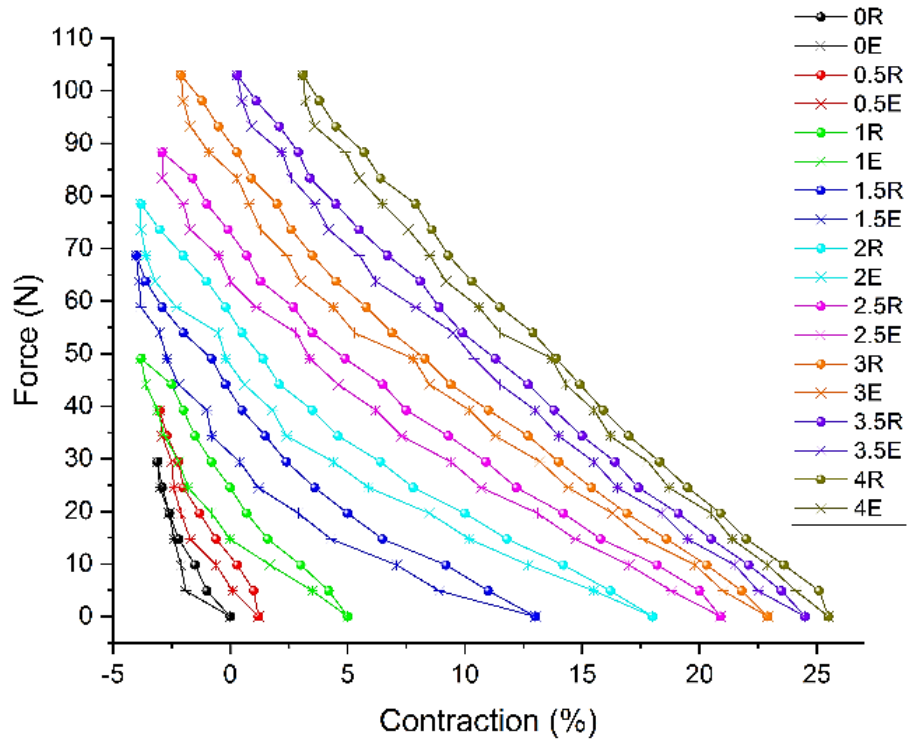
module (NI9237). The LabView program shown in Annexure C records the force generated by the muscle for the applied actuation pressure.

4.2.3 Force Versus Contraction Characteristics

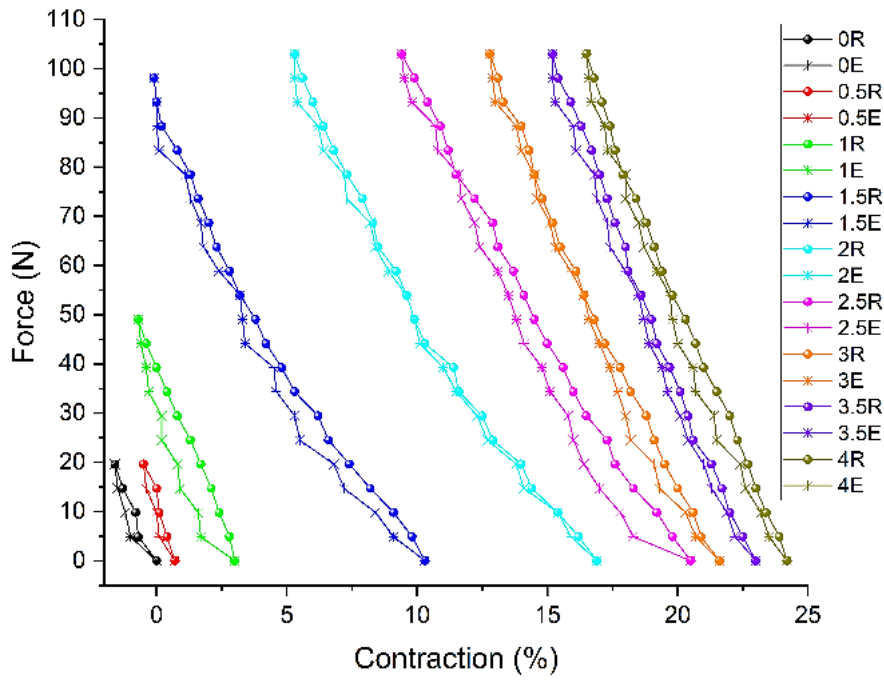
Experimental testing is performed to understand the extent of force and contraction the pneumatic muscle produces for a particular pressure value. For a specific pressure, the PMA produces a maximum force when both ends are fixed, known as blocked force, while it produces maximum deflection if only one end is fixed. In this test, the pressure is maintained constant for every trial (e.g., 0.5R shown in Fig 4.9 indicates the retraction stroke at 0.5 bar pressure). Each trial involves an incremental rise in the force at the free end (or sliding end) of the PMA, which is imparted by hanging dead weights. The variation in contraction percentage with increasing force is observed and presented in the plots shown in Fig 4.9(a-d) - Fig 4.10(a-b). Each trial is conducted up to a weight (equivalent force) of 10 kg, which is increased incrementally at a rate of 0.5 kg per contraction percentage observed. Subsequently, the experiment involves increasing the pressure by 0.5 bar for every trial (extension(E) and retraction(R) cycle) up to a pressure of 4 bar. The 4x6 PMA is tested up to a pressure of 3.5 bar because of its smaller bladder volume.



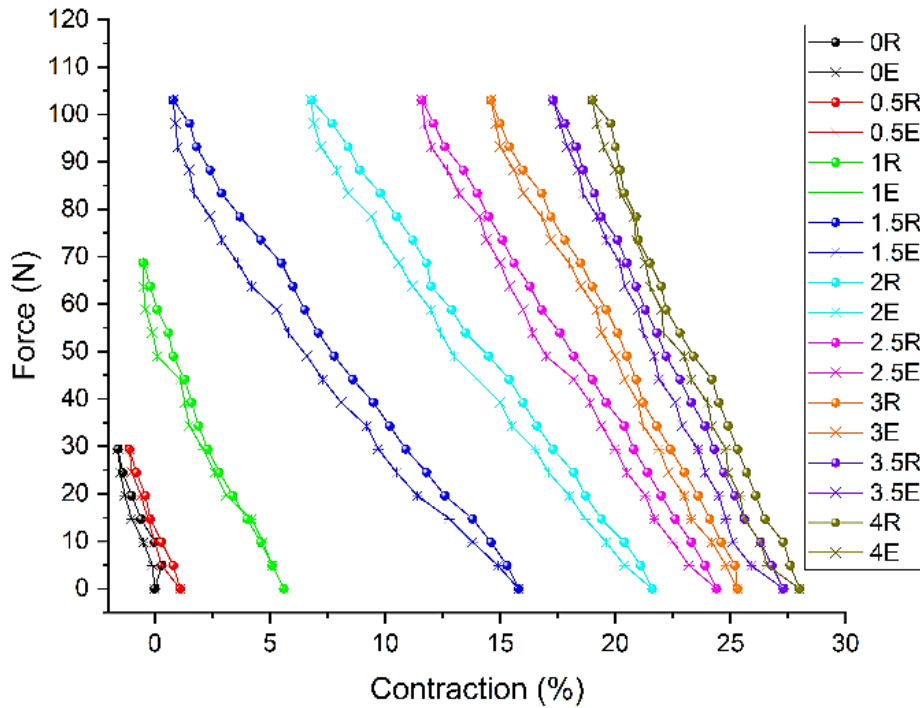
a) 4x6 PMA



b) 6x9 PMA

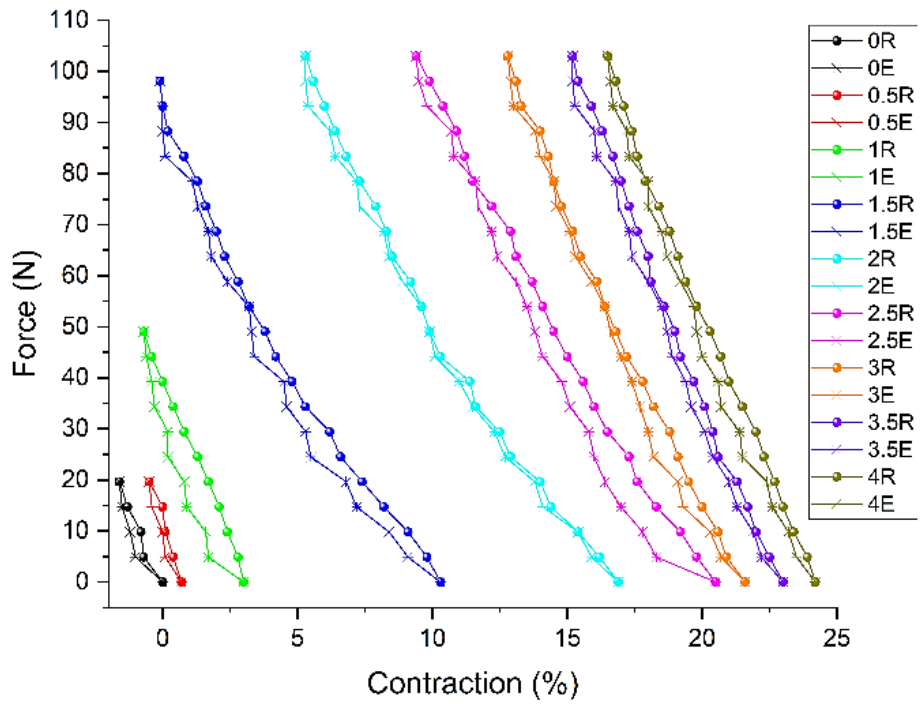


c) 10x14 PMA

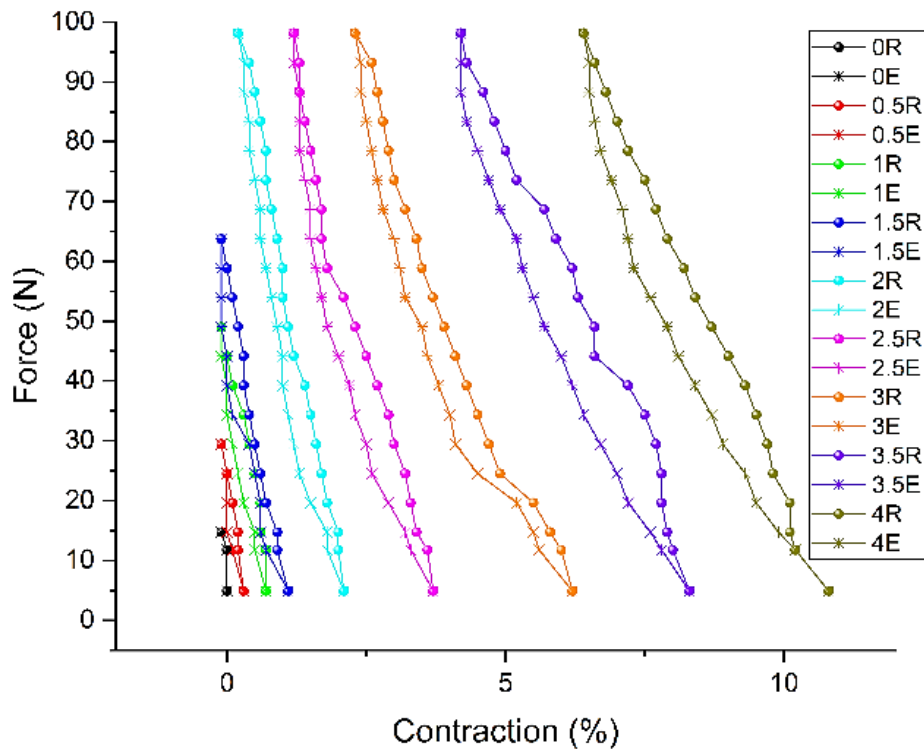


d) 12x17 PMA

Fig 4.9: Force vs Contraction Ratio of Developed PMA (Note: 1R = Retraction Stroke at 1bar; similarly, 1E is Extension Stroke at 1bar)



a) 10x14 Developed PMA



b) Commercial PMA used in this study

Fig 4.10: Force vs Contraction Ratio of Developed and Commercial PMA of identical diameter and actuation length

From the plots shown in Fig 4.9(a-d) and Fig 4.10(a-b), it can be interpreted that for a particular pressure value, the amount of force is inversely proportional to the contraction percentage; as the force increases, the contraction percentage decreases. The smaller size muscles of size 4x6(mm x mm) and 6x9(mm x mm) PMAs show a significant contraction variation, increasing force for a particular actuating pressure. In contrast, the bigger cross-section muscles (10x14 and 12x17) showed a steeper slope (smaller variation in contraction with increasing force). This behaviour is primarily due to the effect of the hyperelastic bladder, whose volume is more prominent in smaller muscles (as shown in Table 4.3). Therefore, PMAs of larger cross-sections offer a better positional stability (and accuracy) and are less affected by the variations in the applied load.

Table 4.3: Ratio of Bladder Volume to Actuator Volume for different PMA sizes

<i>PMA (IDxOD)</i>	<i>V_{bladder}/V_{actuator}</i>
<i>12x17</i>	<i>0.89</i>
<i>10x14</i>	<i>0.73</i>
<i>6x9</i>	<i>0.94</i>
<i>4x6</i>	<i>0.94</i>

Table 4.3 depicts the ratio of bladder volume ($V_{bladder}$) and the total volume of the actuator ($V_{actuator}$) (Pillsbury et al. 2015). The bladder is made of a hyperelastic material and constitutes a significant volume portion of the entire pneumatic muscle actuator; thus, its characteristics profoundly affect the behaviour of the overall PMA. An important observation from Table 4.3 is that the least volume ratio is found in the 10x14 muscle; thus, it shows a tendency to be least affected by the effect of the hyperelastic bladder. Therefore, the 10x14 muscle shows better positional accuracy and low

hysteresis error (higher repeatability of force or deflection achieved for a particular actuation pressure) and is least affected by the increasing payload. The 12x17 PMA (Fig 4.9d) shows a greater drop in contraction with the increase in force compared to the 10x14 muscle (Fig 4.9c). The reason for the reduction in the contraction of the 12x17 PMA compared to the 10x14 muscle is a result of the slightly higher tensile modulus (0.89 MPa) bladder used in the 10x14 PMA, as shown in Table 4.2.

The variation in contraction with increasing force or load is the compliance of the pneumatic muscle, which is due to the hyperelastic bladder and the use of a compressible fluid (air). Compliance is an essential property required in a rehabilitation exoskeleton that prevents harm to a patient resisting the exoskeleton's motion (Vallery et al. 2008). Compliance can be defined as a percentage of elongation of the hyperelastic bladder that resulted from a restriction to the movement of the PMA, which returns to its set position (based on applied pressure) once the restriction is removed. The plots in Fig 4.9a– Fig 4.9d indicate the variation of contraction percentage vs force, which directly depends on the bladder's size and material properties. At higher contraction values, the flexible inner tube is strained beyond the linear stress-strain relation, resulting in a stiffness effect evident in the smaller PMAs compared to their larger counterparts; a similar observation is reported by Hocking et al. (Hocking and Wereley 2012).

The plots also reveal a hysteresis error during the retraction-extension (R-E) strokes in all four developed PMAs (4x6, 6x9, 10x14, and 12x17) and the commercially available muscles. Several factors contributed to hysteresis error, which includes the bladder's hyper-elastic nature, friction between braids, and friction between braided sleeve and bladder. The plot of the 10x14 PMA shown in Fig 4.9c exhibits the least hysteresis error due to the smaller bladder volume and a more significant gap between the bladder and braided sleeve. The better contraction and lower hysteresis error in the 10x14 pneumatic muscle make it great for the rehabilitation application, as it exhibits a perfect balance of compliance and positional accuracy. The slight difference (of +0.05 MPa) in the tensile modulus of the 10x14 PMA shows a significant improvement over the other developed muscles, thus indicating a substantial influence of bladder material and size on the behaviour of the PMA.

The Plots in Fig 4.9(a-d) and Fig 4.10(a-b) show that for an actuation pressure of 4 bar, the PMA developed in the present work contracts by about 30%, while the commercial muscle contracts by only 11% of its actuating length. In this study, the behaviour of the 10x14 PMA shown in Fig 4.10a is compared with the commercially available muscle shown in Fig 4.10b due to their similar dimensional properties (14 mm diameter, 2 mm thickness, and 100 mm length). The plots in Fig 4.10a and Fig 4.10b reveal that the 10x14 muscle follows a similar behaviour to the commercial muscle in terms of force vs contraction characteristics. The plots shown in Fig 4.9(a-d)– Fig 4.10(a-b) reveals that the least hysteresis error is exhibited by the 10x14 muscle, which has the least volume ratio with a tensile modulus slightly lower than the rest of the developed pneumatic muscles. The force and contraction behaviour of both 10x14 (Fig 4.9c) and 12x17 (Fig 4.9d) look similar, as they use a thicker tube and use the exact same size of the braided sleeve (same actuator volume). This test clearly shows a variation in the behaviour of force and contraction for different PMA sizes. The amount of force generated for a particular value of actuation pressure is seen to increase with the increase in the size of the muscles tested, as shown in Fig 4.9(a-d) to Fig 4.10(a-b). The plots also indicate that the variation of contraction with force is higher for the smaller cross-section muscles than the larger muscles. It is concluded that the sizes 10x14 and 12x17 produce stable force and contraction characteristics with incremental actuation pressures.

4.2.4 Pressure vs Deflection Characteristics

The force versus contraction ratio characterization is used to study the overall behaviour of the various pneumatic muscles. In assistive applications such as an elbow exoskeleton, it is essential to control the position of the PMA accurately. The pressure versus deflection behaviour provides a sound basis for deciding the control strategy to actuate the pneumatic muscle. It is established from the force versus contraction study that the 10x14 PMA showed high positional accuracy and a low hysteresis error. Accordingly, the 10x14 PMA is compared with the commercial muscle for the pressure versus deflection test. The displacement test rig shown in Fig 4.8a requires one end of the pneumatic muscle to be mounted at the test rig's top fixed support while the other end is clamped to the sliding assembly, which is loaded with a 5 kg dead weight. As

previously mentioned in the earlier section, the maximum load while actuating the forearm through flexion is less than 5 Kg, which includes the weight of the support structure, patient's hand, payload, and the forearm itself (Chakrabarti Debkumar 1999; Plagenhoef et al. 1983). The laser displacement sensor is used in this test to measure the deflection of the muscle (retraction/extension). The laser displacement sensor recorded the amount of deflection experienced by the loaded PMA for incremental pressure inputs. The test is conducted in pressure steps of 0.5 bar up to a pressure of 4 bar for the 10x14 PMA.

Fig 4.11 shows an almost linear deflection is observed within the pressure range of 1-3bar, while the curve tends to flatten at its ends. This trend indicates a linear relationship between pressure and deflection from 1 bar to 3 bar, thus resulting in the ideal control range for the 10x14 muscle. The flattened portion at the start of the plot is due to the gap between the bladder and braided sleeve (pressure deadband), while that at the end is most likely due to the expanded bladder reaching its maximum radial limit. A hysteresis error visible in Fig 4.11 indicates that it is difficult to achieve the same deflection value during the retraction (R) and extension (E) strokes of the PMA.

The plot in Fig 4.11 showcases two trials (T1 and T2) to check the actuators' repeatability. It is evident from both plots that there is a very slight difference in the deflection between trial T1 and T2 for each value of pressure due to the hyperelastic nature of the bladder. The non-linear nature of pressure vs deflection results from friction (between braids of the braided sleeve and braided sleeve & bladder) and the bladder's hyperelastic nature. A similar observation is reported by Hocking et al. (Hocking and Wereley 2012).

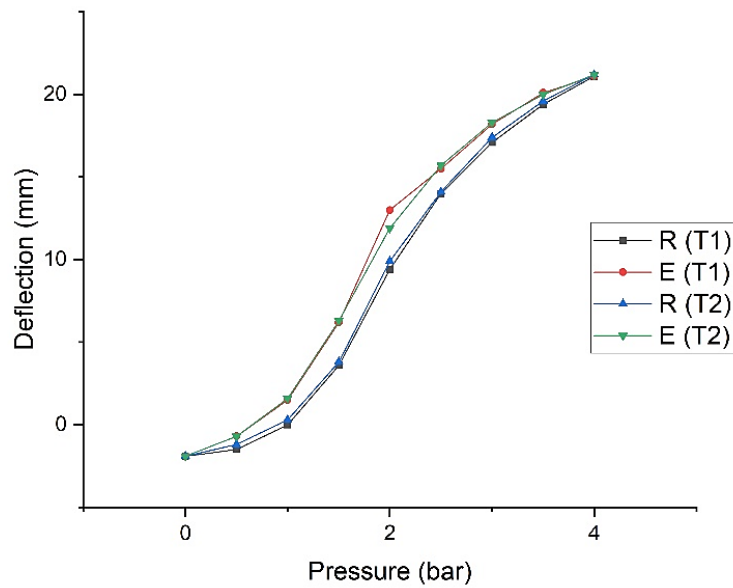


Fig 4.11: Deflection vs Pressure of 10 X 14 PMA (R(T1): Retraction Stroke of the 1st Trial, E(T1): Extension stroke of the 1st trial)

4.2.5 Pressure vs Force Characteristics

The force generated by the PMA is an essential parameter in deciding the size of the pneumatic muscle based on the application's requirement. For instance, the PMA used for an upper limb exoskeleton requires a more significant force to flex the patient's elbow (5 kg payload). The test is conducted using the force test rig shown in Fig 4.8b. A fixed base replaced the sliding mechanism shown in Fig 4.8a with an adjustable top horizontal member. A load cell (HBM 2 KN) is attached to the free end of the PMA, and the other end is anchored to the rigid base of the test rig. A 4-channel strain gauge DAQ (NI9237) acquires the force data from the load cell. The pneumatic muscle is actuated using the proportional pressure regulator, and the force it generates is recorded for various values of pressure. The force vs pressure behaviour of the two developed muscles, 10x14 and 12x17, shown in Fig 4.12, is analyzed to evaluate the effect of size on the force behaviour of the muscle.

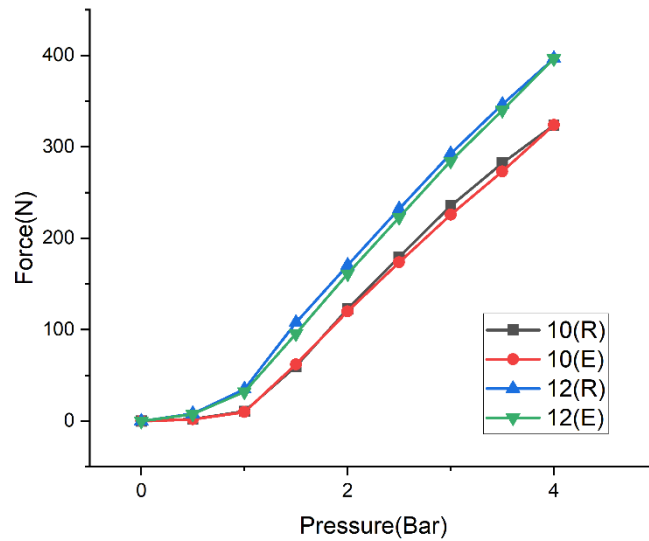


Fig 4.12: Force vs Pressure of 10 X 14 (10R & 10E) and 12 X 17 (12R & 12E) PMA for Extension(E) and Retraction (R) Strokes

Fig 4.12 clearly indicates that the larger diameter muscle 12x17 produces a higher force of 401 N while the 10x14 generates a blocked force of 324 N at 4 bar actuation pressure. Similar to the deflection characteristics, the force value for a particular pressure in the retraction(R) and extension(E) strokes is different, thus indicating a hysteresis error. Fig 4.12 also suggests that the 10x14 PMA shows a smaller hysteresis error than the 12x17 PMA due to the higher tensile modulus bladder used in the 10x14 PMA. The plots in Fig 4.12 shows a linear relationship between force and pressure in the 1 to 4 bar pressure range. The delay in the force generation after the application of pressure (< 0.25 bar) is a result of the pressure deadband (or gap between the bladder and braided sleeve). The plots also indicate a smaller pressure deadband in the 12x17 muscle (a smaller gap between the bladder and braided sleeve), as a result of which it starts producing force at a pressure less than 0.25 bar when compared to the 10x14 PMA (deadband: 0.5 bar).

4.2.6 Comparing Displacement and Force Characteristics of The Developed PMA with a Commercial PMA

The commercial McKibben muscle forms an excellent standard to compare the performance of the PMA developed in this work. The commercial PMA used in this study has the dimensional properties of the 10x14 muscle with a 10 mm internal

diameter, 14 mm outer diameter, and a 100 mm actuation length. The displacement and force tests are conducted up to the maximum operating pressure of 8 bar for the commercial muscle.

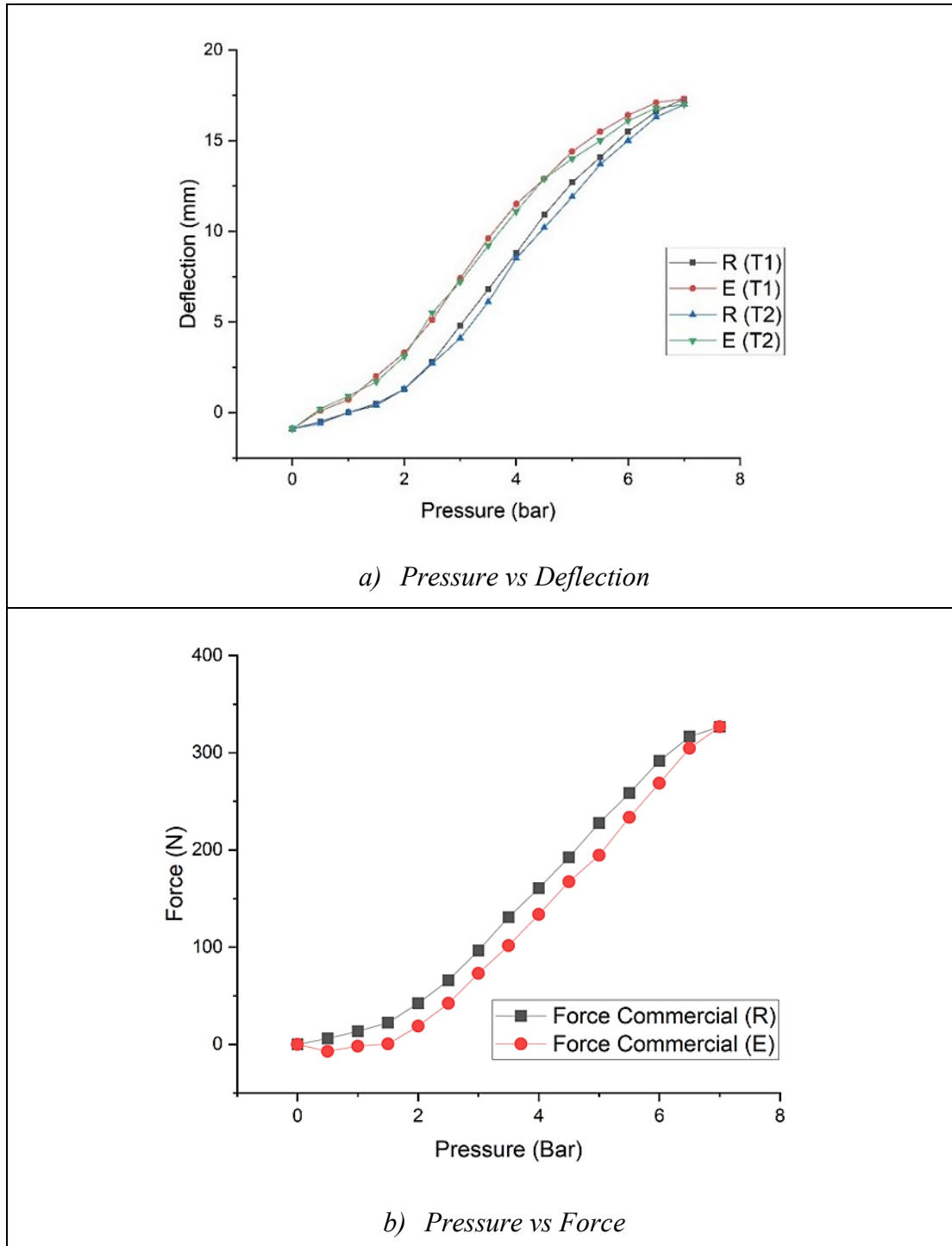


Fig 4.13: Deflection and Force Characteristics of the commercial PMA tested

Fig 4.13 shows the variation of the muscle deflection with increasing actuation pressure. Similar to the 10x14 PMA presented in section 4.2.4, the commercial muscle shows a linear relationship between pressure and deflection in the pressure range of 2 bar to 6 bar. Fig 4.13 also indicates a flattening at the plot's start and end, resulting from pressure deadband and the bladder reaching its maximum limit of radial expansion. From Fig 4.11 and Fig 4.13a, it is clear that the muscle developed in this work (10x14) produced a higher deflection at a lower pressure when compared with the commercial muscle. The plots also indicate a smaller hysteresis error in the developed PMA (10x14) compared to the commercial muscle.

Fig 4.13b is the plot of pressure versus force of the commercial PMA. The force behaviour of the commercial PMA shows an approximate force of 350 N at 8 bar. Fig 4.13b also shows the flattening of the force curve at its ends, thus indicating an initial pressure deadband and a negligible increase in the force with the increase in pressure beyond 7 bar. The developed PMA behaviour shown in Fig 4.12 depicts a linear rise in force with pressure in the operating range of 1 bar to 4 bar, while a similar trend is observed in the range of 2 bar to 6 bar for the commercial PMA as shown in Fig 4.13b. Fig 4.13b shows that the force generated by the commercial PMA at 4 bar is under 150 N, which is much less than the force generated by the developed 10x14 PMA (324 N), as shown in Fig 4.12, having a similar geometric configuration. Therefore, the plots in Fig 4.12 and Fig 4.13b indicate that the developed PMAs using the styrene-based bladder and PET braided sleeve can generate a higher force at a lower actuation pressure, requiring a smaller compressor, thus reducing the cost of the system.

4.2.7 Life Cycle Test

As the developed pneumatic muscle is intended to actuate an exoskeleton for medical rehabilitation, its operational reliability is critical. To test the reliability of the PMA before actually using it to actuate the exoskeleton, an endurance test or life cycle test is designed and implemented. The test is conducted by mounting the muscle onto the test rig shown in Fig 4.8a and loading it with a 5 kg load (actual load of the structure, forearm, hand, and payload) at its free/sliding end. Unlike the previous tests, this test involved additional components, such as a microcontroller (Atmega 2560 clocked at

16MHz), a pressure sensor (P43 Series from Metal Works), and an electro-pneumatic pressure regulator (Regtronics ¼ from Metal Works). The microcontroller is programmed to give a cyclic voltage signal to the pressure regulator to increase and decrease the pressure of compressed air fed to the pneumatic muscle to realize the contraction and extension strokes of the PMA. The pressure sensor connected to the system senses the system pressure and acts as a feedback device for the controller in case of a sudden pressure drop, indicating a rupture (failure) of the pneumatic muscle. The entire program is run in a loop, and the controller records the number of successful cycles the PMA endures. The flow chart in Fig 4.14 gives a detailed overview of the lifecycle test. The life cycle test is conducted on the developed 10x14 muscle with a 5 kg load attached. The life cycle test showed that the developed muscle endured over 200000 cycles over 8.38 days of continuous operation. The test is conducted as close to actual conditions as possible considering the load attached (5 kg) and the maximum operating pressure of 4 bar for 10x14 PMA, fed at each cycle to realize a full contraction stroke.

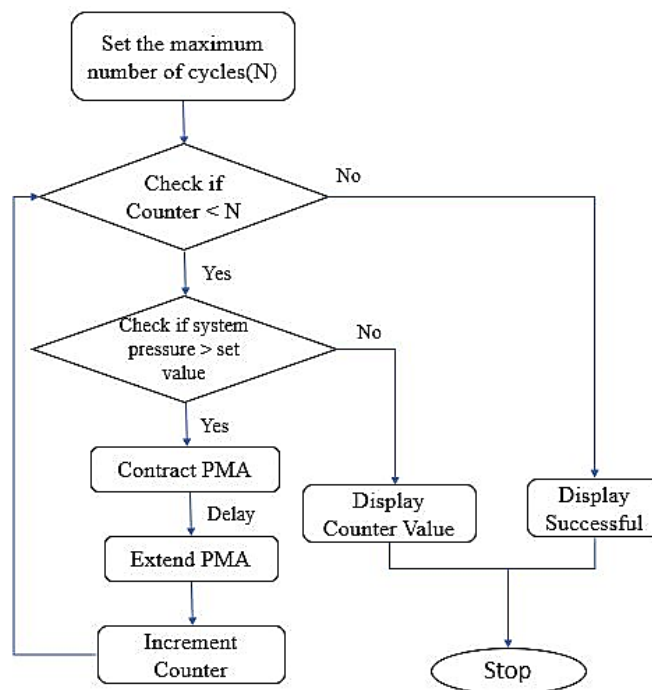


Fig 4.14: Lifecycle Test Flowchart

4.3 Mathematical Model of a Pneumatic Muscle Actuator (PMA)

4.3.1 Mathematical Models of PMA

A mathematical formulation gives the theoretical perspective of the pneumatic muscle in an ideal situation. Previous research has reported modelling pneumatic muscles to simulate and optimize the PMA design for different applications. A comparative study of the various mathematical models is presented in this section to establish a model which closely resembles the fabricated pneumatic muscle. This study helps to optimize a pneumatic muscle and saves both time and resources, which is a downside of a purely experimental approach.

The PMA's volume substantially comprised the hyper-elastic bladder (e.g., latex rubber), thus making the actuator highly non-linear and challenging to model. Fig 4.15 shows a single braided fibre wrapped around the bladder at an initial angle of ' α_0 ' with respect to the central axis of the muscle. 'F' is the force the pneumatic muscle produces when a pressure 'P' is applied.

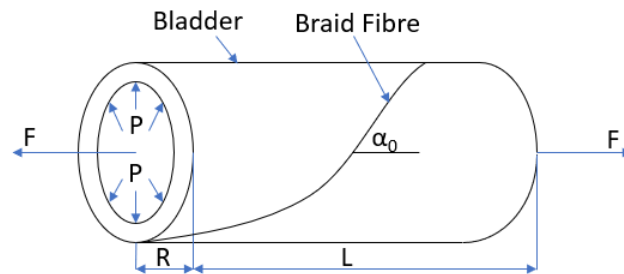


Fig 4.15: Schematic of PMA with braid fibre (F in the X direction)

The actuation of the pneumatic muscle is due to the application of compressed air at a set pressure, 'P,' which causes the outward expansion of the bladder. The outward motion of the bladder is confined by the braided sleeve, which converts the radial motion to axial contraction of the muscle. The contraction ratio given in eq(4.1) is expressed as the axial contraction of the PMA.

$$\text{Contraction Ratio} = \frac{\text{Length of PMA after actuation (L)}}{\text{Original length of PMA (L}_0\text{)}} \quad (4.1)$$

Where $L_0 > L$

Length of PMA after actuation (L) is obtained by deducting the amount of deflection (δ) from the original length of the muscle (L_0) given in eq(4.2):

$$L = L_0 - \delta \quad (4.2)$$

When the pneumatic muscle's motion is restricted by clamping one end and loading the other, it tends to apply a force on the load, which is assumed to be proportional to the applied actuation pressure. This actuation force the pneumatic muscle produced for an applied actuation pressure was first presented by Gaylord (Tondu and Lopez 2000)(Vocke et al. 2012)(Kothera et al. 2009) as depicted in eq 4.3.

$$F_{Gaylord} = \frac{P * (3 * L^2 - B^2)}{4 * N^2 * \pi} \quad (4.3)$$

Where P is the pressure of compressed air applied to the PMA

N is the number of turns of a single braid fibre about the bladder

L is the instantaneous length of the actuator

B is the length of a single braid fibre

The diameter of the flexible bladder and the braid angle play a vital role in the amount of contraction and force generation by the pneumatic muscle. The formulation given by Gaylord does not account for parameters such as friction, the effect of the braided sleeve, or the effect of the hyper-elastic bladder. The effect of the braided sleeve and bladder on the PMAs behaviour is given in the formulation by Tondu (Tondu and Lopez 2000).

The first mathematical model of the PMA is represented as M1 and is given by force (F_{M1}) as per the formulation by Tondu (Tondu and Lopez 2000), which includes Gaylord's Force, and is given by eq 4.4.

$$F_{M1} \tag{4.4}$$

$$= F_{Gaylord} - \frac{\pi * R_0^2 * P * (2 * h_0 * (2 * \cos\alpha_0^2 * (1 - \delta)^2 - 1))}{(1 - \delta) * (1 - \cos\alpha_0^2 * (1 - \delta^2))}$$

Where α_0 represents the initial braid angle ($\alpha_0 = 25.3^\circ$)

R_0 represents the initial radius of the tube ($R_0 = 7$ mm)

t_0 represents the initial thickness of the bladder ($t_0 = 2$ mm)

$h_0 = t_0/R_0$

The bladder material is a hyperelastic material (styrene-based thermoplastic elastomer) whose properties should be considered while modelling the pneumatic muscle. Kothera et al. (Kothera et al. 2009) presented two models; the first model represented as ‘M2,’ considered the hyperelastic nature of the flexible bladder, and the second represented as ‘M3,’ used Newton's second law as the basis.

The model by Kothera et al. (Kothera et al. 2009), which accounts for the hyperelastic bladder, comprises two primary elements. The first is the Gaylord Force term, and the second is a corrective term for the hyperelastic nature of the bladder. The model also considers the effect of the braided sleeve on the force generated by the muscle.

The Mooney Rivlin Force ($F_{hyperelastic}$), as given by eq 4.5, takes into account the hyperelastic nature of the bladder.

$$F_{hyperelastic} = 2 * V_{bl} * [C_{10} * (\lambda_1 * \lambda_1' + \lambda_2 * \lambda_2' + \lambda_3 * \lambda_3') \tag{4.5}$$

$$+ C_{01}$$

$$* (\lambda_1 * (\lambda_2^2 + \lambda_3^2) * \lambda_1' + \lambda_2 * (\lambda_3^2 + \lambda_1^2) * \lambda_2'$$

$$+ \lambda_3 * (\lambda_1^2 + \lambda_2^2) * \lambda_3')$$

C_{01} and C_{10} are Mooney Rivlin constants ($C_{01} = 0.0594$; $C_{10} = 0.00306$) obtained experimentally for the thermoplastic elastomer used in the bladder. λ_1 , λ_2 , and λ_3 are the stretch ratios given as $\lambda_1=L/L_0$, $\lambda_2=(R-t)/(2R_0-t_0/2)$, and $\lambda_3=t/t_0$.

Where t is the instantaneous thickness of the bladder

Assuming a constant volume bladder (V_{bl}), given by eq 4.6

$$V_{bl} = L_0 * [\pi * R_0^2 - \pi * (R_0 - t_0)^2] \quad (4.6)$$

Where L_0 is the initial length of the PMA

t_0 is the initial thickness of the bladder

The bladder's change in radius (R) after applying pressure is given by eq 4.7.

$$R = \frac{\sqrt{B^2 - L^2}}{2 * \pi * N} \quad (4.7)$$

Where B and L are mentioned previously in eq 4.3.

The braided sleeve plays a vital role in the behaviour of the PMA; therefore, considering it as an integral part of the muscle model is essential. The braided sleeve was modelled using eq 4.8.

$$F_{braid} = V_{br} * \left(\frac{4 * \pi^2 * P^2 * B^2 * L}{E_{br} * A_{br} * n^2 * (2 * \pi * N)^4} \right) \quad (4.8)$$

Where V_{br} is the volume of a single braid fibre

E_{br} is the modulus of elasticity of the braid fibre (for the current work, a PET braided sleeve is used)

A_{br} is the cross-sectional area of the braid fibre

n is the number of braid fibres in the braided sleeve

Therefore, using eq 4.3, eq 4.5, and eq 4.8, the PMA force formulation (F_{M2}) can be written as shown in eq 4.9.

$$F_{M2} = F_{Gaylord} - F_{hyperelastic} - F_{braid} \quad (4.9)$$

The third model represented as 'M3' presented in this thesis, proposed by Kothera et al. (Kothera et al. 2009), is based on Newton's second law that uses the force balance

method. The forces in the x-axis (along the length of PMA) and z-axis (radial to the bladder) directions shown in the PMA schematic in Fig 4.15 have been equated with calculating the force F_{M3} produced by the PMA, shown in eq 4.10.

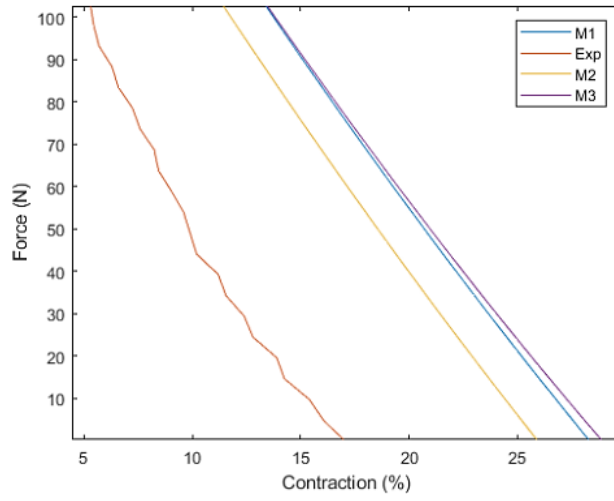
$$F_{M3} = F_{Gaylord} + P * \left(\frac{V_{bl}}{L} - \frac{t * L^2}{2\pi * R * N^2} \right) + E_t * V_{bl} * \left(\frac{1}{L_0} - \frac{1}{L} \right) - \frac{E_t * L}{2\pi * R * N^2} (t * L - t_0 * L_0) \quad (4.10)$$

Where E_t is the tensile modulus of the bladder tube, this research used a styrene-based thermoplastic elastomer bladder with a tensile modulus of 0.893 MPa (obtained experimentally).

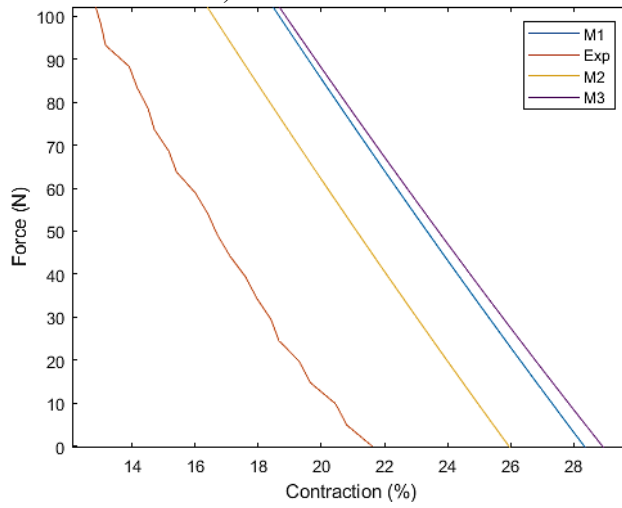
All three models discussed above are programmed in MATLAB (a flowchart of the complete procedure is given in Annexure D) and simulated for various pressures and contraction ratios. In all three models, a constant bladder volume is assumed, and the gap between the braided sleeve and the bladder is accounted for by considering a pressure deadband of 0.2 bar, which is obtained experimentally. The comparative analysis of the simulation results with the experimental findings is presented in section 4.3.2.

4.3.2 Comparing Experimental and Simulated Results

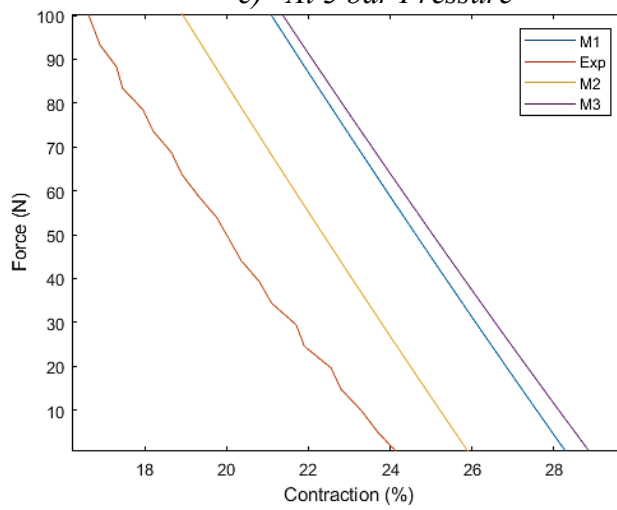
The use of a hyper-elastic bladder makes the pneumatic muscle actuators non-linear in nature. Thus, it becomes essential to determine the mathematical model that best describes the behaviour of the developed muscle. This study evaluates three mathematical models (M1, M2, and M3) of pneumatic muscles and compares their results to the experimental findings. The comparison is conducted for three different pressures, and the results are shown in Fig 4.16a - Fig 4.16c.



a) At 2 bar Pressure



c) At 3 bar Pressure



d) At 4 bar Pressure

Fig 4.16: Force vs Contraction (Where 'M1', 'M2', & 'M3' are Mathematical Models and 'Exp' is obtained experimentally)

The plots reveal that the experimental results match the simulated results more closely as the pressure increases. This trend of experimental results following the simulated values at elevated pressures may be mainly due to increased stiffness and reduced gap between the bladder and braided sleeve, thus demonstrating a close-to-ideal behaviour. The plots in Fig 4.16a - Fig 4.16c shows that the model 'M2' best represents the developed pneumatic muscle. As model 'M2' considers the bladder's hyper-elastic nature and the braided sleeve's effect, it has an accuracy higher than models M1' and 'M3'. The accuracy of the simulation could be further improved by adding a correction factor. Still, the main aim of this study is to find a model which closely resembles the force and contraction characteristics of the developed PMA.

4.4 PMA Characterization for Varying Bladder and Braided Sleeve Configurations

The literature presented in section 2.4.1 indicates that the material and geometric properties of the bladder and braided sleeve influence the performance of the pneumatic muscle. The study carried out in the previous sections also indicates the effect of bladder material, initial braid angle, and bladder-braided sleeve dimensions on muscle performance. This section presents the characterization of the pneumatic muscle utilizing different bladders and braided sleeves and their influence on the pneumatic muscle's performance. The experimental setups discussed in sections 4.2.1 and 4.2.2 are designed for ease of experimentation and autonomous operation. The PMAs are assembled using the novel modular end-fittings, as shown in Fig 4.6, to simplify the process of swapping the bladder and braided sleeve. The experiments were conducted on bladders of different materials and sizes and varied diameters of braided sleeves for various pressures and loading conditions. These experiments aim to find a muscle for actuating an elbow exoskeleton, thus requiring good contraction, compliance, and force characteristics but low pre-extension and hysteresis.

The muscles constructed in this study are broadly divided into two categories, one based on bladder material and the second based on the bladder and braided sleeve size. Fig 4.17 indicates the categories of muscles developed for this study; one muscle is made of a styrene-based thermoplastic elastomer, while the other is made of natural latex

rubber. As the two bladders are procured commercially, they are subjected to tensile tests, which reveal the tensile modulus of the Styrene bladder and Latex bladders as 0.97MPa and 1.21MPa, respectively.

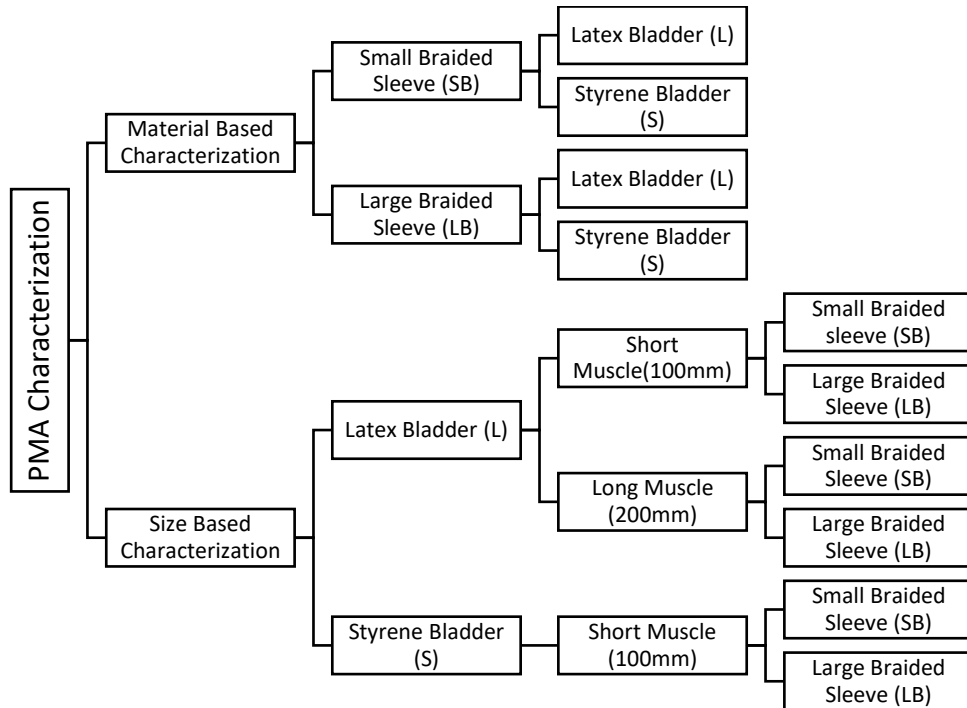


Fig 4.17: Categories of PMA fabricated based on material and dimensional characteristics

Table 4.4 details the muscle actuators constructed using various bladder and braided sleeve combinations. The acronym used in the first column of Table 4.4 indicates the type of bladder (shown as L: for Latex, or S: for Styrene), followed by the size of the bladder (L6: for the Latex bladder of 6 mm ID), and the size of braided sleeve (SB: for Small Braided sleeve, or LB: for Large Braided Sleeve). Table 4.4 also shows muscles of two lengths (100 mm and 200 mm) constructed to study the effect of length on the behaviour of the pneumatic muscle.

Table 4.4: Details of tested PMAs

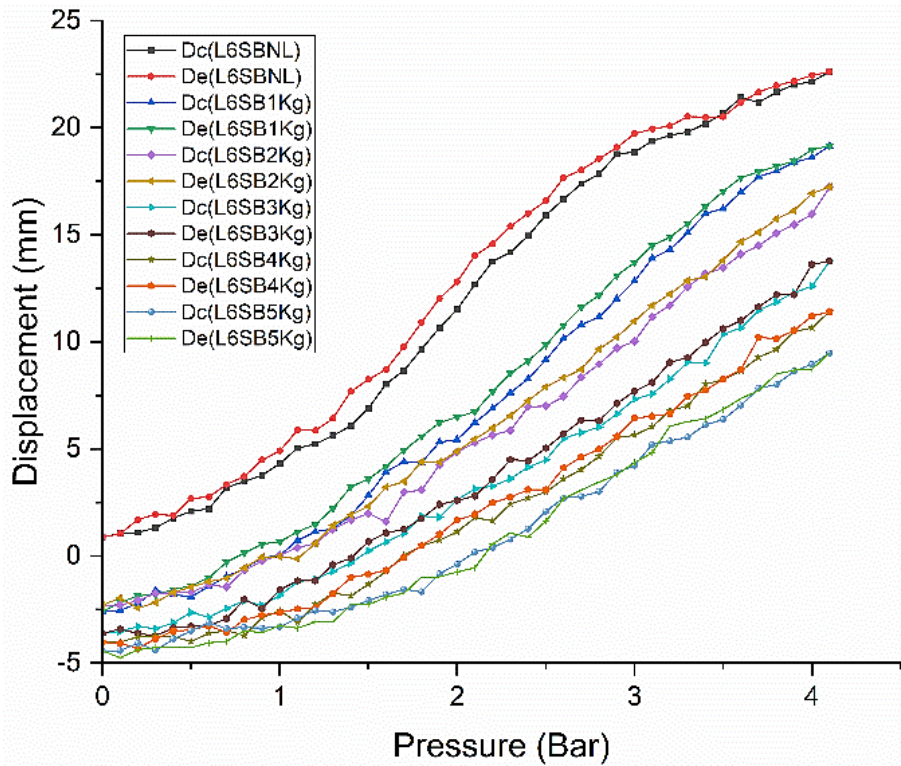
PMA	Bladder (ID x OD), mm	Bladder Wall Thickness, mm	Braided sleeve, mm	Bladder- Braided Sleeve Gap, mm
L6SB/ S6SB	6 x 9	1.5	10	0.5
L6LB/ S6LB	6 x 9	1.5	12	1.5
L8SB/ S8SB	8 x 12	1	14	1
L8LB/ S8LB	8 x 12	1	16	2
L12SB/ S12SB	12 x 17	2.5	19	1
L12LB/ S12LB	12 x 17	2.5	22	2.5

PMAs are constructed with identical dimensional characteristics and varying bladder materials in the material-based characterization. Comparing muscles of the same dimensional features eliminates the effect the size of the bladder and the braided sleeve have on the behaviour of the muscle. On the other hand, size-based characterization involves comparing muscles with the same material characteristics but varying bladder and braided sleeve dimensions. The effect of material and size-based characteristics on the displacement and force generated by the PMA are presented in the following sections. The muscle samples are pre-cycled at a pressure higher than the operating pressure to reduce Mullins effect (Diani et al. 2009), which is the softening effect in fluid filled rubbers due to cyclical loads. Also, note that all tests are performed under quasi-static conditions where the actuation rate is slow to keep the inertial loading effect negligible.

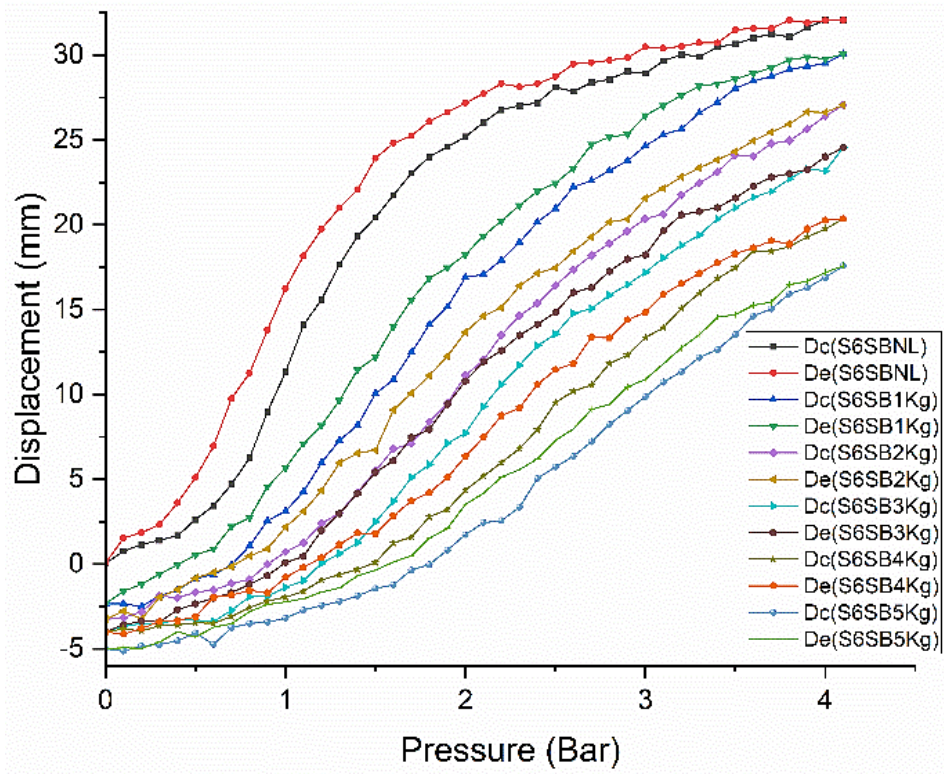
4.5 PMA Displacement Characteristics

The displacement tests are used to study muscle contraction when actuated at different pressures and loading conditions. The test is conducted on the displacement test setup shown in Fig 4.8a by attaching one end of the PMA to the fixed upper bracket and the

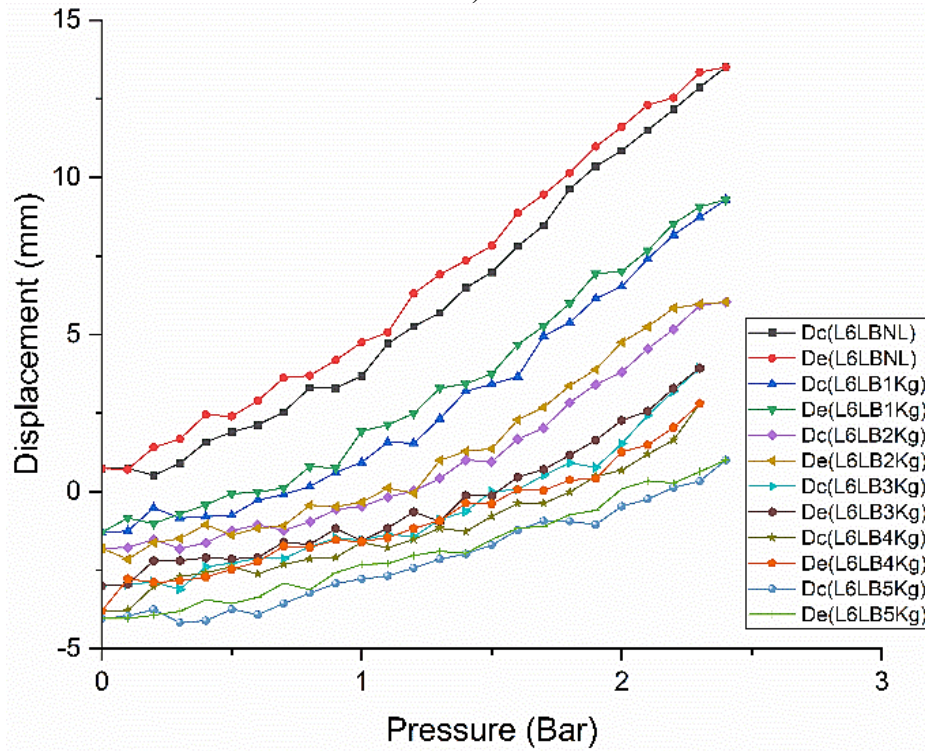
other to the test setup's sliding horizontal member. This study aims at finding a suitable muscle for the actuation of an elbow joint exoskeleton which requires an actuator with a load-carrying capacity rated under 5Kg (weight of support structure, forearm, and payload (Chakrabarti Debkumar 1999; Plagenhoef et al. 1983)). Tests are conducted from the no-load state up to a maximum load of 5 kg, with an increment of 1 kg every trial. The plots in Fig 4.18-4.19 gives the experimental variation between displacement (or contraction) and pressure of the various pneumatic muscles tested.



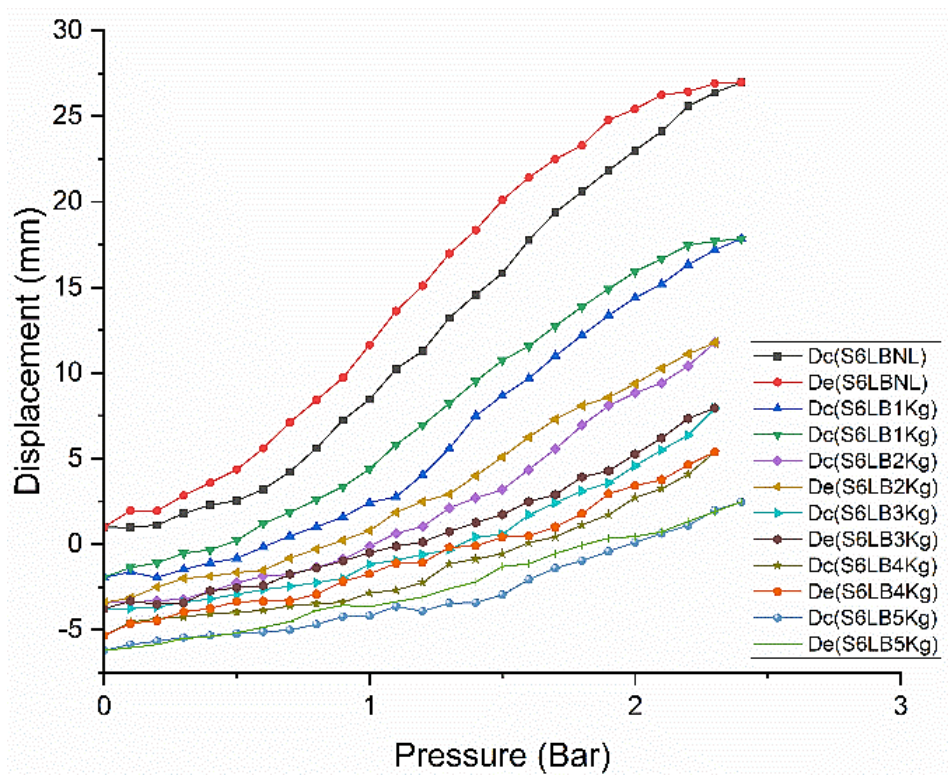
a) L6SB



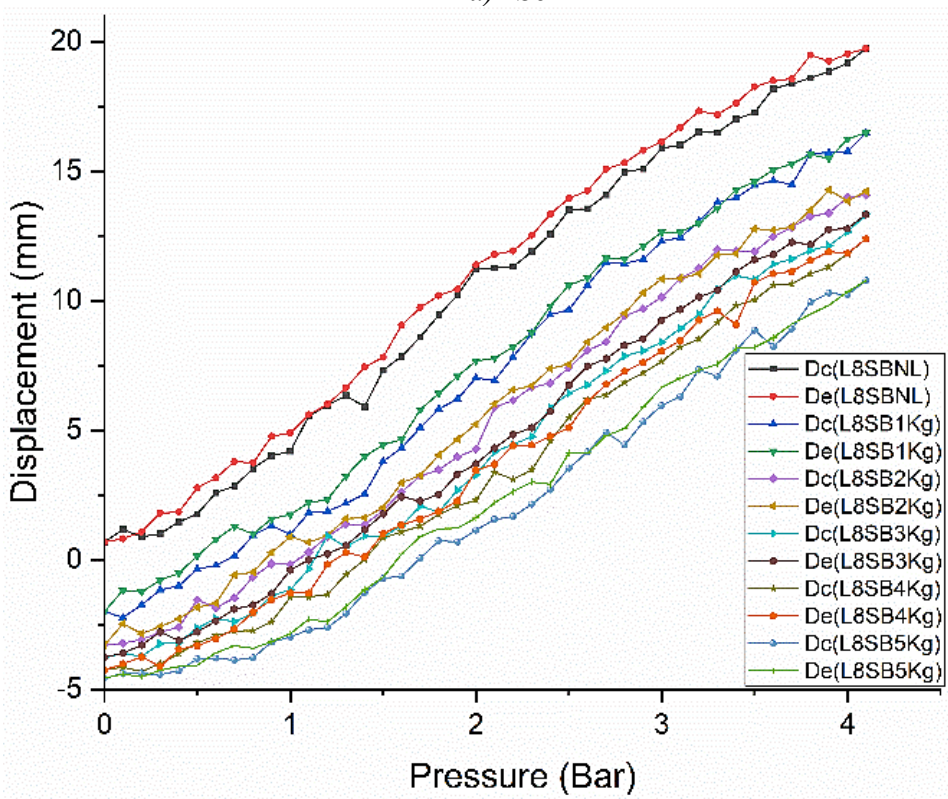
b) S6SB



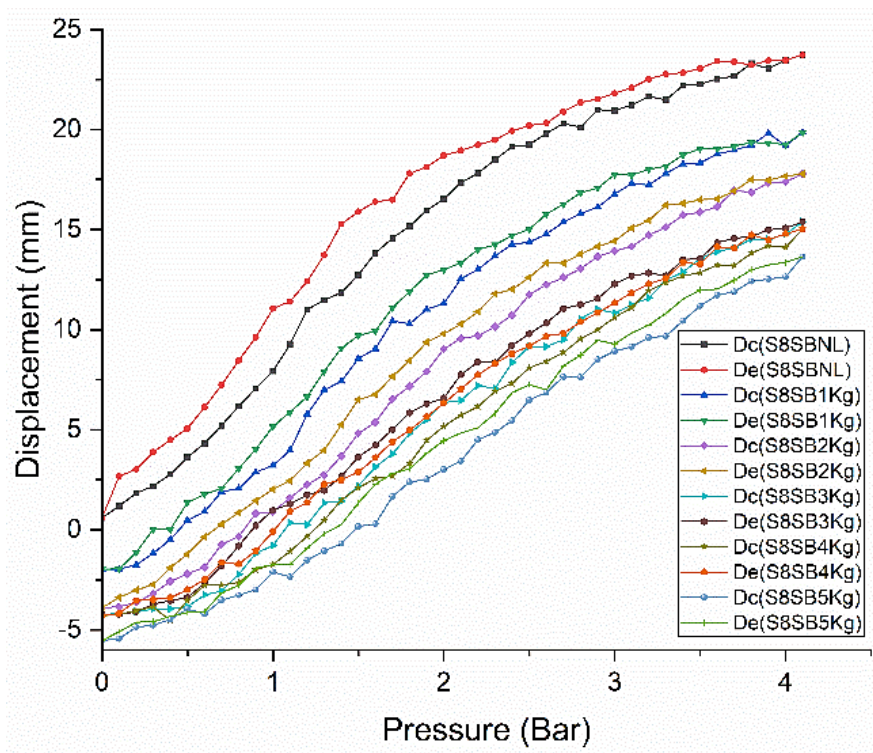
c) L6LB



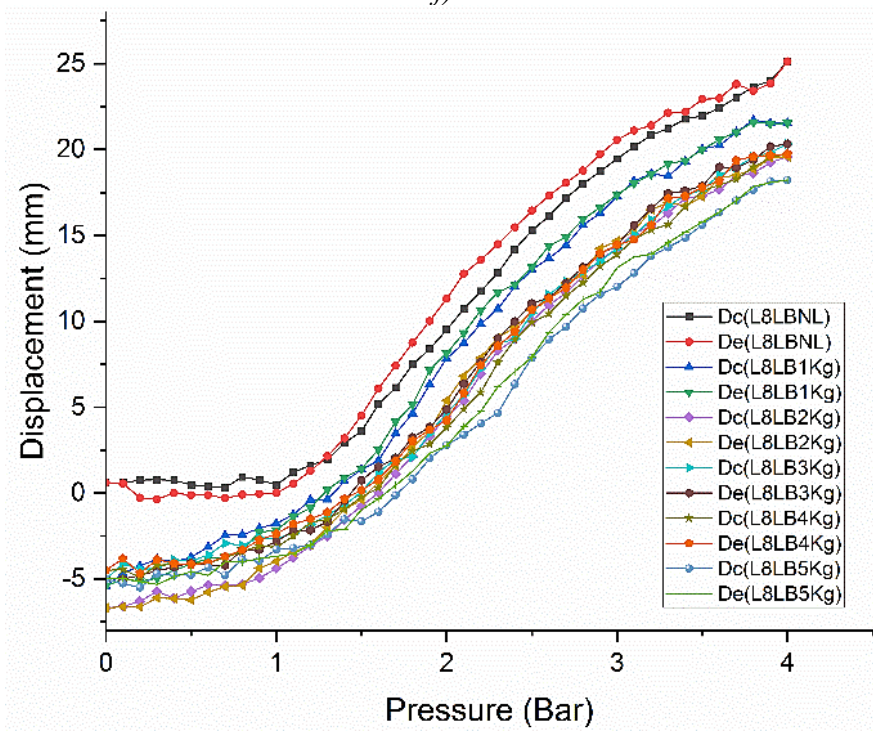
d) S6LB



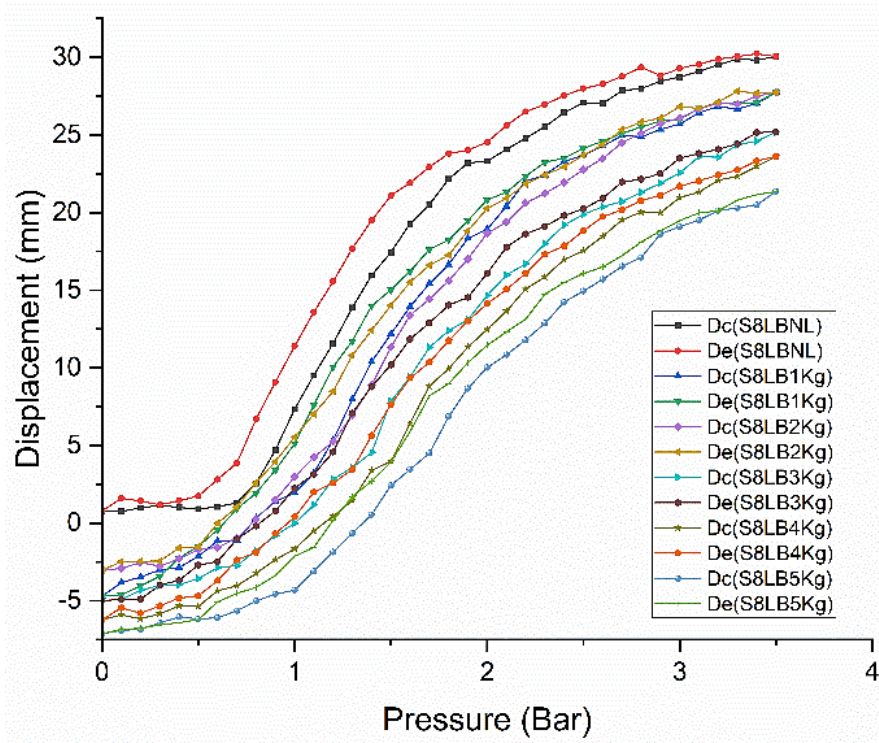
e) L8SB



f) S8SB

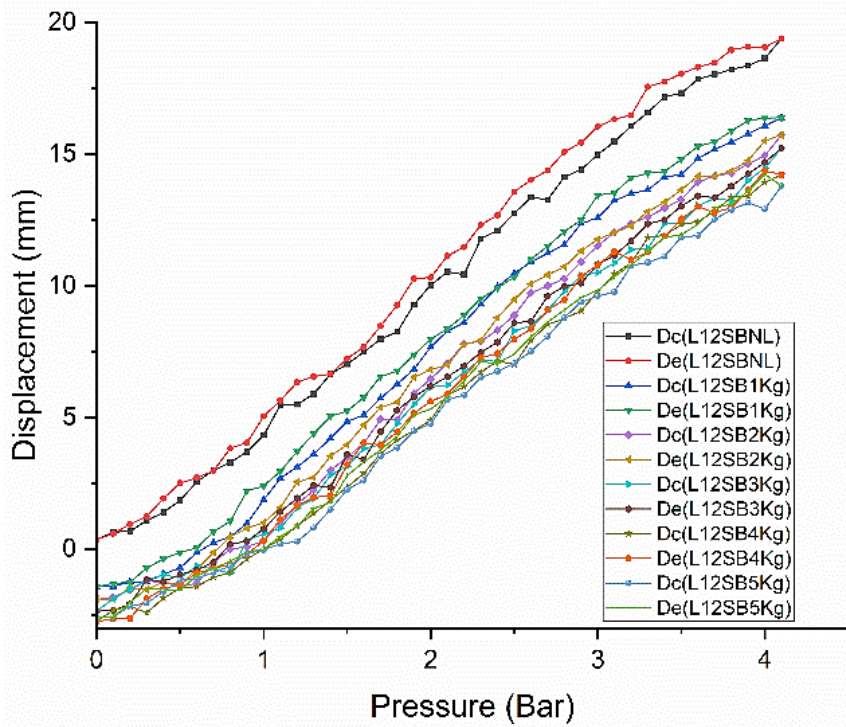


g) L8LB

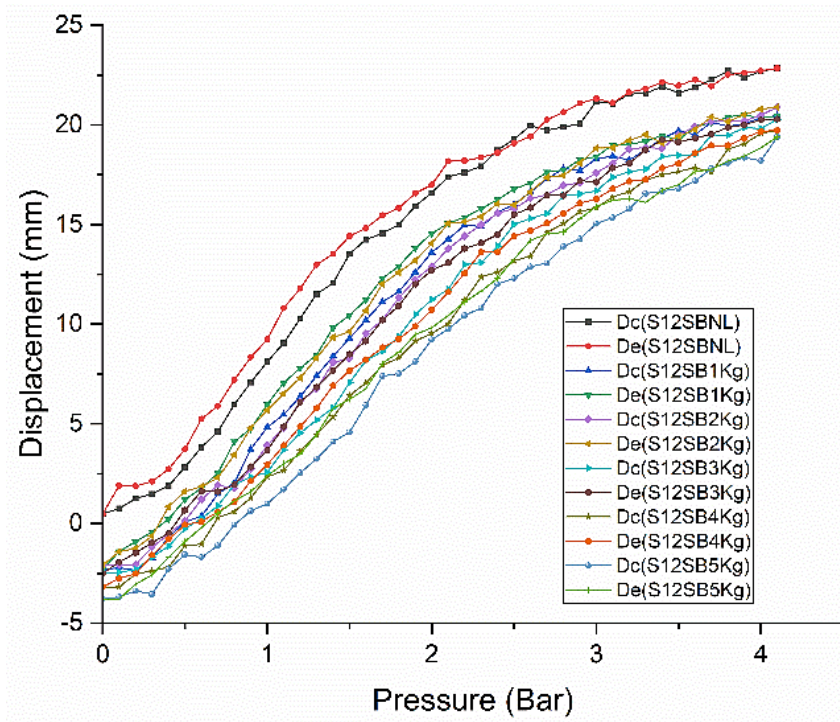


h) S8LB

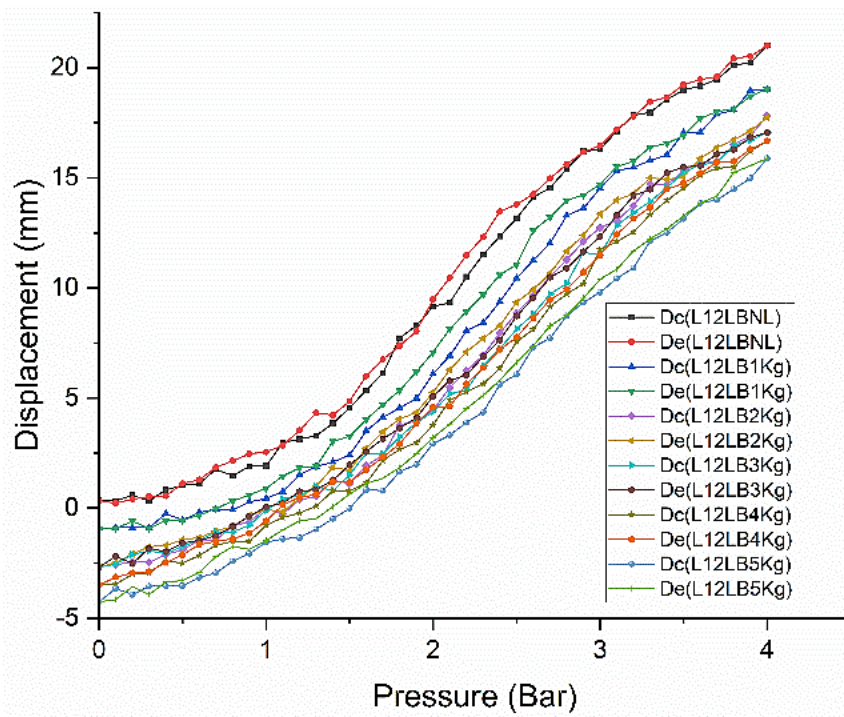
Fig 4.18: Displacement vs Pressure of 6 mm and 8 mm ID (Bladder Internal Diameter) Muscles



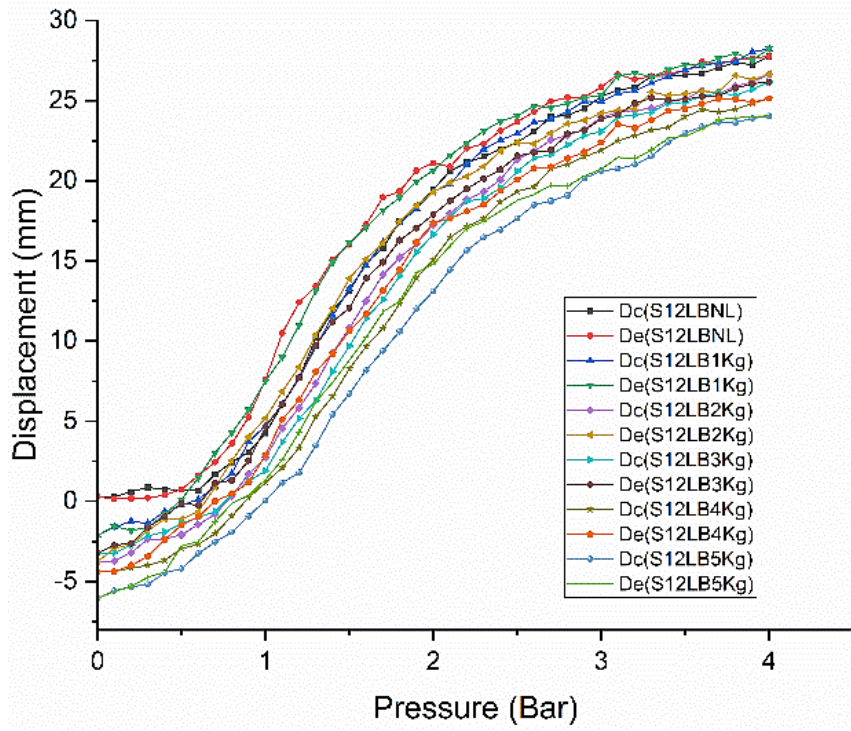
a) L12SB



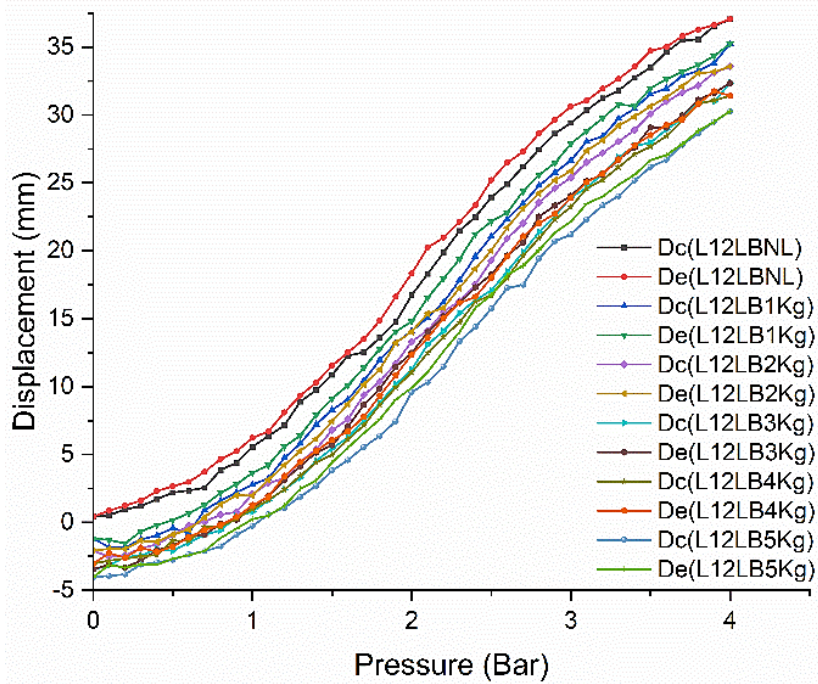
b) S12SB



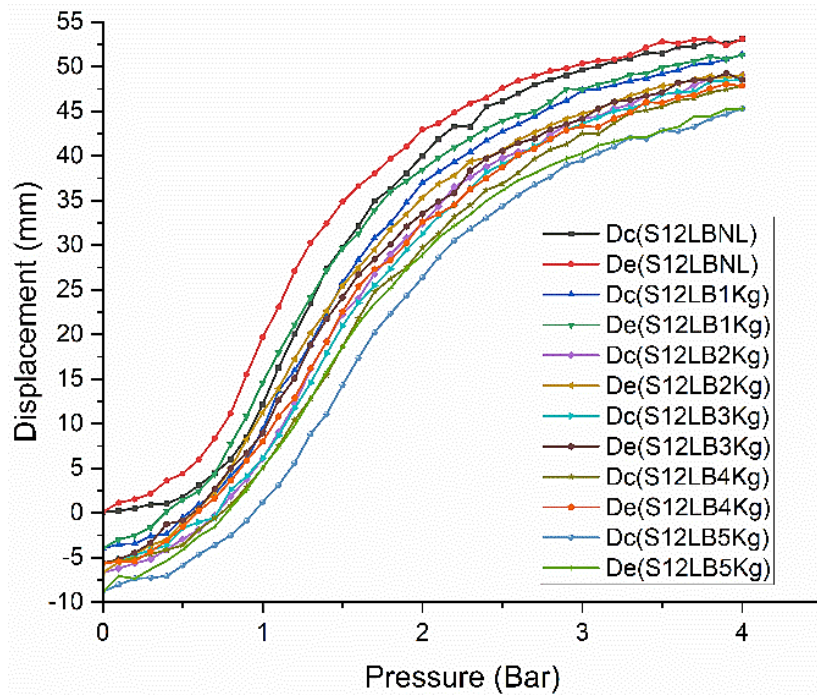
c) L12LB



d) S12LB



e) L12LB (200 mm)



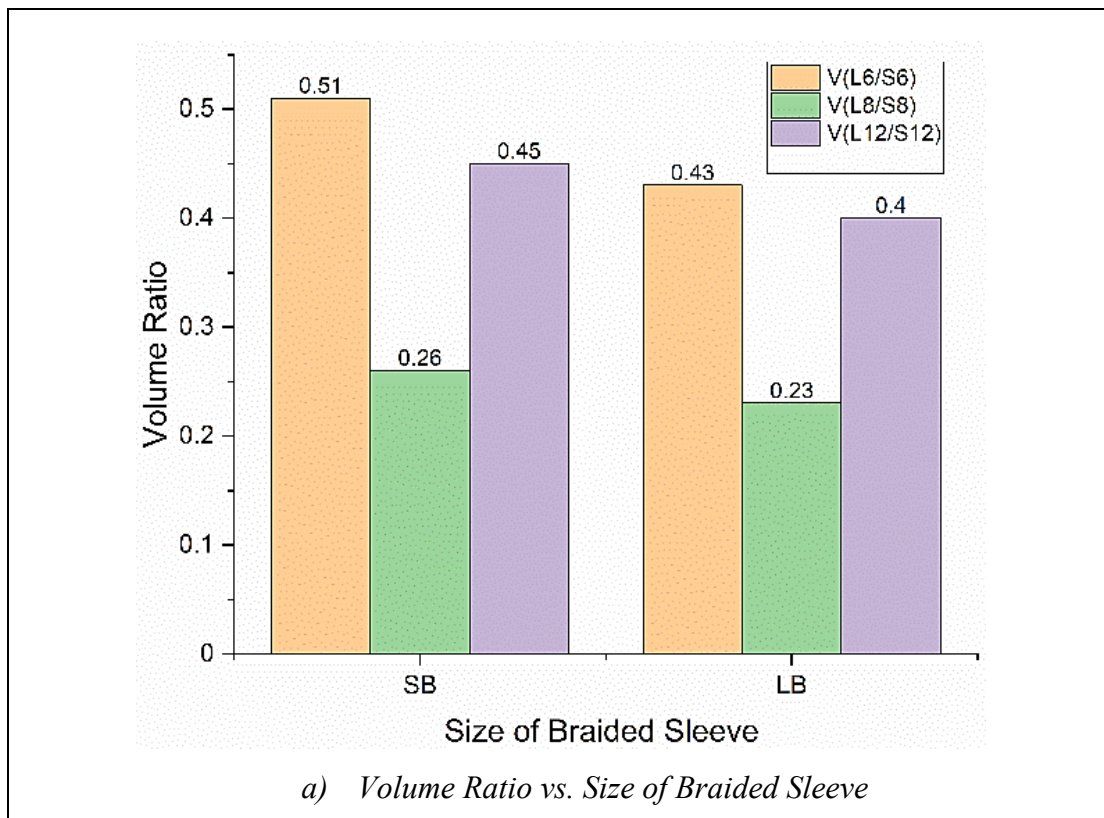
f) S12LB (200 mm)

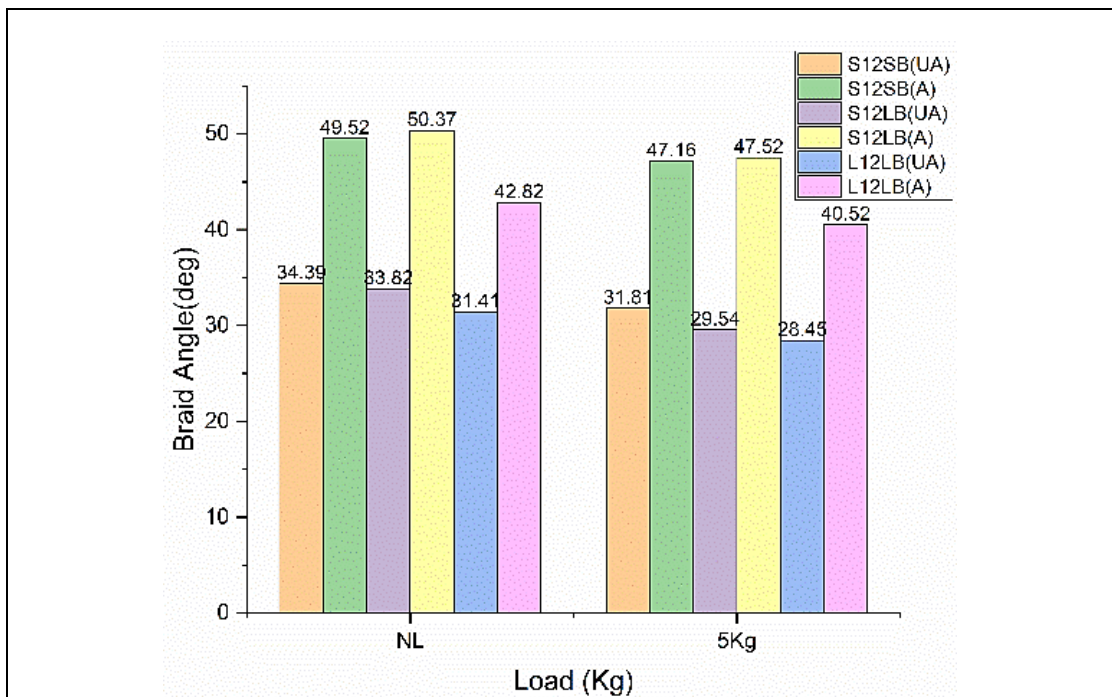
Fig 4.19: Displacement vs Pressure of 12 mm ID Muscles

The plots in Fig 4.18 and Fig 4.19 show the contraction (or deflection) characteristics of the latex and styrene-based muscles' for varying pressures and loading conditions. The striking feature observed from the plots in Fig 4.18 and Fig 4.19 is a steeper slope in the Styrene-based muscles than their latex counterparts, which shows a more gradual slope. The steeper slope in the styrene-based muscles could be the result of the lower tensile modulus of the styrene bladder, which makes it expand rapidly when pressurized air is supplied. The second most prominent feature is the lower hysteresis error in the latex-based muscles compared with the styrene-based muscles. The structure of pneumatic muscle has two components: the bladder and braided sleeve, which causes unavoidable friction, resulting in the hysteresis error between the contraction and extension strokes of the muscle. The hyper-elastic bladder also adds a damping effect, contributing to the muscle actuator's hysteresis error. Similar behaviour is also observed by Hocking et al. (Hocking and Wereley 2012).

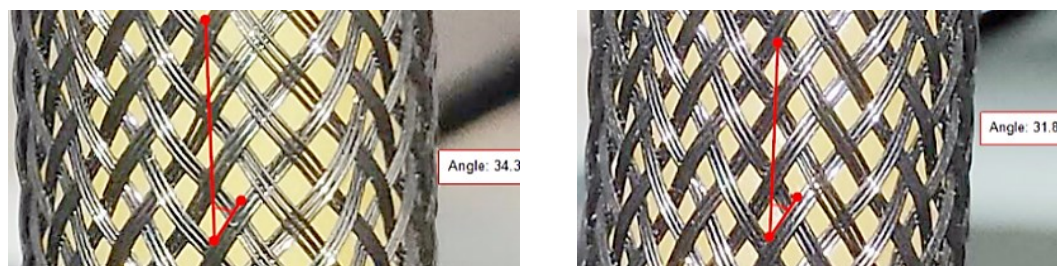
The smaller diameter muscles appear to act differently compared to the larger sizes. Fig 4.18(a) vs Fig 4.18(c) and Fig 4.18(b) vs Fig 4.18(d) show the 6 mm muscle with a small braided sleeve contracting to a larger extent when compared with its larger

braided sleeve counterparts. Comparing the 6 mm latex muscle L6SB with the styrene muscle S6SB shows the styrene muscle produces a more significant contraction. This behaviour of the 6 mm muscle can be explained by two factors: a lower-pressure deadband and a high-volume ratio. Pressure deadband is the initial pressure required for the bladder to fill the gap between the bladder and braided sleeve before producing any axial contraction. The second reason for the behaviour seen in the 6 mm muscle is its high-volume ratio compared to the 8 mm and 12 mm muscles (Table 4.4). Volume ratio is the amount of volume the bladder occupies in the actuator. A high-volume ratio indicated a more significant influence of the bladder on the behaviour of the PMA (Pillsbury et al. 2015). The high-volume ratio and lower tensile modulus of the styrene-based muscles resulted in a higher contraction ratio than its latex counterpart.



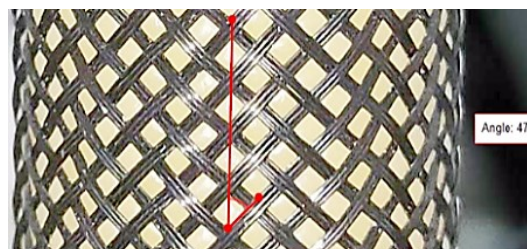


b) Braid Angle For various loading conditions when unactuated (UA) and actuated (A)



NL UA

5Kg UA



5Kg A(4Bar)

c) Braid Angle For various loading conditions when un-actuated and actuated

Fig 4.20: Volume Ratio and Braid Angle of PMA

The muscle with 8 mm ID in Fig 4.18(e-h) shows the most significant contraction compared to the other two muscle sizes (6 mm and 12 mm). This behaviour is due to

its lower volume ratio, as seen in Fig 4.20a, and bladder thickness, shown in Table 4.4, compared to the other muscles (6 mm and 12 mm). A low value of volume ratio indicates a lower hysteresis error and a greater positional accuracy (as shown in Fig 4.18 and 4.19). A bladder having a thinner wall has increased force and contraction characteristics and is also less affected by pressure deadband (Pillsbury et al. 2015). The drawback of using a thinner-walled bladder is its higher pre-extension and lower load-bearing capability (Fig 4.18 e-h).

The 12 mm PMA having a thicker bladder, as shown in Table 4.4, demonstrates a lower contraction and pre-extension. Lower pre-extension also indicates a better load-bearing capacity of the 12 mm muscle when compared to the smaller-sized muscles. The comparison of the latex and styrene-based muscles depicted in Fig 4.19 shows a lower pre-extension in the higher tensile modulus latex-bladder muscles. Comparing Fig 4.19a vs Fig 4.19c and Fig 4.19b vs Fig 4.19d shows that the larger braided sleeve (LB) muscle pre-extends to a larger extent than the smaller braided sleeve (SB) muscle. However, the S12LB muscle has a larger pre-extension (6.04 mm), owing to the lower tensile modulus styrene bladder being stretched to a greater extent due to the wider gap between the bladder and braided sleeve when loaded. The lower tensile modulus also results in the S12 muscle producing a higher contraction (24.03 mm) than its latex counterpart (15.87 mm) when actuated at 4 bar. The volume ratio (Fig 4.20a) of the 12 mm ID muscle is valued between the 6 mm and the 8 mm ID muscles, making it the muscle with balanced compliance and positional accuracy. Compliance is an important feature required in assistive applications, but too much compliance (increase in hysteresis error) can affect the positional accuracy of the muscle. Therefore, it is essential to find a balance between compliance and accuracy.

The contraction percentage of a particular pneumatic muscle actuator is independent of the actuator's length, but the amount of contraction is directly dependent on the actuator's length. Two muscles of a larger length (200 mm) are constructed using the latex (L12LB(200)) and styrene bladders(S12LB(200)) to show the relationship between contraction and muscle length. Comparing Fig 4.19c vs Fig 4.19e, it is evident that the L12LB muscle with a longer form factor (200mm) contracts to a greater extent (36.0 mm) than the latex muscle of 100mm length (20.3 mm). The same behaviour is

seen in the styrene muscles of varying lengths, where S12LB(200) produces a greater contraction (51.7 mm) than its 100 mm counterpart (S12LB)(29.1 mm). Fig 4.19e and 4.19f clearly show a steeper slope in the styrene muscle, thus indicating a smaller actuation pressure range of 1-3 bar (linear relation between displacement vs pressure). The usable pressure range of the latex muscle is much more extensive due to its gradual slope characteristics throughout its operating pressure range. The steeper slope in the styrene PMAs provides the advantage of requiring a smaller power pack (compressor). The styrene-based muscles are also seen to plateau beyond their usable pressure range of 3 bars, indicating that the bladder has reached its maximum limit of radial expansion.

The braid angle is formed by a single braid of the braided sleeve with the muscle's central axis (α in Fig 4.15). The initial braid angle is vital in deciding the amount of contraction and blocked force capability of the pneumatic muscle (Gentry and Wereley 2009). Fig 4.20b and Fig 4.20c show the braid angles for the various muscles constructed. Fig 4.20(c) shows the braid angle variation with load for the S12SB PMA. Fig 4.20c (NL UA) shows the initial braid angle of the muscle in the no-load (NL), unactuated (UA) state. Fig 4.20c (5 Kg UA) shows a decrease in braid angle when loaded with a 5Kg load in the unactuated state. Lastly, Fig 4.20c (5Kg A(4 bar)) shows the same loaded muscle (5 Kg) whose braid angle increases as the muscle is actuated with a 4 bar pressure supply. The plot of braid angle vs load is given in Fig 4.20(b), showing the lower initial braid angle muscle achieving a higher contraction value at 4 bar actuating pressure. As seen in Fig 4.20b, the least initial braid angle for the S12LB muscle is 33.82° compared to its smaller braided sleeve counterpart S12SB, which is 34.39° ; therefore, it contracts to a greater extent, as seen in Fig 4.19b vs Fig 4.19d. Fig 4.20b also indicates the L12LB showing a smaller increase in braid angle (31.41° to 42.82°) as compared to the S12LB muscle (33.82° to 50.37°). The smaller contraction in the L12LB muscle results from its higher tensile modulus bladder. This high tensile modulus does not allow the bladder to expand significantly compared to the S12 bladder having a lower tensile modulus. Therefore, even though the large braided sleeve of both the muscles (S12LB and L12LB) are identical, the property of the bladder restricts the full potential of contraction of the larger braided sleeve. Fig 4.20b also shows a higher amount of pre-extension in the styrene bladders, which is evident from the larger

decrease in angle from no-load (NL) to 5 Kg loading condition seen in the S12LB muscle (33.82° to 29.54°) when compared to the L12LB muscle (31.41° to 28.45°).

The displacement vs pressure study reveals a lower hysteresis error and a gradual slope in the latex-based muscles. The displacement characterization shows that the 8 mm ID muscle produces the highest contraction at no-load using the large braided sleeve. The main downside of the 8 mm muscle is its lower load-bearing capacity, thus making it preferable for applications having to handle negligible payloads. According to the displacement analysis, the 12 mm muscles exhibit the optimal balance of contraction, compliance, and load-carrying capabilities. When actuated with an attached payload, the S12LB muscle shows the highest displacement but suffers from higher hysteresis error and pre-extension. Though the L12LB muscle produces a lower amount of displacement, it demonstrates a lower hysteresis error and a better load-handling capability. The study on the more prominent length muscles shows an increase in the contraction, indicating that a muscle L12LB with better behavioural characteristics produces a more significant contraction by increasing its length to 200 mm.

4.6 PMA Force Characteristics

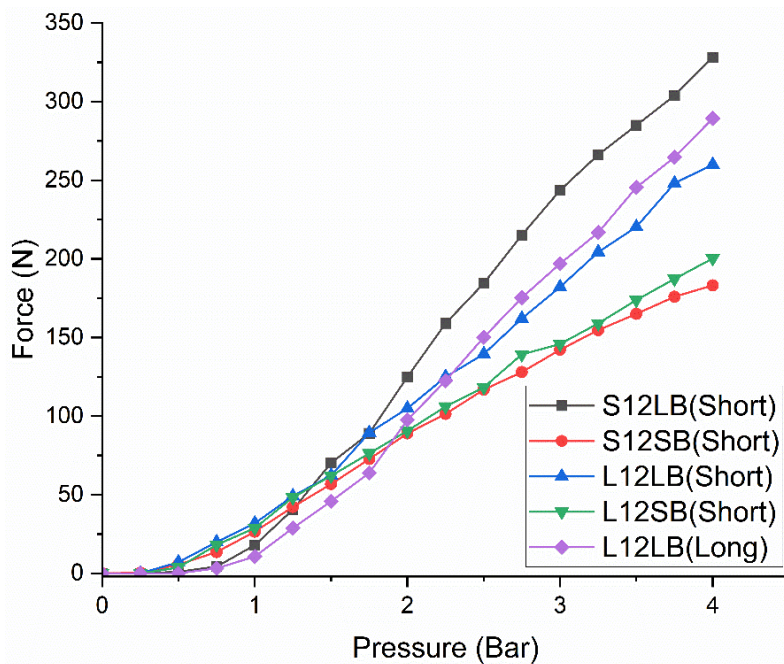


Fig 4.21: Force vs Pressure for 12 mm ID PMA

The pneumatic muscle has two output parameters maximum contraction and maximum blocked force. The PMA's force is influenced by the actuation pressure, contraction ratio, material characteristics, and nominal length (Takosoglu et al. 2016). The force test is conducted by mounting the muscle on the force test rig and evaluating the force characteristics with the rise in actuation pressure. The deflection test reveals a significant contraction in the S12 and L12 muscles. Therefore, the 12 mm ID muscles are the most preferred choice for actuating the exoskeleton. The displacement test also proves better contraction capabilities of the longer-length muscles; therefore, the S12 and L12 muscles of 100 mm (Short) and 200 mm (Long) have been tested and compared. The plot in Fig 4.21 shows that the S12LB muscle produces the highest force (328.2 N) compared to its latex counterpart L12LB (260 N). Among the smaller braided sleeve (SB) muscles (Fig 4.21), it is seen that the L12SB produces a slightly greater force (200.3 N) when compared to the same-sized styrene muscle S12SB (183.2 N). Fig 4.21 also shows the larger length L12LB(Long) muscle (289.3 N), producing a slightly greater force when compared to the L12LB(Short) muscle (260 N).

4.7 Conclusion

In this study, an easy-to-assemble pneumatic muscle actuator is designed, developed, fabricated, and experimentally characterized. The designed PMA highlights the novel end fittings, which are 3D printed and used along with a commercially available bladder and braided sleeve to prove operational versatility. The design and development of a modular test rig helped to conduct all tests with minor adjustments to the test setup. The muscle characterization is carried out w.r.t. parameters such as pressure, contraction ratio, deflection, and force. The force versus contraction ratio is used to give the overall performance of the pneumatic muscle. This test shows that the four developed muscles demonstrate a hysteresis error, but the amount of this error seems to decrease in the larger diameter muscles (10x14 and 12x17). This study also compares the 10x14 pneumatic muscle to a commercial muscle, that exhibits a similar behavioural pattern of force and contraction with pressure variation. The following are the advantages of the developed muscle in comparison to the commercial muscle:

1. The novel end-fittings facilitate the easy and quick assembly and maintenance process of the developed PMA.
2. The novel end-fittings also help to build a PMA of a smaller form factor without compromising its contraction percentage. Since the end-fittings are 3D printed, they even help to realize an overall lightweight and cost-effective PMA.
3. The developed muscles produce 18% more contraction than commercially available one at an actuation pressure of 4 bars.
4. The developed muscles generate 50% higher force than the commercial muscle tested at an actuation pressure of 4 bars. The developed muscles also demonstrate a linear increase in force with the increase in actuation pressure.
5. The developed muscles operate at a lower pressure than the commercial muscle; therefore, they require a smaller power pack (compressor).
6. The 10x14 muscle demonstrates a smaller hysteresis error than the commercial muscle, which is most likely because the bladder occupies a smaller overall volume within the actuator than the other developed and commercial PMAs.
7. The lifecycle test reveals a life of over 200000 cycles at actual loading of 5 kg for the elbow exoskeleton and a maximum operating pressure of 4 bars.

Three mathematical models of the PMA are formulated, evaluated, and compared with the experimental results. Observations made from the force versus contraction plots showed the following:

1. At higher pressure values, the experimental results match the simulation results of the three models, M1, M2, and M3.
2. The plots reveal that the results of model M2 closely resemble the experimental results compared to the other models, M1 and M3. As model M2 considers the bladder's hyper-elastic nature and the braided sleeve's contribution, thus amounting to a more realistic result than models M1 and M3.

This research also studied the effect of material and geometrical characteristics of the bladder and braided sleeve on the behaviour of the pneumatic muscle actuator. The

study revealed a higher contraction in the styrene-based muscles but a lower pre-extension in the latex-based muscles. The comparison study between the Latex and Styrene bladders, showed that the latex-based muscles had a lower hysteresis error, thus making them more accurate and easier to control. The Latex muscles also showed a gradual increase in contraction with an increase in pressure compared to the styrene-based muscle having a steeper slope. The latex muscle's gradual slope and low hysteresis make it a good choice for actuating an assistive exoskeleton with good position accuracy and control.

The S12LB exhibited a good amount of contraction and force characteristics but suffered from hysteresis error and pre-extended to a greater extent when loaded due to the lower tensile modulus of the styrene bladder. Thus, making the styrene-based muscle suitable for space-constrained applications such as a direct actuator-mounted exoskeleton (section 5.1). The 6 mm ID muscles using the smaller braided sleeve had the smallest bladder-braided sleeve gap among all the muscles developed in this study, thus making it more responsive to variation in actuation pressure. The pressure deadband arising from the gap between the bladder and braided sleeve was eliminated by setting an initial actuation pressure equal to the deadband pressure. Therefore, by setting the initial pressure of 0.5 bar for the 12 mm ID muscles, the negative effects of the deadband were eliminated, and the muscle response time was made similar to the 6 mm ID muscles. L12LB muscle is found to be most suitable for assistive applications with negligible space constraints (e.g., indirect cable-actuated exoskeleton discussed in section 5.2), which also had the perfect balance of contraction, force, and compliance. The L12LB also showed a lower hysteresis error and greater load-bearing capacity. The reasons for selecting the L12LB PMA are listed below:

1. The higher tensile modulus of the latex bladder in comparison to the styrene bladder makes the muscle more resistant to payloads (lower pre-extension).
2. The L12LB volume ratio (0.4) is set between the 6 mm and 8 mm ID muscles. Therefore, the hyper-elastic bladder has a balanced effect on the behaviour of this muscle, which results in a good amount of compliance and lower hysteresis error.

3. The larger braided sleeve used in the L12LB muscle has a lower initial braid angle ($\sim 31^\circ$) than the smaller braided sleeve. This lower initial braid angle facilitates the muscle to contract to a greater extent and produce a larger force.
4. The longer length L12LB (L12LB(long)) muscle produces a force and contraction much more significant than its shorter latex counterpart. Therefore, the L12LB(long) muscle is most suitable for the indirectly actuated upper limb exoskeleton application (discussed in section 5.2).
5. The biodegradable nature of the latex bladder also makes it a preferable choice compared to the Styrene bladder. As the bladder is prone to wear and has to be replaced more often than the other components of the PMA, using a biodegradable bladder can be very advantageous. Thus, the latex bladder with the biodegradable 3d printed end-fittings makes the muscle an eco-friendly construction.

5 EXOSKELETON

The exoskeleton is a device to support and impart physical therapy to the user's limbs. The exoskeleton presented here is designed and built to give repetitive therapy to the elbow joint. The elbow exoskeleton is designed with two degrees of freedom, one to flex and the other to pronate the forearm. As the exoskeleton is intended for a medical application, it is designed for lightweight, modular, and safety criteria. The most preferable actuator for this application is the pneumatic muscle actuator (PMA). As discussed in the previous section, the PMA is inherently compliant, lightweight, and safe to be used in a sterile medical environment. The pneumatic muscles have certain deficiencies, such as antagonistic nature, hysteresis, and inability to produce a perfect linear actuation. The exoskeleton has to be designed to incorporate a particular mechanism and method to overcome or reduce these limitations of the pneumatic muscle actuator to make it suitable for the rehabilitation application. At first, an exoskeleton with a direct actuator mounting arrangement is designed to test the PMA whose design is discussed in the previous section. The direct actuator-mounted exoskeleton's performance is analyzed when actuated with the newly developed pneumatic muscle actuator. The tests reveal a few shortfalls of the existing direct actuated exoskeleton, which led to the development of an improved exoskeleton system called the EXPHYSIO. EXPHYSIO is short for 'Exoskeleton for Physiotherapy,' an indirectly actuated exoskeleton system to impart repetitive therapy to the elbow joint.

5.1 Design and Development of an Exoskeleton for the Actuation of the Elbow Joint

The upper extremity of a stroke patient is known to be weak and delicate. Therefore, it is essential to design a structurally strong and lightweight structure. The exoskeleton also needs to be designed to be modular in construction to accommodate the varying anthropometric dimensions of the Indian demographic, with minor adjustments to the structure. The aluminium t-slot is a lightweight and modular aluminium extrusion with T-shaped slots on its face, thus making it easy to build various forms and adjust with the help of special modular fittings (e.g., T-nuts).

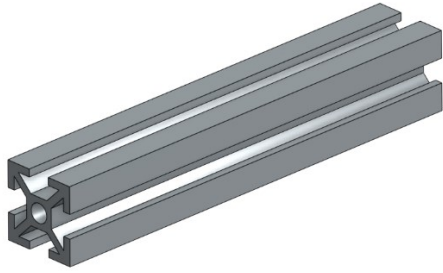


Fig 5.1: Aluminium T-slot (Isometric View)

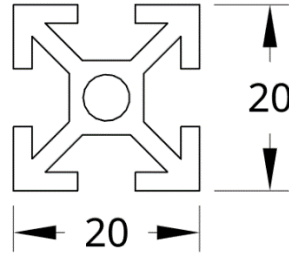
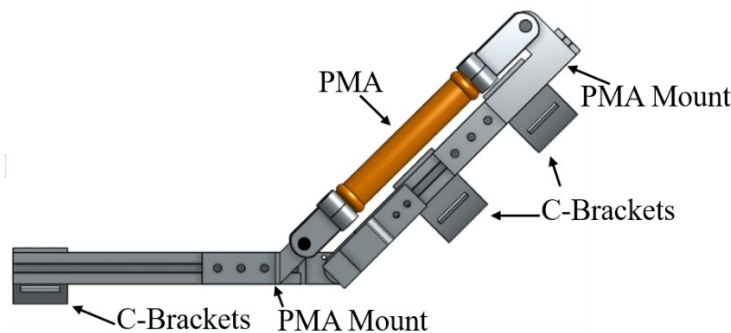


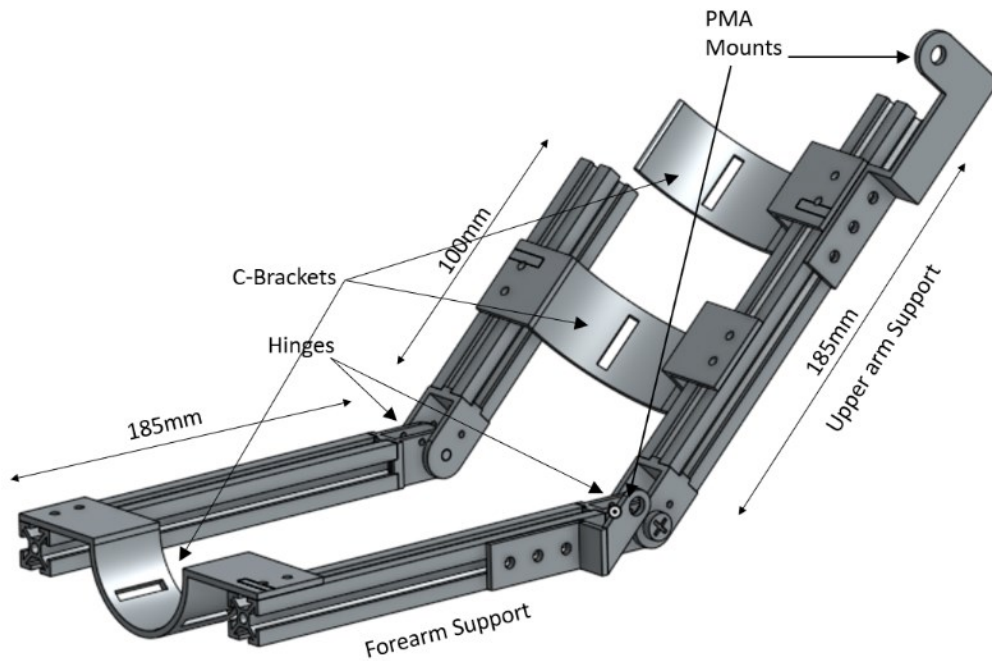
Fig 5.2: Aluminium T-slot (Cross-section)

The smallest size of the most commonly available commercial T-slot of 20 mm X 20 mm section is shown in Fig 5.1 and 5.2. This size of T-slot is most appropriate to build the upper extremity exoskeleton as it is lightweight yet sturdy enough to support the upper extremity.

As previously discussed, the exoskeleton's size should be universal as far as possible to fit most Indian patients. The anthropometric data of the Indian population (Chakrabarti Debkumar 1999) in Table 5.1 helps to decide the required dimensional variation of the structural setup. The data suggests that the minimum size of an Indian forearm is 186 mm, and that of the upper arm is 234 mm. The exoskeleton has been designed with a forearm and upper arm support of 185 mm as per the anthropometric data, making it a universal fit for most Indian upper extremities. The upper arm inner support is kept at 100 mm due to the space restriction between the upper arm and the torso, which would otherwise be uncomfortable for the user. The primary assembly of the exoskeleton is shown in Fig 5.3a.



a) Direct actuator mounted exoskeleton



b) Design features and dimensions of the direct actuator mounted exoskeleton

Fig 5.3: Designed Exoskeleton Assembly with direct actuator mounting arrangement

The 20 mm x 20 mm aluminium T-slots make up the main frame of the exoskeleton structure. Three C-shaped brackets depicted in Fig 5.3 (a & b) have been designed to mount the patient's arm to the exoskeleton. These C-brackets function as load-bearing members that transfer the load of the patient's arm onto the exoskeleton frame. The design includes two C-brackets at the upper arm and one at the forearm, whose position can be easily adjusted depending on the patient's anthropometric data. Fig 5.4 demonstrates the fabrication process of the C-bracket. The fabrication of the C-brackets involves precisely laser cutting a 3 mm stainless steel plate to form rectangular sections of five lengths: "extra-small," "small," "medium," "large," and "extra-large," depending on the diameter of the patient's upper limb, as shown in Table 5.2. Slots are then cut into the rectangular sections to accommodate the Velcro band, which is used to fasten the patient's arm to the exoskeleton. The rectangular sections are bent into a semi-circular shape of the required sizes depending on the anthropometric data (Chakrabarti Debkumar 1999) in Table 5.1. The ends of these semi-circular sections are flattened, and two holes are punched to mount these C-brackets to the aluminium frame of the exoskeleton.

Table 5.1: Anthropometric data of upper extremity

Part of the Upper Extremity (UE)	Minimum Size	Maximum Size
Elbow	62.10 mm	97.13 mm
Forearm	58.91 mm	98.72 mm
Wrist	41.40 mm	60.82 mm
Arm Length	234 mm	395 mm
Forearm Length	186 mm	350 mm
Wrist to Fist Length	24 mm	83 mm

Table 5.2: Sizes of C-Brackets

Part of UE\Size	XS	S	M	L	XL
Upper arm\Forearm	60 mm	70 mm	80 mm	90 mm	120 mm

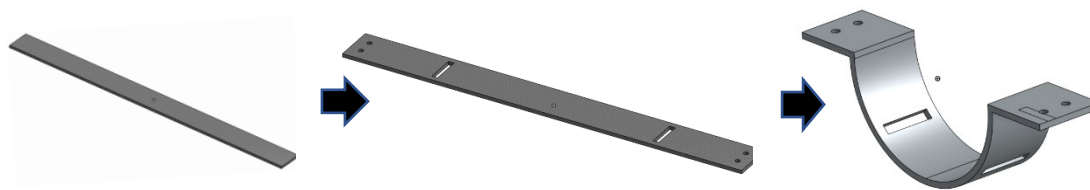


Fig 5.4: C-Bracket manufacturing process

As the exoskeleton is to be actuated using pneumatic muscles, which bulge radially to produce a force in the axial direction, the placement and mounting locations of the muscles are crucial. Z-shaped PMA mounts are designed, as shown in Fig 5.5, to prevent the inflated pneumatic actuator from coming in contact with the patient's arm. These PMA mounts are designed to keep the pneumatic muscle at an offset from the main structure, as shown in Fig 5.3, while still being able to place it close to the elbow

fulcrum for maximum mechanical advantage. The offset distance has been decided based on the amount of the muscle bulge at maximum actuating pressure (4 bar). Experimental data shows that the pneumatic muscle bulged radially by 2 mm when actuated. Thus, the mounts are designed with an offset of 5 mm, allowing for their safe operation while flexing the exoskeleton. For the PMAs to produce maximum elbow joint flexion, their location at the forearm and upper arm are essential; as a result, the PMA mounts are strategically fixed. One actuator mount is positioned at the extreme end of the upper arm aluminium section. In contrast to this, the second mount is fixed onto the forearm section close to the hinge to achieve maximum angular deflection of the elbow joint.

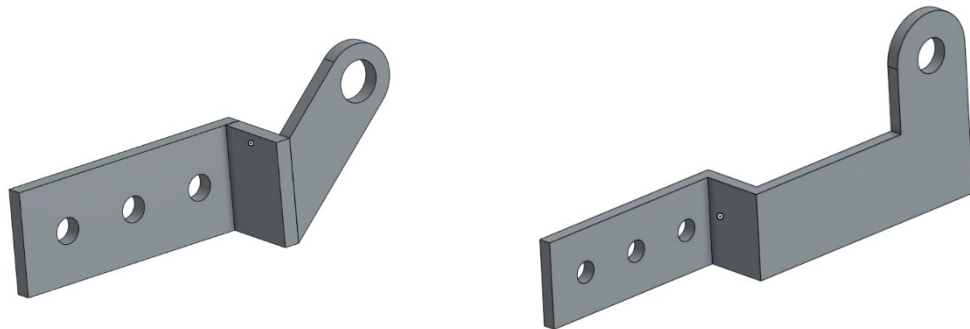


Fig 5.5: PMA Mounts; forearm mount (left), upper arm mount (right)

The forearm mount is designed with a tilt of 135° , while the upper arm mount is angled at 90° to allow free rotation of the pneumatic muscle about the PMA mounts when actuated. The fabrication process of the PMA mounts is similar to the C-brackets; these have been made from the same 3 mm stainless steel plate. The Z-shaped mounts are provided with three holes to attach these mounts to the exoskeleton frame. The Z-mounts also have a larger hole to accommodate a pin joint to mount the end-fitting of the PMA, forming a 1 DOF rotary joint.

The discussion of the exoskeleton structure remains incomplete without the hinge, which forms an integral part of the design. The hinge is designed to join the forearm support with the upper arm, thus allowing the elbow joint a one-degree of freedom motion (flexion/extension). Initially, a commercially available hinge shown in Fig 5.6 was used, but this resulted in a smaller range of angular motion (0° - 90°); thus, a hinge with an appropriate degree of movement for the elbow joint had to be designed.

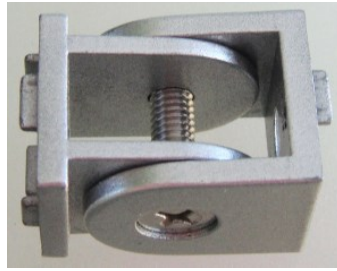


Fig 5.6: Commercial Hinge

Fig 5.6 shows the commercial hinge. It has a short operating range due to its short legs, which limit its motion to 90° . Therefore, the hinge for the elbow exoskeleton is designed with longer legs. The length of the leg of the inner section measured from the face attached to the aluminium T-slot to the fulcrum is 21 mm, while that of the outer section is 19 mm. These changes in the design allow a 220° of motion (110° clockwise and 110° anticlockwise), which is greater than the required range of motion of the normal elbow joint of 110° in the clockwise direction. The back plate of both the inner and outer sections have four protrusions that secure the hinge to the T-slot, thus preventing any unwanted rotary motion. All these design considerations are mainly with reference to the provision of free movement to the elbow joint. The new hinge design shown in Fig 5.7 also addresses other deficiencies of the exoskeleton structure's overall working.

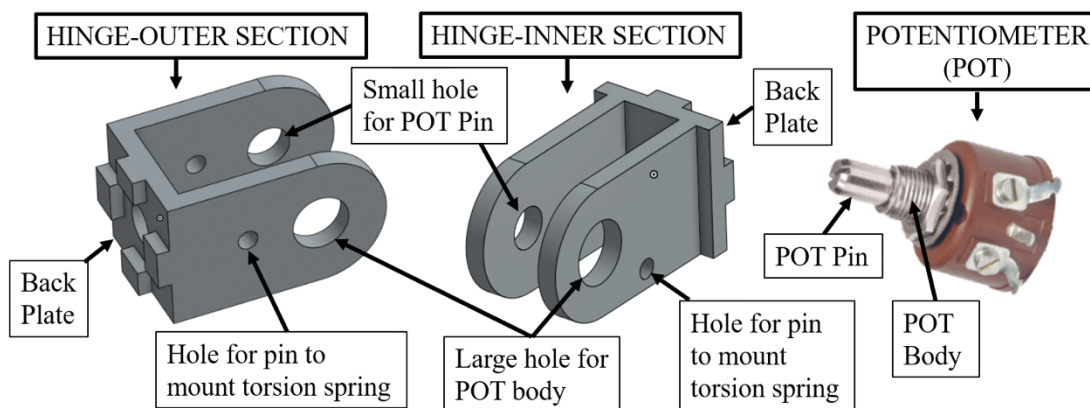


Fig 5.7: Hinge Design with shaft type potentiometer

Pneumatic muscle actuators are compliant, which is an ideal choice for manipulating the fragile upper extremity of stroke patients. Though compliance is an advantage for assistive applications, it resulted in an actuator that is difficult to be controlled accurately. In order to accurately control the position of the exoskeleton arm using the pneumatic muscle actuator, a position feedback sensor is required. The hinge forms the best location to position the rotary feedback sensor as it is the fulcrum about which the forearm rotates with respect to the upper arm. A shaft-type potentiometer shown in Fig 5.7 is used, with its body attached to the outer section of the hinge, while its rod/POT pin has an interference fit with the inner section. Thus, the rod of the potentiometer acts as the pin about which the hinge rotates. The method of using a shaft-type potentiometer gives accurate angular measurements. Still, it compromises the strength of the hinge as one hole in both the hinge sections has to be large enough to allow the body of the potentiometer to fit.

As discussed in the previous section, the exoskeleton is being actuated using pneumatic muscle actuators. A significant drawback of pneumatic muscles is their inability to produce force in both strokes (antagonistic nature); thus, a mechanism is required to bring this actuator back to its initial position. Several past researchers used two pneumatic muscles, one to flex and another to extend the elbow joint. Using two pneumatic muscles to actuate a single anatomical joint result in a bulky system and increases the overall cost, as each pneumatic muscle requires a separate valve to control its operation. In this research, the antagonistic nature of the pneumatic muscle actuator is resolved in a novel way. Here a torsion spring is used to act in the extension stroke of the pneumatic muscle. The hinge is designed to incorporate a torsion spring, providing a reverse torque at about 110° of elbow flexion. At angles greater than 90° (Fig 5.8), the forearm can extend with gravity when air from the pneumatic muscle is released. Therefore, the torsion spring is made to act at about 110° to build sufficient torque to extend the forearm against gravity when the angle between the forearm and upper arm is less than 90° (Fig 5.9).

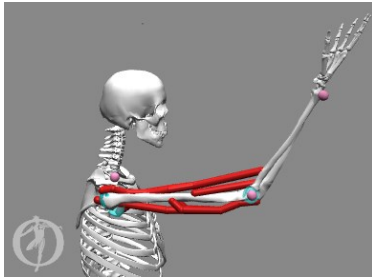


Fig 5.8: Elbow Flexion greater than 90deg (gravity assisted extension)

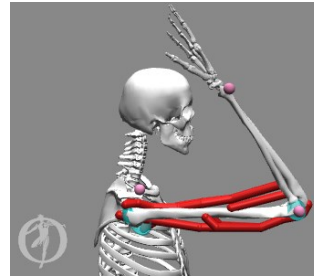


Fig 5.9: Elbow Flexion less than 90deg (Extension requires force against gravity)

The basis for the torsion spring design is finding the torque required to lift the forearm. The free-body diagram of the forearm and the forearm exoskeleton support is shown in Fig 5.10.

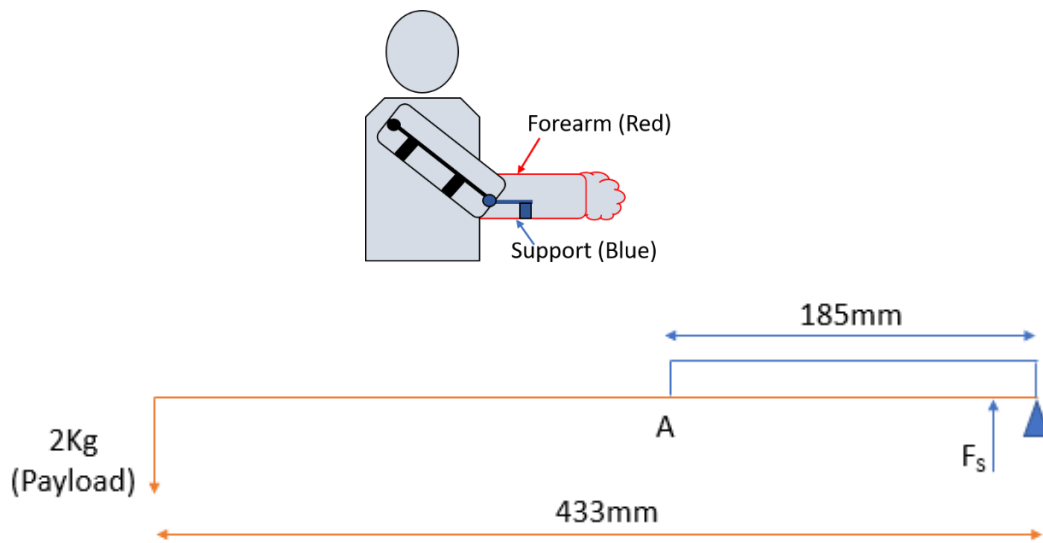


Fig 5.10: FBD of forearm-exoskeleton pair for calculation of required spring torque

The beam represented in red colour is the patient's forearm with a self-weight assumed to have a uniformly distributed load (UDL) of 0.0049 N/mm. In contrast, the beam represented by blue colour is the forearm exoskeleton support with a self-weight given by a UDL of 0.0098 N/mm. Point 'A' represents the point at which the C-bracket of the exoskeleton supports the forearm. The free body diagram shown in Fig 5.11 is drawn to find the reaction R_A , representing the forearm's effective force on the exoskeleton support.

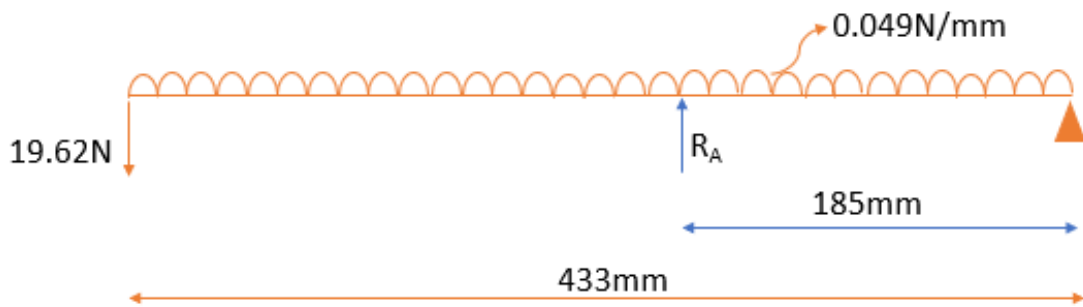


Fig 5.11: FBD of the forearm

The free body diagram in the Fig 5.11 is further simplified in Fig 5.12.

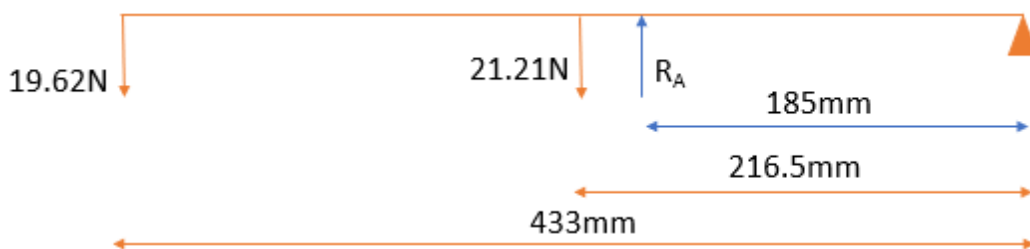


Fig 5.12: Simplified FBD of the forearm

Solving for reaction R_A in Fig 5.12,

$$19.62 \times 433 + 21.3 \times 216.5 = R_A \times 185$$

Therefore, $R_A = 70.73 \text{ N}$

Applying the reaction R_A onto the support member, as shown in Fig 5.13, the required spring torque R_S is calculated.

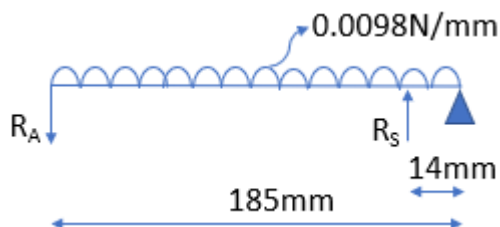


Fig 5.13: FBD of exoskeleton support for the forearm

Fig 5.14 represents the simplified FBD shown in Fig 5.13.

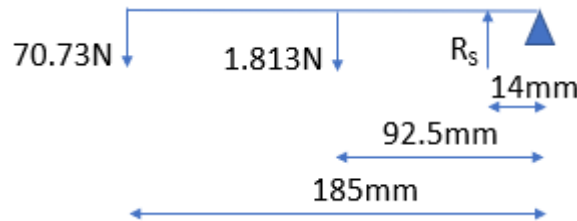


Fig 5.14: FBD of the exoskeleton support for the forearm

Solving for R_s , we get

$$70.73 \times 185 + 1.813 \times 92.5 = R_s \times 14$$

$$R_s = 946.62\text{N}$$

The required spring torque = $R_s \times 14 \text{ mm} = 13252.75 \text{ Nmm}$

The spring is designed with the parameters given in Table 5.3 to generate the required torque as calculated above.

Table 5.3: Torsion Spring Design parameters

SPRING PARAMETERS	VALUES
Material	ASTM A228 Music Wire
Wire Diameter	3 mm
Outer Diameter	22 mm
Total Coils	3.7
Spring Rate	64.99 Nmm/degree

The spring rate of the designed spring given in Table 5.3 is 64.99 Nmm/degree. Thus, the torque built up by the spring when actuated to 0° (maximum flexion angle assumed between the arm and forearm) from 110° (the angle at which spring is activated) is 7148.9 Nmm. This value of spring torque is much less compared to the required torque. The exoskeleton is designed with two hinges on either side of the elbow joint, and each hinge is designed to house one torsion spring. Therefore, the two springs together

develop a combined torque of 14297.8 Nmm, which is higher than the required value calculated.

5.1.1 Testing the PMA on the Designed Elbow Exoskeleton

Plots in Fig 5.15 and 5.16 show the elbow exoskeleton's angular deflection behaviour versus pressure when it is actuated using the S12LB PMA at various loading conditions.

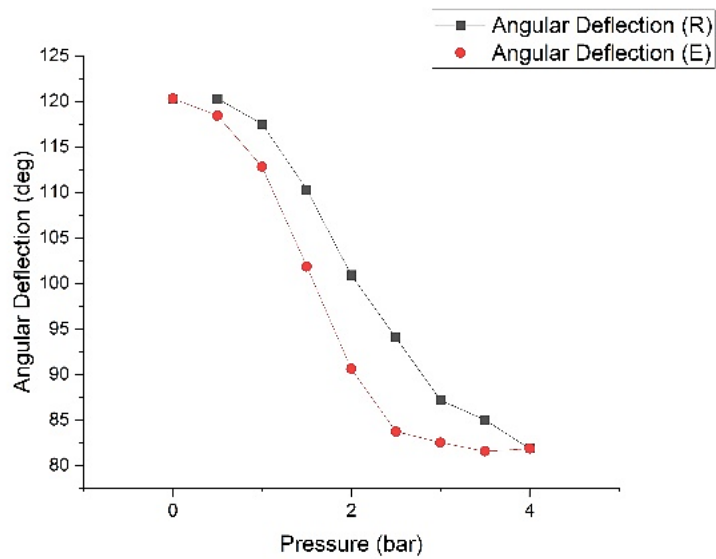


Fig 5.15: Pressure vs deflection with no load

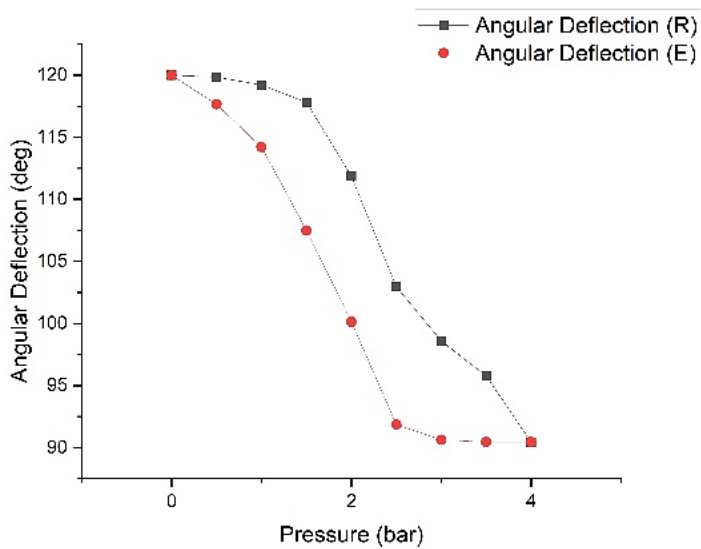


Fig 5.16: Pressure vs Deflection with an attached load

Fig 5.15 gives the angular deflection of the exoskeleton for various pressure values, while Fig 5.16 shows the angular deflection with a simulated arm (load) attached. The integrated angular position sensor in the hinge senses the angular position of the forearm with respect to the upper arm. The angle sensor is connected to an ATmega2560 controller board that records the angular deflection at different incremental pressure values, as depicted in Fig 5.17. From the Plots in Figures 5.15 and 5.16, it is evident that the hysteresis widens as the load, which represents the patient's arm on the exoskeleton, increases. This occurs due to the hyper-elastic nature of the PMA's bladder. A slight reduction in the angular deflection of the elbow joint is observed in Fig 5.16 compared to Fig 5.15. This reduction results from the pre-extension of the muscle due to the added payload. Another important observation is the linear relation of pressure and angular deflection between pressures of 1bar and 3bar, while the plot tends to flatten at the ends. The plateauing at the beginning and end of the plots indicates that the muscle is building up a force to overcome the weight of the exoskeleton structure and the added payload. The integrated angular sensor within the hinge design makes it a suitable feedback sensor for the accurate angular flexion control of the exoskeleton.

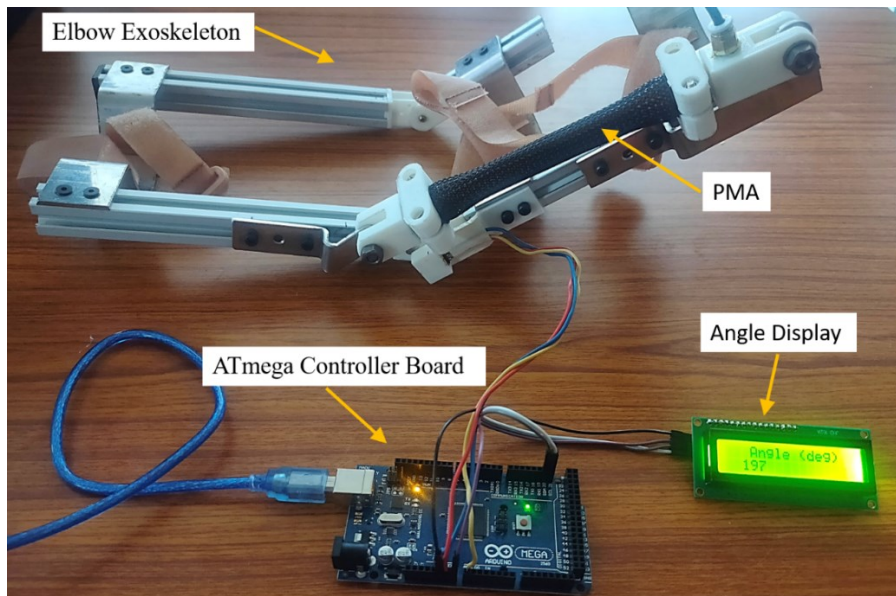


Fig 5.17: Experimental setup for determining pressure vs. angular deflection characteristics of the exoskeleton

5.2 Improved Exoskeleton Design

Fig 5.3 shows the initial exoskeleton configuration with PMAs directly attached to the exoskeleton frame using PMA mounts. The preliminary tests revealed a few limitations of the direct actuator-mounted exoskeleton that must be addressed and are listed below:

1. The developed PMA, though designed shorter than the commercial PMA, still occupies a considerable bulk of the exoskeleton structure, especially when the user's forearm is short.
2. Adding additional degrees of freedom (Pronation/Supination) becomes difficult due to space constraints.
3. Adding additional actuators in a parallel configuration to compensate for higher loads is difficult in the direct arrangement.
4. A safety concern that could arise as a consequence of placing the muscle actuators too close to the user is it being tampered with or an accidental rupture of the bladder, whose sound could startle the patient.
5. Accurate position sensing of the pneumatic muscle actuator is complex in the direct configuration.

A new exoskeleton system involving an actuator block with cable arrangement in Fig 5.18 and 5.19 is designed to avoid the disadvantages of the direct muscle-mounted arrangement shown in Fig 5.3 and 5.19. The new design is called the EXPHYSIO, or exoskeleton for physiotherapy, depicted in Fig 5.18.

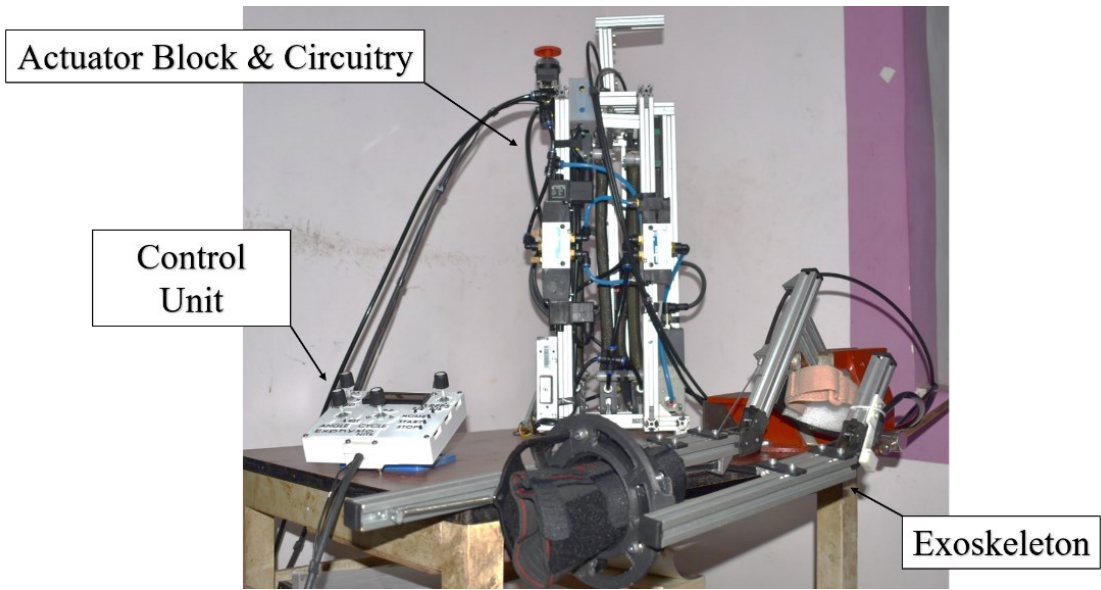


Fig 5.18: EXPHYRIO (Exoskeleton for Physiotherapy) System

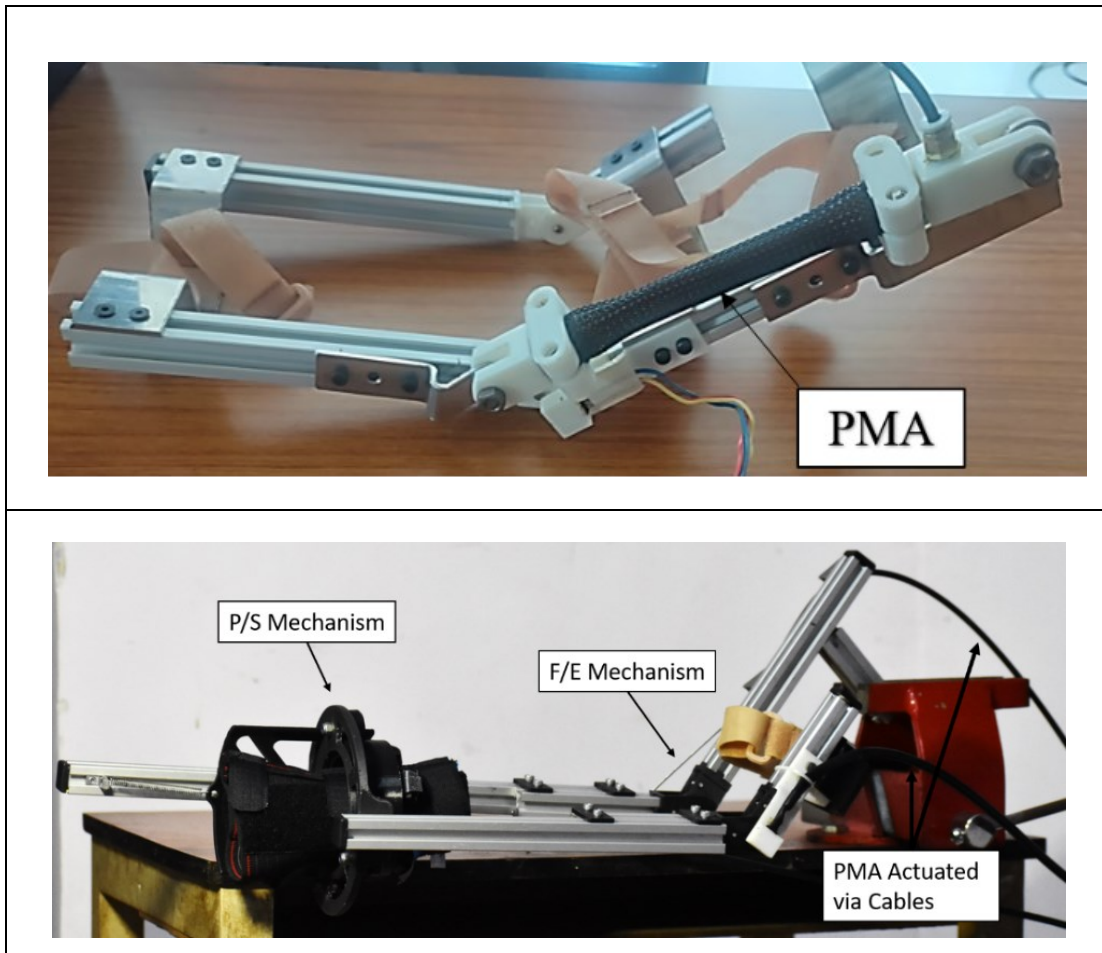


Fig 5.19: Exoskeleton with Direct (Top) vs Indirect (Bottom) actuation

The EXPHYSIO mainly consists of three components:

1. The *exoskeleton* that is attached to the user's upper limb.
2. The *actuator block* that houses the muscles driving the exoskeleton.
3. The *control unit* which is used to program and control the EXPHYSIO.

5.2.1 The Exoskeleton of the EXPHYSIO

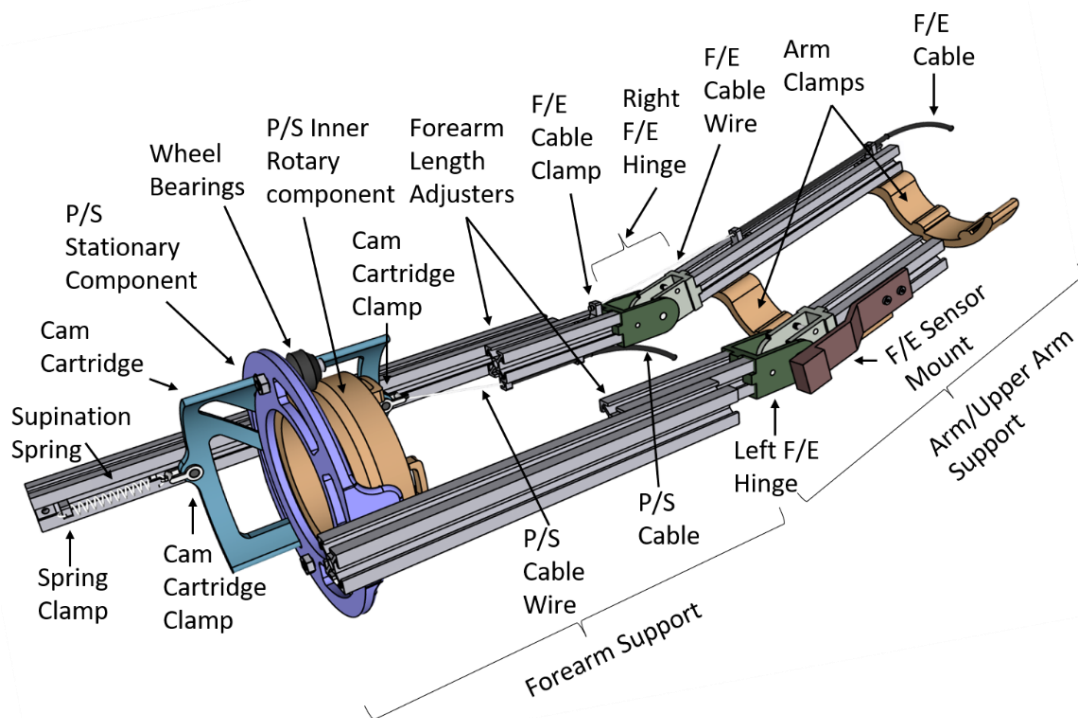


Fig 5.20: Exoskeleton of the EXPHYSIO

The exoskeleton is redesigned to accommodate both degrees of freedom viz F/E and P/S in a single device, as shown in Fig 5.20. In this design, the basic structure of the exoskeleton remains the same, with 20x20 aluminium sections forming the main structural element. The upper arm is almost identical to the directly actuated exoskeleton except for the two 3D-printed arm clamps. The arm clamps depicted in Fig 5.21 are 3D printed using carbon fibre PLA to make the structure lighter by 0.5 kg compared to the direct actuator mounted exoskeleton of weight 1.5 kg. The clamps are designed in a C-shape, with parallel flat ends to accommodate holes in order to bolt them to the upper arm exoskeleton frame. The C-clamps are attached to the two t-slot

sections on either side of the arm, ensuring that the two sections are maintained parallel and in the correct position. Two raised portions with grooves are designed on the inner surface of the C-clamps to attach the Velcro straps, securing the user's upper arm to the exoskeleton.

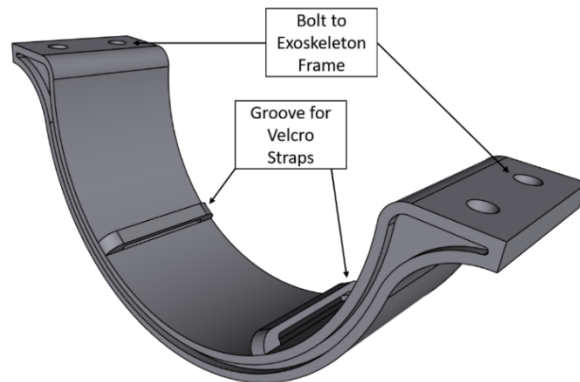
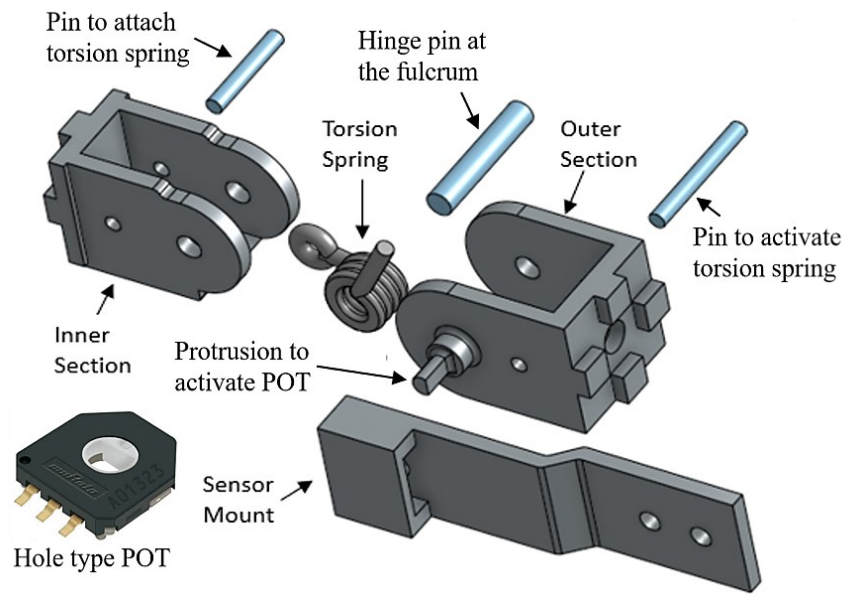


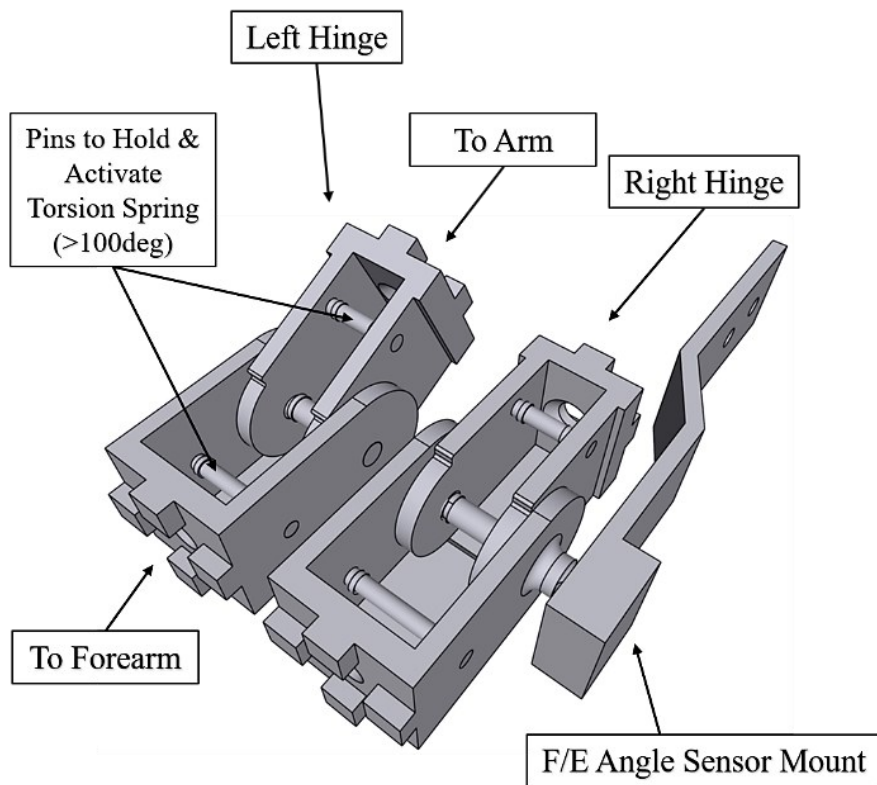
Fig 5.21: New design of 3D Printed Clamps

The hinge is the component that connects the upper arm support structure to the forearm. The hinge of the exoskeleton is responsible for achieving the flexion and extension of the elbow joint, thus giving the system one degree of freedom. The newly designed exoskeleton has two hinges, the left and the right hinge, located at either side of the elbow joint. The main difference between the two hinges is the flexion angle sensing arrangement in the left hinge, which is absent in the right counterpart.

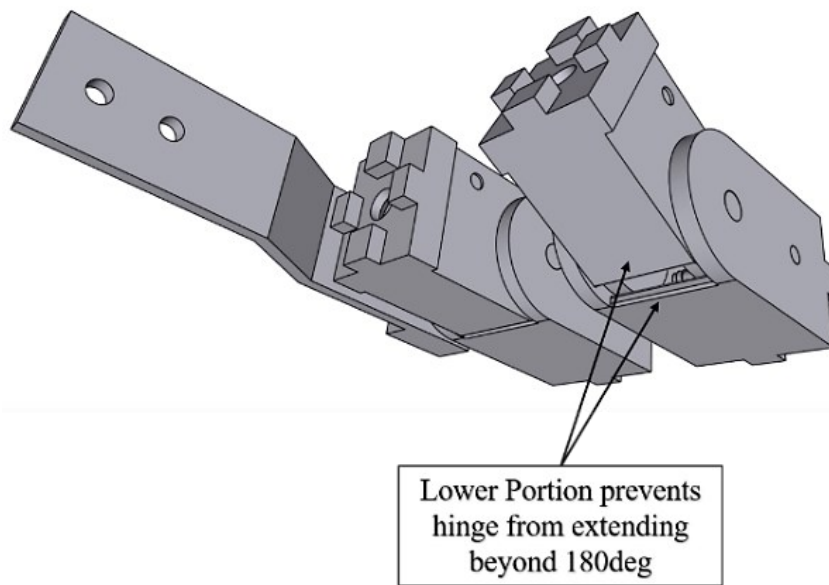
The hinge in the previously designed direct actuator-mounted exoskeleton shows a few drawbacks, such as lower strength and lack of proper angle sensing mechanism. As a result, a new hinge is designed. The new hinge shown in Fig 5.22 has an outer and inner component like the previous design, with a few design improvements, such as larger flexion ROM, an accurate angle sensing mechanism, and improved safety.



a) Exploded view of the newly designed hinge



b) Assembled view of the newly designed hinge



c) The safety feature of the newly designed hinge

Fig 5.22: New 3D printed hinge

The F/E angle arrangement consists of a hole-type rotary potentiometer from Murata with a measurement range of 0° to 333.3° . The potentiometer is mounted in the F/E angle mount or sensor mount shown in Fig 5.22a attached to the exoskeleton's arm support frame. The potentiometer is engaged by a small semi-circular protrusion designed in the hinge's forearm portion, resulting in the POT's rotation as the user's forearm is actuated in flexion. The rotating POT records the accurate value of elbow flexion in real-time. The hinge also uses aluminium pins that support and actuate a torsion spring responsible for the extension of the elbow joint due to the antagonistic nature of the PMA. The pins were arranged strategically to activate the spring at 110° of forearm flexion, therefore allowing to build a sufficient amount of reverse torque in both hinges to extend the forearm when it is flexed below 90° as depicted in Fig 5.9b. The hinges also have a design safety feature in Fig 5.22c, preventing the user's forearm from extending beyond 180° . This angle restriction is provided by the lower flat portion of the hinge sections, which restrict the inner and outer hinge sections from extending beyond 180° . The hinge body is printed in Carbon-fibre PLA, while the pins are machined in Aluminium, thus making them lightweight and allowing them to sustain the torque built up by the torsion spring supported by these aluminium pins.

The forearm support of the new exoskeleton is designed differently from the direct actuator-mounted model to accommodate the pronation/supination and length adjustment mechanisms. As per the Indian Anthropometric data published by Chakrabarti Debkumar (Chakrabarti Debkumar 1999), the forearm length shown in Table 5.1 ranged from 186 mm to 234 mm; therefore, to accommodate the various sizes, two mechanisms are designed in the forearm exoskeleton structure. The P/S mechanism is the exoskeleton's only point supporting the forearm. Therefore, it is designed with the flexibility to adjust its position along the forearm exoskeleton frame. Accordingly, depending on the length of the user's forearm, the position of the P/S mechanism can be adjusted. The amount of length adjustment possible at the P/S mechanism is restricted by the length of the cam-cartridge (of the P/S mechanism), which requires enough space to move when actuated to pronate the user's forearm. Therefore, two additional length adjustment plates called 'forearm length adjusters' shown in Fig 5.20 are provided to make more extensive length adjustments, giving the additional length adjustment capability to the new exoskeleton.

The Pronation/Supination(P/S) mechanism is an essential feature of the new exoskeleton design, and its design is inspired by the cam follower mechanism. The P/S mechanism is the main component of the exoskeleton's novel design, which is depicted in Fig 5.23(a-f). Previous research reports that the pronation/supination mechanism is achieved through a rotating handle held by the user to pronate the elbow joint, therefore restricting the movement of the hand and fingers. This prevents physical therapy to the fingers, hand, and wrist, especially while training for activities of daily living such as grasping or strength training such as squeezing. The novel P/S mechanism designed in the EXPHYSIO performs the pronation and supination of the user's elbow joint without hindering the motion of the user's hand and fingers. The pronation/supination mechanism is depicted in Fig 5.20. Figures 5.20 and 5.23e clearly show the assembled P/S mechanism, consisting of three sections. The outer stationary section shown in Fig 5.23a is attached to the forearm frame of the exoskeleton. The inner rotary section depicted in Fig 5.23c and f is attached to the user's wrist, and a sliding cam cartridge in Fig 5.23d converts the linear motion of the muscle to the rotation of the user's forearm.

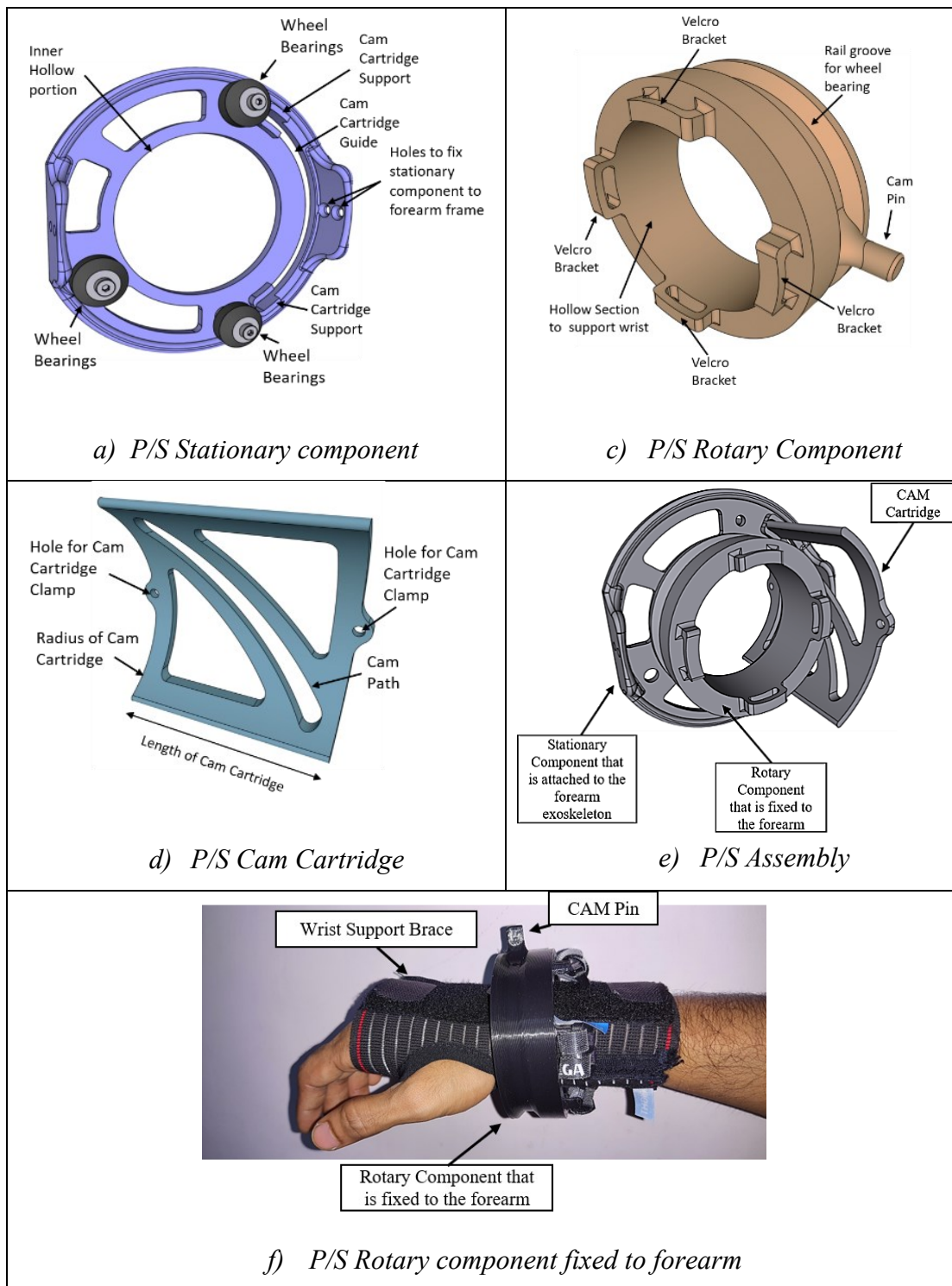


Fig 5.23: Novel Pronation/Supination Mechanism

The stationary component of the P/S mechanism shown in Fig 5.23a has two pairs of holes on raised portions on either side, which are used to mount it to the forearm section of the exoskeleton, as shown in Fig 5.20. The stationary component has three v-wheel

bearings positioned around its hollow centre section, which allow the free rotation of the inner rotary component mounted between the v-wheel bearings. One of the three v-wheel bearings is fixed using an eccentric nut which allows the position of the v-wheel to be easily adjusted with respect to the other two bearings; this allows to adjust the compression force of the v-wheels on the P/S inner rotary component. The stationary component also has a cam-guide that allows the cam-cartridge to slide along easily while being actuated by the contracting muscle via the P/S cable. The ends of the cam guide have a raised portion depicted as 'cam cartridge support,' which offers support to the cam-cartridge as it slides through the cam-guide. The hollow centre of the stationary component has a radius slightly larger than the hole in the rotary component, allowing the user's hand to easily fit through it without causing discomfort to the pronating forearm.

The second important component of the novel pronation/supination mechanism is the inner rotary component shown in Fig 5.23(c and f). The inner rotary component is the section of the pronation/supination mechanism attached to the user's forearm via a wrist brace, as shown in Fig 5.23f. The V-shaped rail groove along the circumference of the rotary component acts as a guide rail for the v-wheel bearings of the stationary component. The inner rotary component, with the v-rail assembled between the three v-wheel bearings, is shown in Fig 5.20 and 5.23e. These v-wheel bearings allow the inner rotary component to easily rotate about its central axis. The cam pin is a protrusion on the circumference of the inner rotary component that glides along the cam path of the cam-cartridge, resulting in the rotation of the inner rotary component. The four velcro brackets depicted in Fig 5.23b are used to attach the user's forearm to the inner rotary component using Velcro straps attached to the wrist brace that is worn over the user's hand and wrist. The inner rotary component also has a hollow section designed with a diameter large enough to fit most Indian wrists.

The last component of the novel pronation/supination mechanism is the cam-cartridge shown in Fig 5.23d. The cam-cartridge is a curved plate structure with a radius equal to the arch radius of the cam-cartridge guide of the stationary component. The main feature of the cam-cartridge is the cam-path. The cam-path is the portion along which the protruding cam pin of the inner rotary component glides as the cam-cartridge is

moved forward or backward, thus producing the rotation of the inner rotary section, which is free to rotate about the v-wheel bearings on the P/S stationary component. The slope of the cam-path plays a vital role in deciding the speed and amount of rotation of the inner rotary component. A steeper cam-path produces a greater rotation of the inner rotary component with a smaller movement of the cam-cartridge. A steeper slope also results in a cam-cartridge of shorter overall length. The cam-cartridge has two holes at either end, shown in Fig 5.23d as 'hole for cam-cartridge clamp.' The purpose of the holes is evident and shown in Fig 5.20. The left cam cartridge clamp is attached to a tension spring which compensates for the antagonistic nature of the P/S pneumatic muscle and cable mechanism. The spring develops tension when the cam-cartridge is pulled by the retracting P/S muscle and acts to supinate the user's forearm when air from the muscle is released. The other end of the tension spring is attached to the forearm frame of the exoskeleton using the spring clamp depicted in Fig 5.20. The other cam cartridge clamp is connected to the pneumatic muscle in the actuator block via the P/S cable.

The cam-cartridge forms an essential component of the P/S mechanism, which decides the range and rotation rate of the inner rotary component. A steeper cam profile results in a faster rate of pronation and supination of the forearm. A cam cartridge with a cam path of 45° slope and 114 mm length is designed to test the capability of the P/S system. The real-time measurement of the pronation or supination angle using this mechanism is challenging; therefore, the cam-cartridge displacement, equal to the pneumatic muscle contraction, is used to calculate the amount of pronation. The contraction of the pneumatic muscle is measured by a linear potentiometer attached to the horizontal sliding member of the actuator block. The logic for the real-time P/S angle measurement is shown in Fig 5.24.

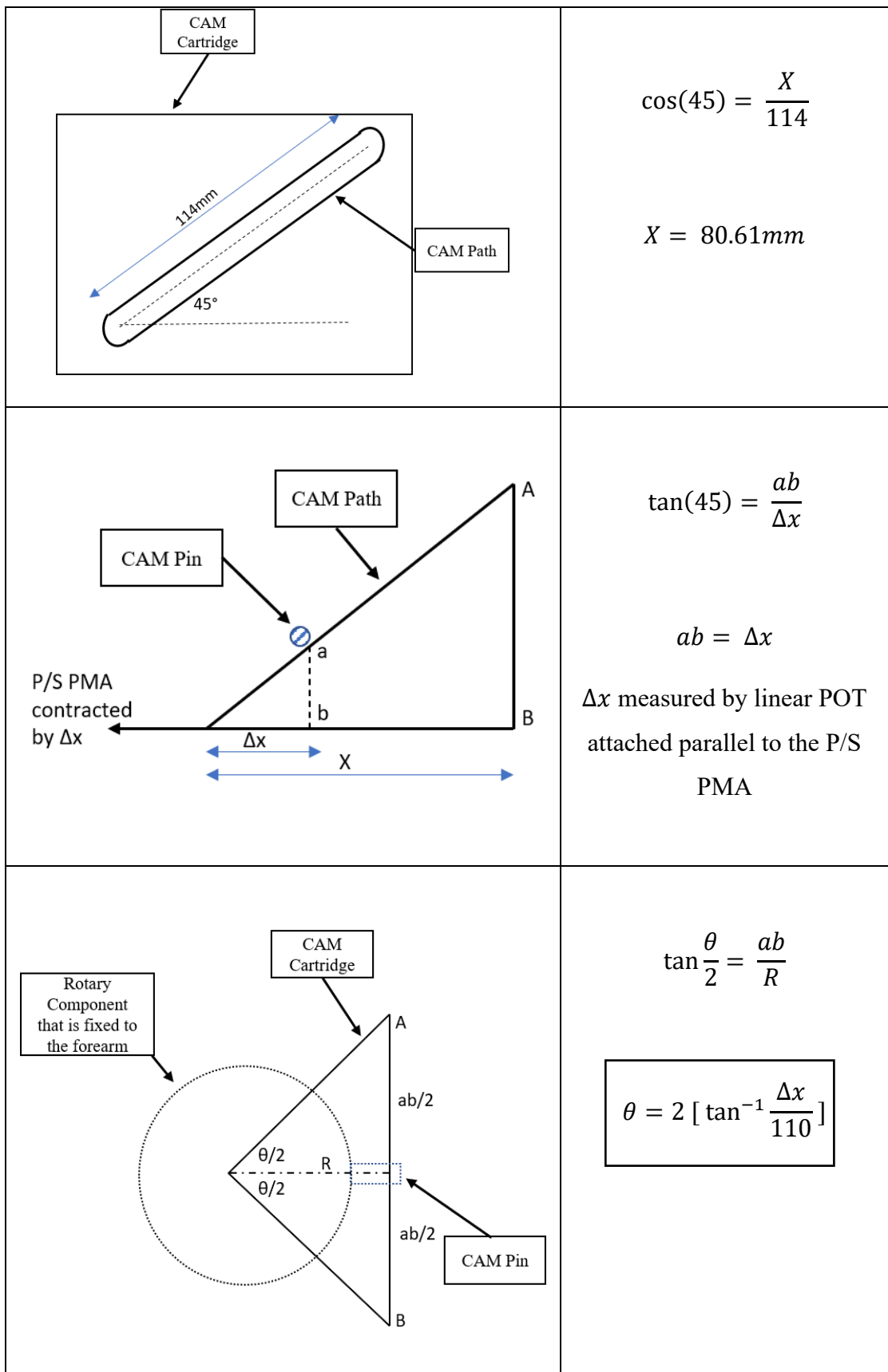


Fig 5.24: Method to record real-time Pronation Angle Measurement

Fig 5.24 shows the calculation for programming the controller to measure the real-time angle of the elbow joint through pronation and supination motion. This method of using linear displacement of the PMA to measure the P/S angle avoids the requirement of having any additional sensor to measure the elbow joint angle through P/S motions.

5.2.2 The Actuator Block (AB) of the EXPHYSIO

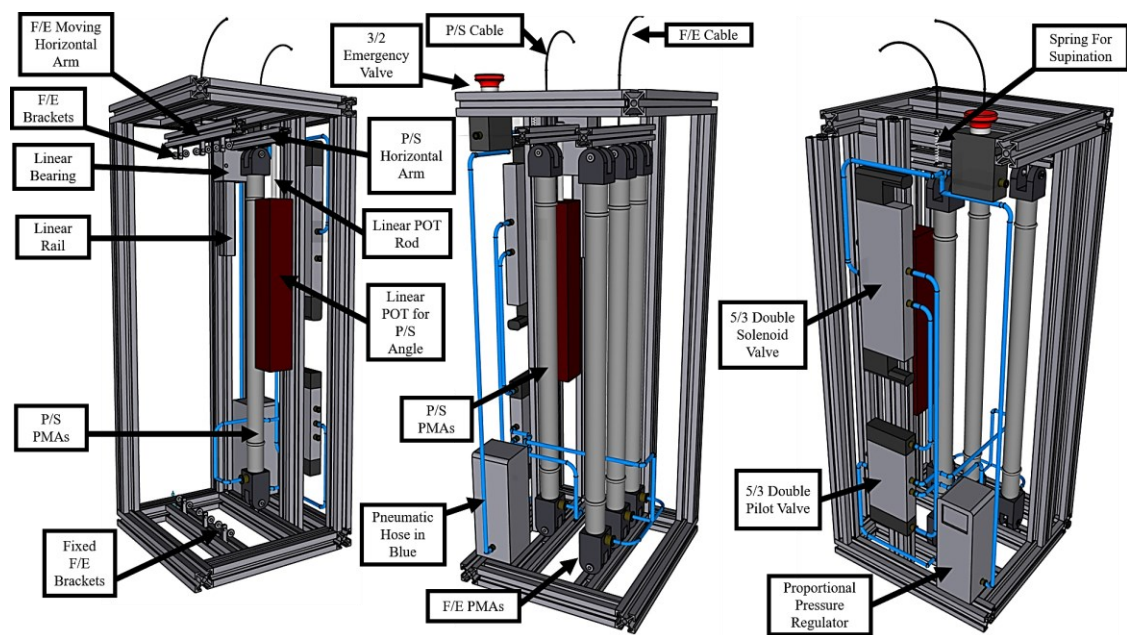


Fig 5.25: Actuator Block Design

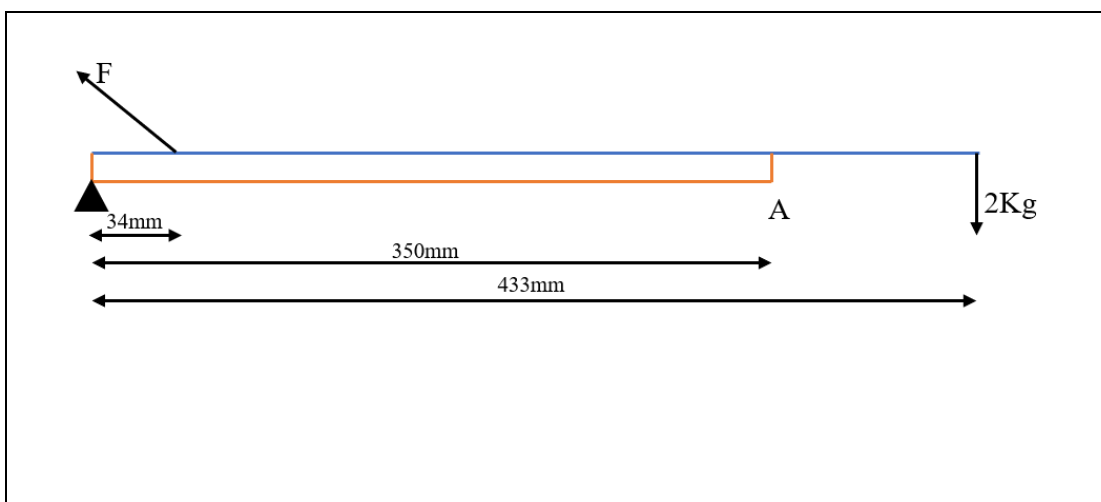
The actuator block shown in the Fig 5.25 is the main component of the EXPHYSIO exoskeleton system. The actuator block is responsible for housing the pneumatic muscles, and other circuitry used to drive the elbow exoskeleton. Soft linear actuators, such as pneumatic muscle actuators, are inherently compliant and excellent for human interactive systems (e.g., exoskeletons). The main disadvantage of soft linear actuators is their inability to achieve perfect linear actuation. The actuator block shown in Fig 5.25 restricts the muscle to linear motion using linear rails and bearings (for the P/S muscles) without compromising its compliance. In applications requiring the manipulation of heavier loads, a single soft actuator would not suffice; therefore, multiple muscle actuators have to act in parallel to produce the required force. Using multiple soft linear actuators requires additional space, thus making the system bulky, which is a significant concern in a space-constraint application such as the exoskeleton.

The actuator block allows several soft linear actuators to drive a single joint (e.g., elbow flexion) via an indirect actuation mechanism using cables. The contraction produced by the pneumatic muscle actuator is directly proportional to the length of the actuator. The previous section has shown that the contraction is lower in the Latex PMA L12LB muscle than in the S12LB muscle, but the L12LB PMA demonstrates a lower hysteresis error and good compliance characteristics. Therefore, a more significant length of latex muscle is required to actuate the elbow exoskeleton through its full range of motion. The directly mounted exoskeleton does not have sufficient space to accommodate the actuator of a more extended formfactor (length). Therefore, the indirectly actuated exoskeleton system (EXPHYSIO) has been designed and built. The actuator block allows the flexibility of adding muscles of varying lengths and sizes without affecting the bulk or weight of the exoskeleton attached to the user's upper extremity. The actuator block also provides a solution for the limitation of real-time accurate position sensing by incorporating a linear position sensor (linear potentiometer).

The actuator block is constructed using t-slot aluminium sections of size 20 mm x 20 mm, known for their lightweight and modular nature. The actuator block is constructed in the form of a cuboid structure of size 500 x 180 x 180 (in mm). The actuator block is divided into two compartments, one to actuate the exoskeleton in flexion (F/E PMAs) and the other for pronation (P/S PMA). The flexion/extension section consists of a base section, two vertical sections, and a horizontal top section. The bottom section has fixed brackets, shown in Fig 5.25, which are used to mount one end of the pneumatic muscle. The free/contracting end of the pneumatic muscle set (F/E PMAs) is connected to a horizontal t-slot member, which is connected to the F/E cable clamp on the exoskeleton via the F/E cable shown in Fig 5.20. The P/S section of the actuator block consists of only one muscle, as the force required to pronate the elbow joint is much less than that needed to flex the elbow. The main difference between the P/S section and the F/E section is the presence of the linear mechanism. The linear mechanism consists of two linear rails and bearings fixed to either side of the horizontal member connected to the P/S PMA. The main reason for having a linear mechanism for the P/S muscles is the requirement to monitor the elbow pronation angle accurately. The F/E hinge on the exoskeleton has an angle sensing mechanism, but having such an arrangement is

complex in the P/S mechanism due to space constraints. Therefore, the P/S angle is monitored indirectly by measuring the real-time P/S muscle displacement, as depicted in Fig 5.24, using a linear potentiometer parallel to the P/S muscle, as shown in Fig 5.25. The working principle of the actuator block involves the downward motion of the horizontal sliding member due to the contraction of the actuated soft muscle actuator. The downward movement of the horizontal sliding member pulls the F/S cable and results in the flexion of the forearm portion of the exoskeleton. When the P/S muscles are actuated with controlled air pressure, they contract and pull the P/S cable attached to the horizontal sliding member. The P/S muscle contraction also causes the retraction of the linear potentiometer, which records the accurate muscle displacement in real-time. This displacement measurement is used to precisely calculate the pronation angle in real time, as depicted in Fig 5.24.

The cable used in the EXPHYSIO is a commercial bicycle brake cable with a tensile strength of 1960MPa. There are two sets of pneumatic muscles in the actuator block, one to flex and the other to pronate the elbow joint. The PMA used to flex the elbow joint needs to produce sufficient force to overcome the weight of the forearm, the forearm exoskeleton structure, the hand, and the payload. The free-body diagram of the elbow flexion using the cable mechanism with relevant calculations is shown in Fig 5.26. As seen in Fig 5.26, the red colour beam represents the forearm support of the exoskeleton, while the blue coloured beam represents the user's forearm. Point 'A' in Fig 5.26 represents the P/S mechanism, which supports the user's forearm.



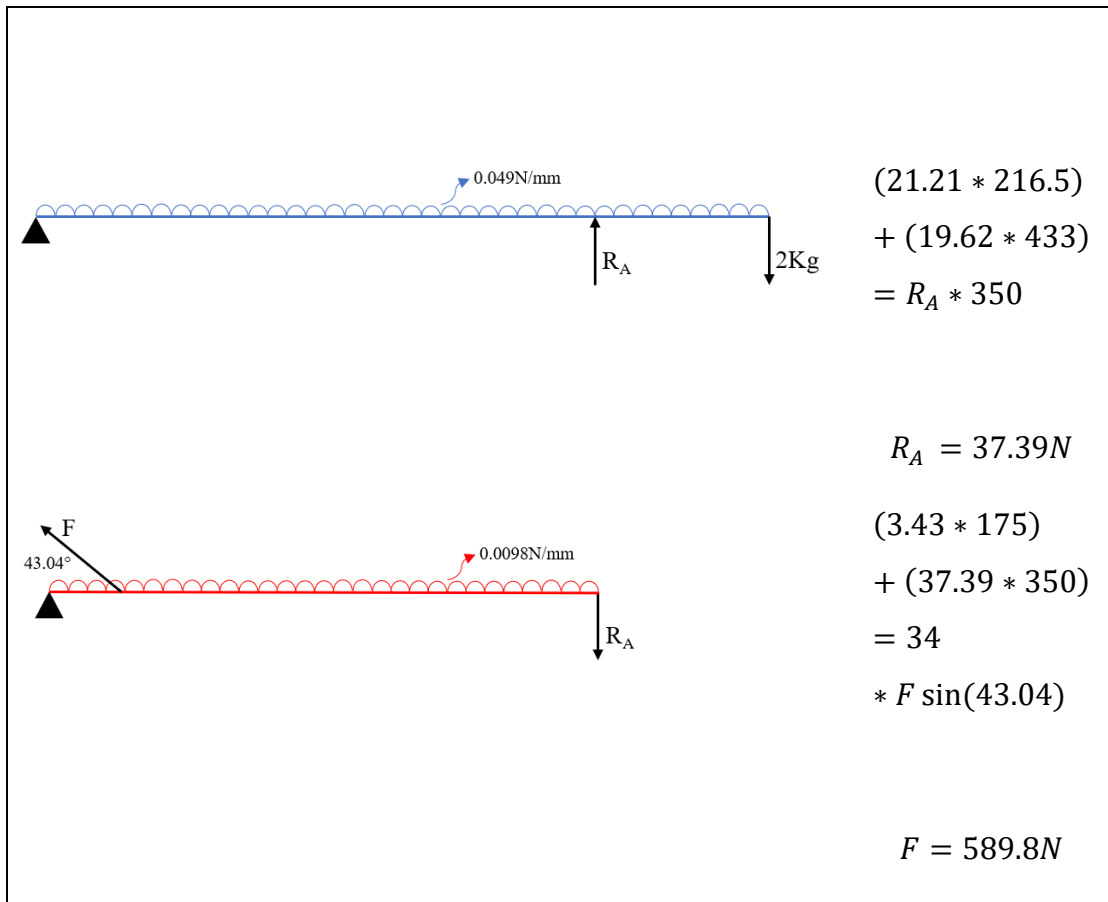


Fig 5.26: FBD for forearm actuated indirectly by PMA via cable mechanism

The forearm FBD is solved to find the reaction force R_A exerted on the forearm exoskeleton support. The support structure FBD is further simplified to find the actuator force F required to lift the user's forearm and the exoskeleton supporting the forearm at point 'A' given by reaction R_A . The maximum force the PMA needs to generate, shown in Fig 5.26, is approximately 600 N. The PMA with Latex bladder (discussed in the previous section) produces a force of approximately 300 N (L12LB(Long): 289.3 N). Therefore, a group of three parallel PMAs is used to actuate the elbow joint through flexion-extension motion by developing a cumulative force of approximately 900 N. Though a set of two muscles would have satisfied the requirement of 600 N, an extra muscle offered an additional factor of safety to the system. Using more than one muscle in parallel also acts as a safety feature that prevents the sudden extension of the elbow joint in case one of the muscles fails/ruptures. The second set of PMAs is used for the elbow joint's pronation. This set is made of a single muscle as it does not require much force to rotate the elbow through pronation motion. The v-wheel bearings further assist

the pronation motion by allowing the smooth rotation of the inner rotary component of the P/S mechanism. The P/S muscle's free end is fixed to a P/S horizontal member attached to linear guide bearings at either end, allowing the smooth linear contraction of the P/S muscle. The horizontal member is also connected to the rod of a linear potentiometer which records the liner deflection of the pneumatic muscle. This aspect is presented in the previous section, in which the muscle displacement feedback Δx is used to calculate the pronation angle of the elbow joint.

The basic principle of operation of the pneumatic muscle actuator involves the controlled supply of pressurized air, which results in its contraction or extension motion. The EXPHYSIO requires a mechanism to control the pressure of air supplied to the muscle sets to control the elbow exoskeleton's two degrees of movement. Therefore, the pneumatic circuit forms an integral part of the actuator block design. Fig 5.27 and 5.28 show the pneumatic circuits designed to actuate the elbow joint through the two degrees of freedom.

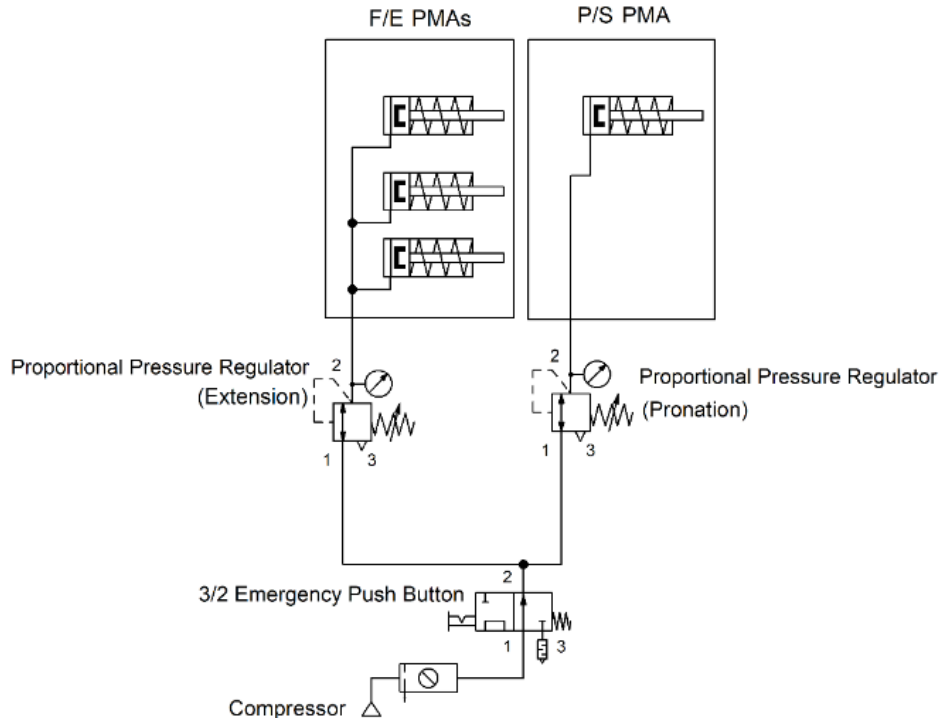


Fig 5.27: Pneumatic circuit using two proportional pressure regulators (PPR)

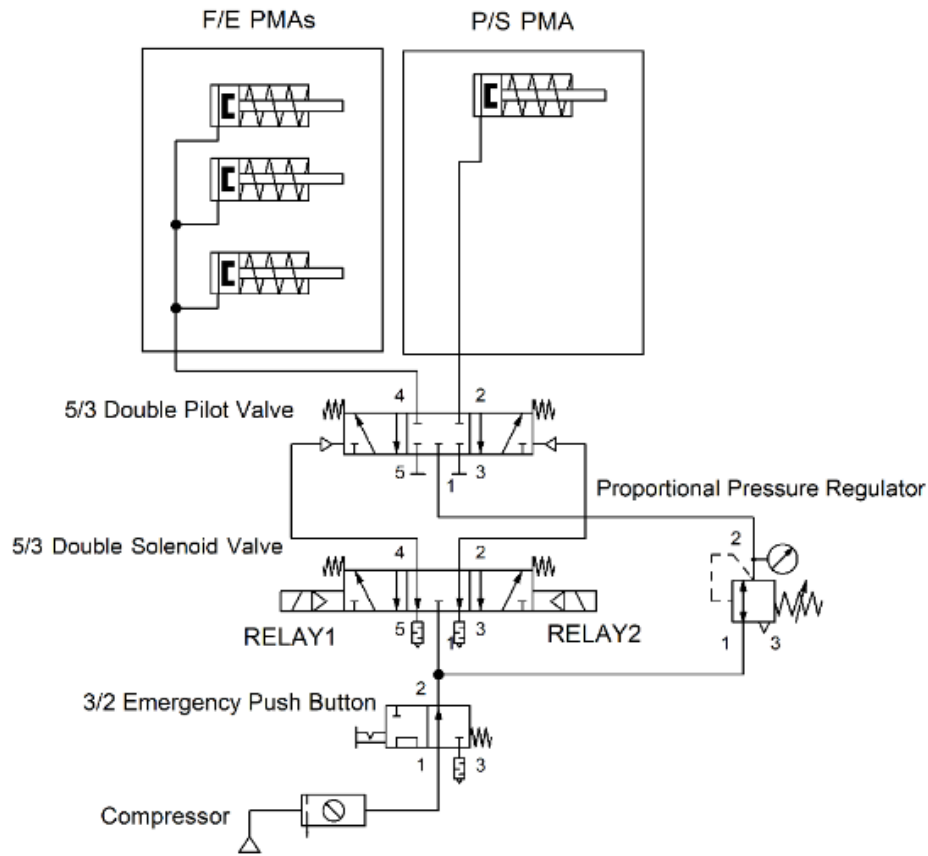


Fig 5.28: Pneumatic circuit using a single proportional pressure regulator (PPR)

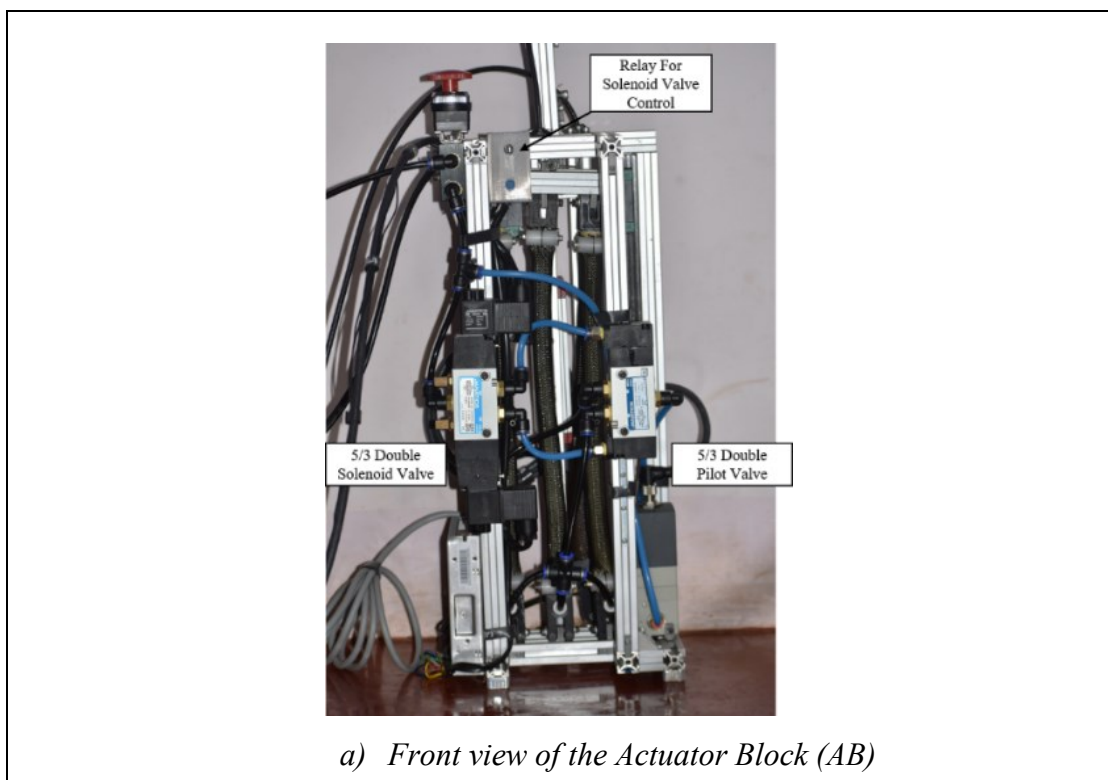
Fig 5.27 and 5.28 represents the PMA as single-acting cylinders with spring return, similar to the antagonistic muscle with spring return. The pneumatic circuit design for the EXPHYSIO is initially achieved using two proportional pressure regulators (PPRs) depicted in Fig 5.27. This is further improvised with a single PPR, as shown in Fig 5.28. The proportional pressure regulator used in this study is the Regtronic $\frac{1}{4}$ by Metal Works, which is responsible for supplying an incrementally increasing air pressure supply with varying input voltage. This incremental air pressure from the proportional pressure regulator allows the linear positional control of the PMA. The initial portion of both circuits is the same, wherein the compressor provides a $1887790 \text{ mm}^3/\text{min}$ (or 4cfm) flow rate air supply at a pressure of 4 bars. The compressed air from the compressor is treated in the Air filter Regulator (AFR) to regulate the pressure and remove any impurities and moisture from the air. The filtered compressed air is then passed via a push-button emergency 3/2 directional control valve, shown using a red button in Fig 5.25, to stop the EXPHYSIO in case of emergencies. The initial design of

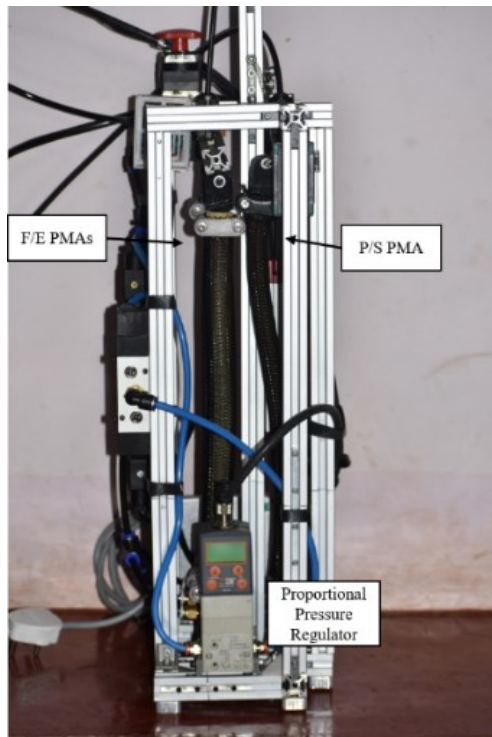
the pneumatic circuit depicted in Fig 5.27 has two proportional pressure regulators, one for actuating the F/E PMAs and the other for the P/S PMA. The advantage of using two proportional pressure regulators is that it allows easy control of individual groups of muscles, but this makes the system more costly. The second circuit is constructed with only one proportional pressure regulator to control both flexion and pronation of the elbow joint. The second circuit is designed with a 5/3 double pilot-operated direction control valve with a closed centre, controlled by a 5/3 double solenoid-operated directional control valve (DCV) with an exhaust centre. The reason for using not just a single 5/3 DCV is the minimum operating pressure requirement for the internal piloting of the valve, which is rated above 2 bar.

As the proportional pressure regulator has to supply a pressure of 0-4bar to actuate the muscle, it does not provide a pressure of above 2 bars at all times, thus making it insufficient for the internal pilot of the DCV to switch the state of the valve. The solution to this problem is the addition of a 5/3 double pilot DCV controlled by a double solenoid 5/3 DCV. The 5/3 double solenoid DCV supplied with a 4 bar pressure supply allows sufficient pressure for the 5/3 double pilot valve to switch between the F/E and P/S muscle set. As the 5/3 double pilot valve is externally piloted, it does not depend on internal piloting to change its state. The inlet port to the 5/3 double pilot valve is connected to the outlet of the proportional pressure regulator, which supplies an incremental air pressure supply to either F/E or P/S muscle sets based on the active state of the DCV. The two 5/3 DCVs are spring-centred, thus acting as a safety feature for the EXPHYSIO. When the 5/3 double pilot valve is centred with all ports closed, it prevents air from entering or exiting the muscles, maintaining the exoskeleton's position. The exhaust centre of the 5/3 double pilot valve ensures that the pilot ports are free from air supply when the solenoid valve is unactuated, thus preventing any accidental movement of the muscles. The safety feature is evident when the system's pressure drops below 2 bar, resulting from the compressor losing power, an air leakage, or the emergency push-button being engaged. The moment the system pressure drops below 2 bar, the 5/3 double solenoid valve would centre, thus resulting in the pilot ports of the 5/3 double pilot valve being connected to the exhaust. As the 5/3 double pilot valve loses pressure in its pilot ports, it is spring-centred, thus blocking air supply in or

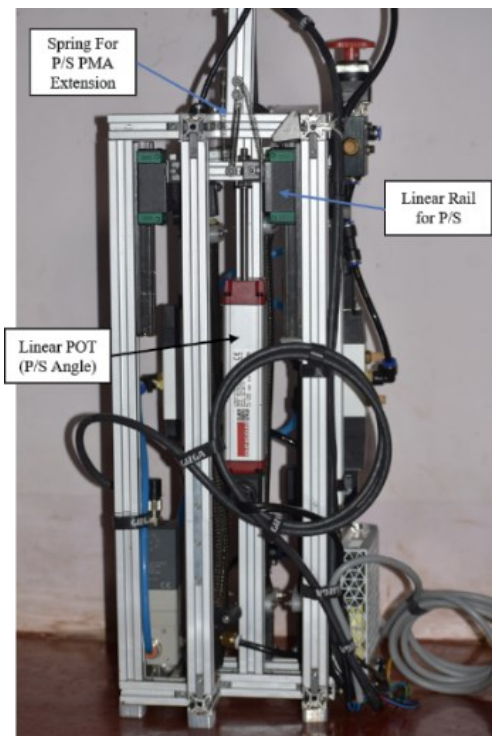
out of the PMAs. The inclusion of the 5/3 DCVs in the EXPHYSIO circuit facilitates the use of a single PPR, thus reducing the cost of the system and making it much safer for the intended medical application.

The elbow joint has two degrees of freedom: flexion/extension and pronation/supination. Achieving both degrees of freedom makes the exoskeleton structure bulky, especially when the actuators are directly mounted. Using the actuator block resolves the problem of the direct actuator arrangement represented in Figures 5.25 and 5.29. The compliant soft actuators attached to the actuator block actuate the exoskeleton via a cable mechanism. Thus, making the system less bulky, lightweight, and safe. The actuator block makes the exoskeleton system safer as it provides an enclosure for the soft actuators, thus protecting them from damage. Soft actuators such as pneumatic muscle actuators have a risk of accidental ruptures due to sudden high pressures or damage to the bladder due to wear, whose sound could startle the user (e.g., patient) if the actuator is attached directly to the exoskeleton. Therefore, it is much safer to operate the exoskeleton indirectly via cables from the actuator block, keeping the user at a safe distance from the actuators. The actual photos of the actuator block constructed for the EXPHYSIO system are shown in Fig 5.29(a-c).





b) Side view of the AB



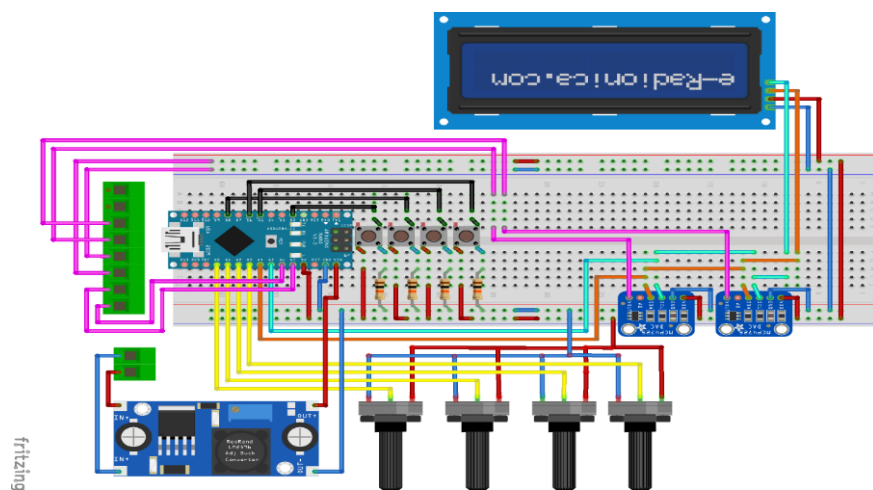
c) Back view of the AB

Fig 5.29: Photos of Actuator Block (AB)

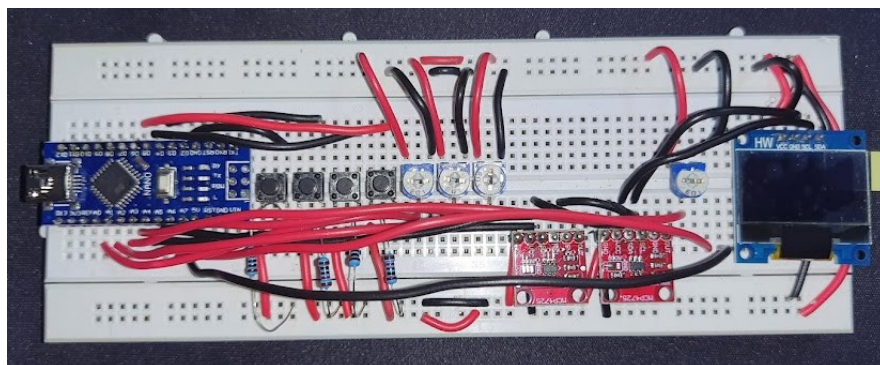
Fig 5.29(a & b) shows the actuator block with two sets of muscles (F/E & P/S PMAs), the pneumatic circuit with PPR and DCVs, and the emergency push button. Fig 5.29c shows the P/S linear mechanism with the linear rails and bearings and the linear potentiometer (POT) attached in parallel to the P/S muscles. The relay box houses a relay that actuates the 5/3 double solenoid DCV based on the signal received from the controller.

5.2.3 The Control Unit of the EXPHYSIO

The control unit of the EXPHYSIO consists of the electronic circuitry, program, and human-machine interface (HMI). The electronic circuit is developed through a series of tests and processes, as depicted in Fig 5.30(a-f).

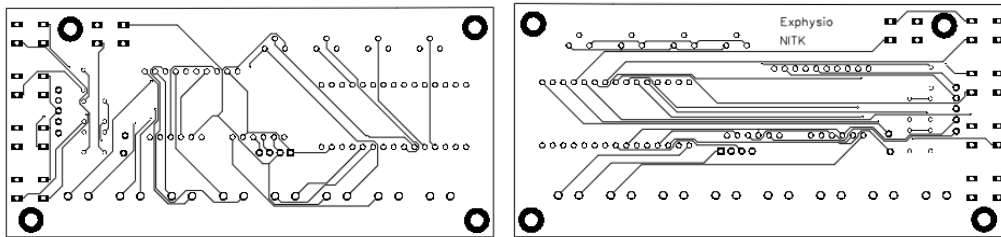


a) Control unit circuit design

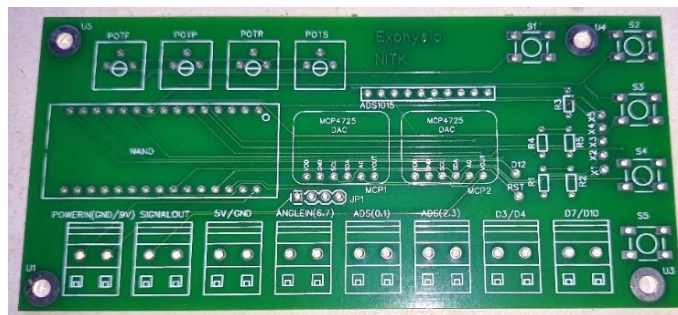


b) Testing the control circuit design on the breadboard

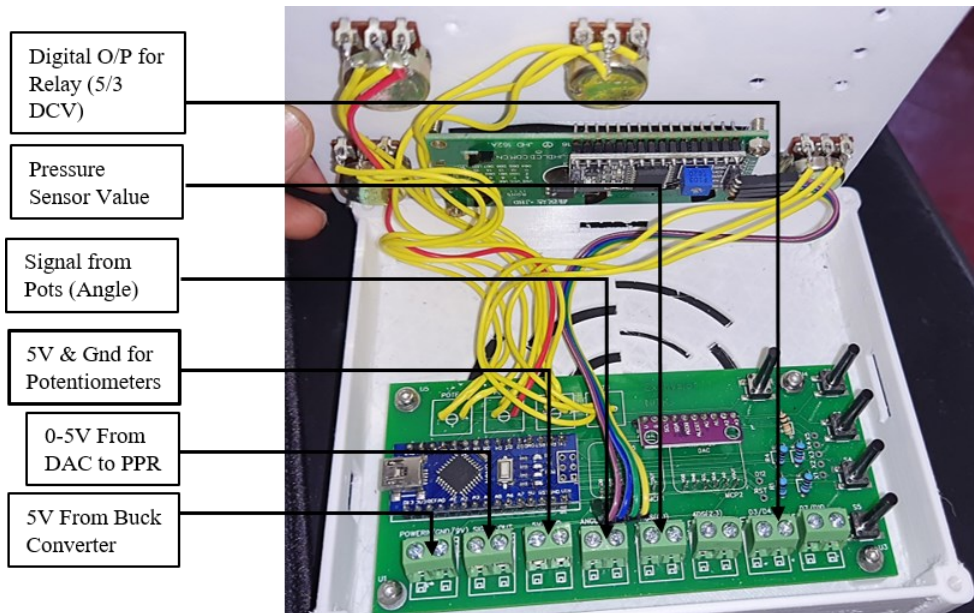




c) Generating the Gerber files of the designed circuit



d) PCB fabrication



e) Assembly of the components onto the PCB





f) Actual photo of the fully assembled control unit

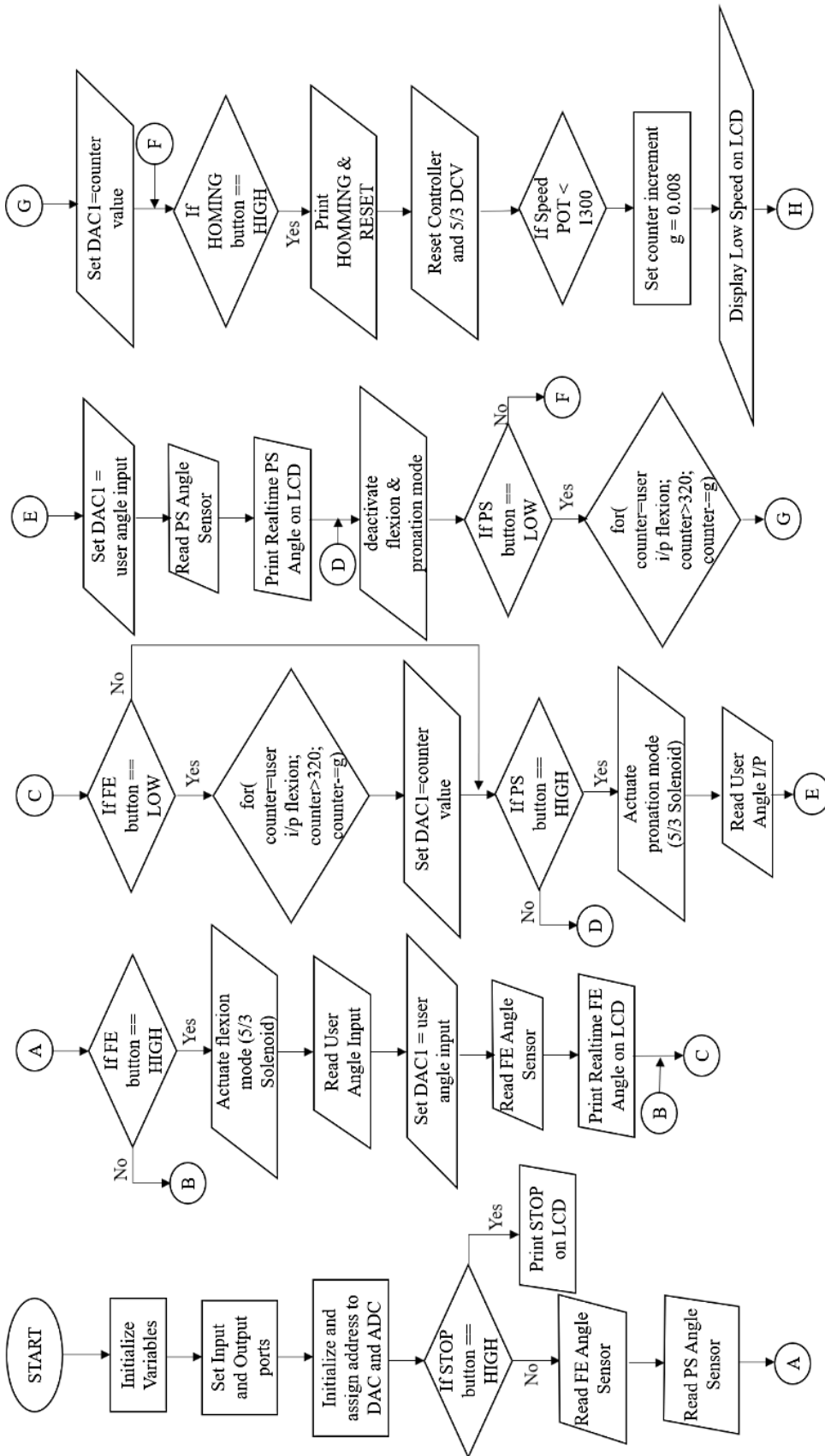
Fig 5.30: Control Unit Development process for the EXPHYSIO

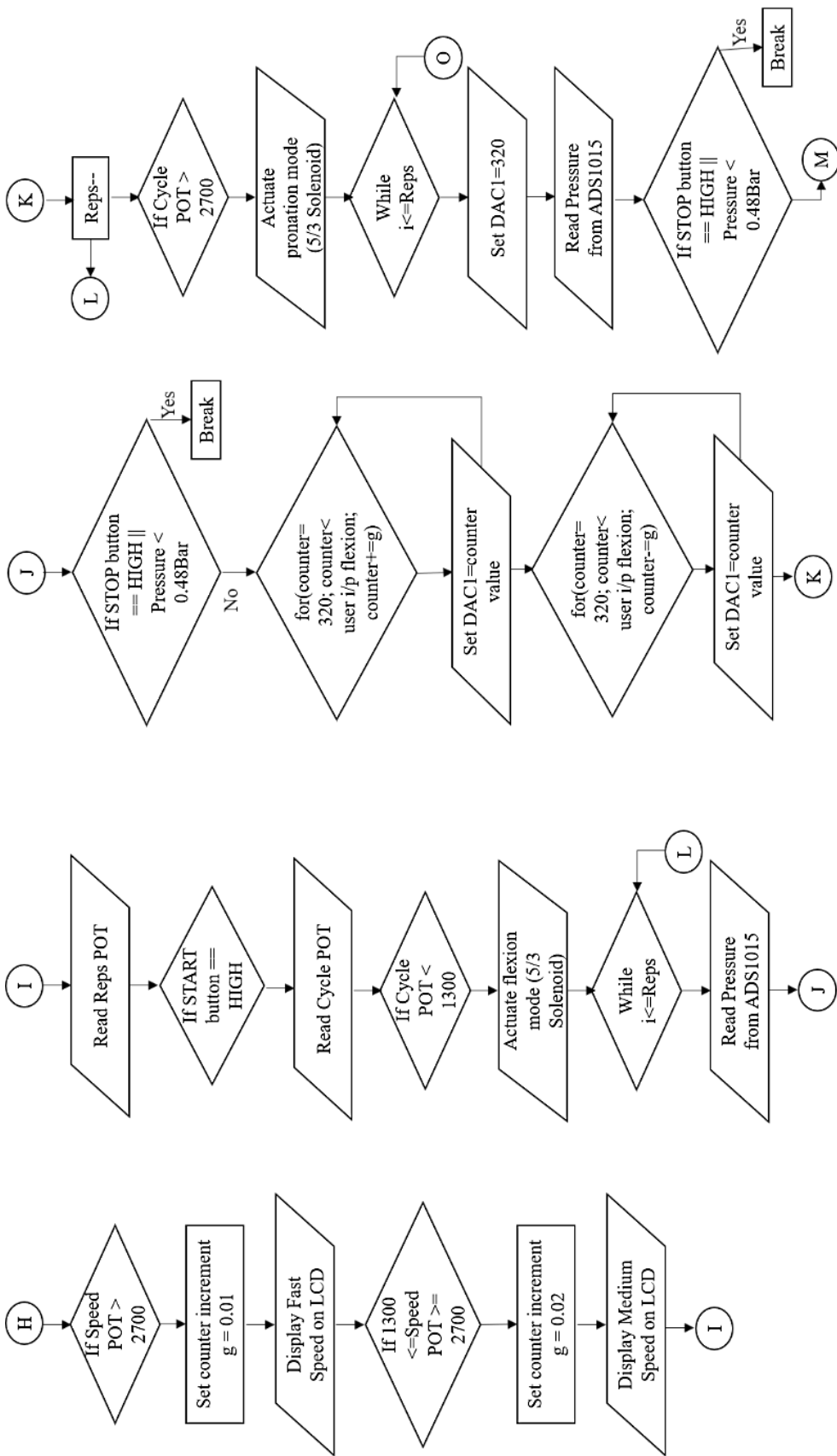
The first step in developing the electronic circuit is the selection of the microcontroller depicted in Fig 5.30a. The microcontroller chosen for the EXPHYSIO is the ATmega328 operating at 5V and having a clock speed of 16MHz. This microcontroller has eight analog input ports and 22 digital IO ports, and it also comes with I2C support, which allows it to be easily connected to several IO devices. The ATmega328 does not have any analog output ports, which makes it challenging to generate a pure analog signal to operate the PPR. Two MCP4725 DACs (digital to analog converters) have been connected over I2C to add analog output functionality to the controller. The MCP4725 is a low-powered, high-accuracy, 12-bit single-channel digital-to-analogue converter (DAC). The initial pneumatic circuit design shown in Fig 5.27, presented in the previous section using two PPRs, requires two separate analog outputs from the controller. Accordingly, the electronic hardware has been designed with two DAC modules. The main power to the actuator block is provided by a 24V SMPS, which powers the PPRs. A buck convertor module LM2596 is used to step down the voltage to a steady 5V supply in order to use the same power source to supply power to other electronics and sensors.

Four potentiometers are provided for the operator to give input for parameters such as angle, speed, cycle type, and the number of repetitions. The circuit also has several push

buttons, which allow the user to set the flexion/extension angle (F/E) and the pronation/supination (P/S) angle. There are dedicated buttons to start and stop the cycle (START/STOP). A 'HOME' button allows the exoskeleton to be brought to its initial position and reset all parameters. A red toggle switch is provided on the control unit as the Emergency switch, which stops the program and stops the motion of the exoskeleton when activated. An additional analog input module ADS1015 is added to the circuit to increase the number of analog inputs of the ATmega328 (via I2C) to read additional parameters, such as pressure in the PMAs. This pressure value at the PMAs also acts as a safety feature that stops the EXPHYSIO in case of a sudden drop in pressure, which could result from a muscle rupture. The ADS1015 has four analog input ports, allowing the flexibility of adding additional analog sensors (e.g., EMG) in the future.

The designed circuit is tested on a breadboard, as shown in Fig 5.30b and connected to the actuator block to check it's working. After satisfactory testing and optimization of the circuit on the breadboard, the Gerber files depicted in Fig 5.30c are prepared to fabricate the circuit board. The Gerber files are designed and generated using EasyEDA software, and the PCB is manufactured using these files. The fabricated PCB is shown in Fig 5.30d. Next, all the electronic components and accessories are soldered onto the fabricated PCB, as shown in Fig 5.30d. Screw terminal connections are used to connect the control unit to the actuator block, thus making it very easy to connect and disconnect in case of any modifications or maintenance required in the system. The control unit panel shown in Fig 5.30e is designed and 3D printed in PLA, thus making it lightweight and easy to be held and used by the operator. The control panel design also includes ventilation slots for thorough cooling of the electronic hardware and a clamp for securing the cable entering the control unit from the actuator block. Precise grooves are also provided in the panel for the assembled push-buttons, toggles, and potentiometers. The side face of the control panel has a small cut-out to plug in a USB cable for programming and debugging the microcontroller of the control unit. The flowchart depicted in Fig 5.31 explains the program logic used in the EXPHYSIO.





5.2.4 Programming and Using the EXPHYSIO

The program shown in Fig 5.31 communicates with the hardware of the EXPHYSIO via the control unit circuitry. The operator or physiotherapist must first set the compressor's initial pressure. A pressure of 5 bar is set on the FRL of the compressor, which is slightly higher than the required pressure of 4 bar, in order to compensate for any losses in supply pressure. The exoskeleton is donned onto the user's upper limb and securely fastened using the Velcro straps provided at the arm clamps. The user's wrist is fixed to the inner rotary component of the P/S mechanism via a wrist brace using small Velcro straps. The user's forearm is fixed to the exoskeleton at the P/S mechanism by mating the v-rail of the inner rotary component with two v-wheel bearings at the P/S outer stationary component. Once the inner rotary component is positioned correctly between the two v-wheel bearings, the third v-wheel bearing is bolted in place using the eccentric nut. The eccentric nut allows the position of the third v-wheel bearing to be adjusted with respect to the other two bearings, thus securing the inner rotary component and allowing its smooth rotation about the v-wheel bearings. The emergency switch is engaged during the donning phase to prevent sudden motion due to the accidental actuation of the PMAs.

Once the exoskeleton is securely donned onto the user's arm, the operator performs the teaching process. The teaching process begins with initializing all the settings on the control unit to prevent any sudden actuation which could harm the user. When all the knobs on the control unit are initialized, it is switched on. The teaching/training process on the EXPHYSIO is very advantageous as it allows the operator to visualize the motion of the exoskeleton in real time. The first step involves setting the flexion and/or pronation angles. The flexion angle is set by clicking the F/E push button on the control unit. While the F/E push button is still being pressed, the operator needs to rotate the angle dial; this action generates a signal for the pneumatic circuitry to supply air to the flexion muscles, thus resulting in the real-time flexion of the elbow joint. Once the required flexion angle is set, the F/E pushbutton is released. This results in the control unit storing the set value of the flexion angle. The release of the F/E button also results in the exoskeleton extending back to its home/initial position. After the flexion angle is set, the user has to teach the required pronation angle. The pronation angle is

programmed by pressing and holding down the P/S pushbutton and rotating the angle dial. This action results in the exoskeleton's real-time movement, allowing the operator to visualize and efficiently teach the required pronation angle. Once the necessary pronation angle is trained, the operator has to release the P/S button, storing the set pronation angle and also supinating the exoskeleton back to its home position. An important safety protocol that must be followed while teaching, is the initializing of the angle dial after teaching either the flexion (releasing the F/E button) or pronation (releasing the P/S button) angles to avoid sudden actuation of the PMAs, which could harm the user.

Once the flexion and pronation angles are trained on the EXPHYSIO, the operator needs to set other parameters such as speed, cycle type, and repetitions. The control unit is designed with dials for each parameter. The speed dial is used to set the speed of movement of the exoskeleton. The speed dial is calibrated into slow (S), medium (M), and fast (F), depending on the requirement of the physiotherapy routine. The following parameter is the type of repetitive cycle. The EXPHYSIO is designed to impart three types of exercise cycles. The first type of cycle is the F-cycle, which only imparts repetitive flexion/extension motion to the elbow joint. The second is the P-cycle which imparts repetitive pronation/supination motion to the elbow joint. The third and last type of cycle mode is the F+P cycle type which gives a repetitive alternating flexion/extension and pronation/supination cycle motion. The final stage of the teaching phase involves setting the number of exercise repetitions or REPS on the control unit.

The following portion discusses the working of the EXPHYSIO system once it is in auto mode by clicking the START button on the control unit. The values of angle, speed, cycle type, and the number of repetitions set by the user in the teaching phase are stored in the control unit's memory. Once the start button is engaged, the controller reads the type of cycle set by the user to choose the relevant program shown in Fig 5.31 to perform the motion cycle. Considering that the user selects the F-cycle mode. Once the controller detects the F-cycle, it sends a signal to the 5/3 double solenoid valve via relay 1. The activated 5/3 double solenoid valve supplies pressure to the pilot port of the 5/3 double pilot valve to switch its state, therefore establishing a connection

between the F/E PMA set and the PPR via the 5/3 double pilot valve. The next part of the program is run in a while loop where a counter helps to achieve the set value of repetitions set by the user during the teaching phase. The program is designed to constantly monitor two critical parameters, the STOP button and the system air pressure. The pressure sensor communicates with the controller via an analogue-to-digital converter ADS1015. The set of flexion PMAs, which are connected to the PPR via the 5/3 double pilot valve, are actuated via a variable voltage signal received from the controller via the digital-to-analogue converter MCP4725. The variable voltage signal (incremental and decremental) to the PPR results in a proportional air supply of increasing and decreasing pressure. The incremental increase in pressure results in the smooth contraction of the muscle actuator, while the decrementing signal results in its smooth extension.

The maximum pressure given to the PPR is set based on the value of the flexion angle set by the operator during the teaching phase. The program of the cyclical motion of flexion/extension of the elbow joint resulting from the contraction and extension of the flexion PMAs is repeated until the set value of REPS is reached. Once the set value of repetitions is reached, the exoskeleton automatically stops at the home position. On completion of the repetitive therapy, the exoskeleton is doffed from the user's arm, and the system is switched off. The following section summarises the sequential operation of the EXPHYSIO.

Pre-Setup:

1. Switch on the air compressor.
2. Set the outlet air pressure to 5 bar at the FRL on the air compressor.
3. Set all potentiometers on the control unit to a minimum (or zero).
4. Switch on power to the EXPHYSIO.
5. Release the P/S rotary component by un-screwing one v-wheel bearing of the P/S stationary component.

Donning the EXPHYSIO:

1. Activate the Emergency button on the actuator block to prevent accidental actuation while donning.
2. Insert the user's hand in the P/S rotary component.
3. Insert the wrist brace on the user's hand and wrist.
4. Use the Velcro strips to connect the wrist brace to the rotary component.
5. Place the user's arm on the exoskeleton clamp supports, ensuring the hand is inserted in the hollow portion of the P/S stationary component and the rail groove is in contact with two-wheel bearings.
6. Secure the user's upper arm to the upper arm support using the Velcro straps in the C-clamps.
7. Connect the third wheel bearing, thus securing the P/S rotary component in place and free to rotate about the stationary component bearings.
8. Release the Emergency button on the actuator block after ensuring the user's arm is secured to the EXPHYSIO.

Training the EXPHYSIO:

1. Switch on the control unit.
2. Keep the F/E button pressed and rotate the ANGLE dial to set the maximum required flexion angle. While the ANGLE dial is turned, the exoskeleton flexes, thus making it easy for the physiotherapist to visualize and set the required angle.
3. Release the F/E button once the required flexion angle is set. Releasing the F/E button stores the set value of the flexion angle and gets the exoskeleton back to its initial position.
4. After releasing the F/E button, rotate the ANGLE dial in the anticlockwise direction to its minimum value. This ensures that when the P/S button is pressed in the next step, there is no sudden pronation of the elbow joint.

5. Now press and hold the P/S button. Rotate the ANGLE dial while holding down the P/S button; this would cause the pronation of the user's forearm.
6. Release the P/S button once the required pronation angle is set. The exoskeleton would automatically supinate due to the spring action.
7. After releasing the P/S button, rotate the ANGLE dial in the anticlockwise direction to its minimum value.
8. Now turn the SPEED dial to select the required speed of the exoskeleton motion.
 - a. S: Slow
 - b. M: Medium
 - c. F: Fast
9. Next, select the required cycle of operation on the CYCLE dial.
 - a. F: This performs only Flexion-Extension of the elbow joint.
 - b. P: This performs only Pronation-Supination of the elbow joint.
 - c. F+P: This dual cycle mode alternates between F/E and P/S motions.
10. Set the maximum number of required repetitions on the REPS dial of the control unit.

Cycle Operation of the EXPHYSIO:

1. Check all the values set during the training phase on the LCD of the control unit.
2. In case of any discrepancy in the set values, the operator can click HOME to reset all values and bring the exoskeleton to its initial position.
3. If all settings are satisfactory, the operator needs to click the START button on the control unit to start the repetitive cycle motion of the EXPHYSIO.
4. Suppose the operator needs to stop the exoskeleton before the completion of the programmed repetitions. Clicking the STOP button stops the exoskeleton motion after completing the current motion cycle.

5. In case of an Emergency stop, there are two options:
 - a. The red toggle switch on the control unit.
 - b. The emergency push button on the actuator block shuts off the air supply to the EXPHYSIO, thus centring the 5/3 valves and causing the exoskeleton to stop.

The link below contains a video showing the summary of this research with the process of training and testing the newly developed EXPHYSIO exoskeleton system.

https://drive.google.com/file/d/1g_q1S_iqRWkL-Qp4OS9mbjvU4B7XKW7F/view?usp=sharing OR scan the QR code:



5.2.5 Testing the EXPHYSIO using the Developed PMA

The L12LB muscle is used to actuate the exoskeleton of the EXPHYSIO to test the motion behaviour of the exoskeleton for various loading and pressure conditions. As discussed in the previous sections, three L12LB(long) muscles are used to flex, and one L12LB(long) muscle is used for pronating the elbow exoskeleton. Fig 5.32 and 5.33 show the angle vs pressure for the two degrees of motion of the EXHYSIO exoskeleton.

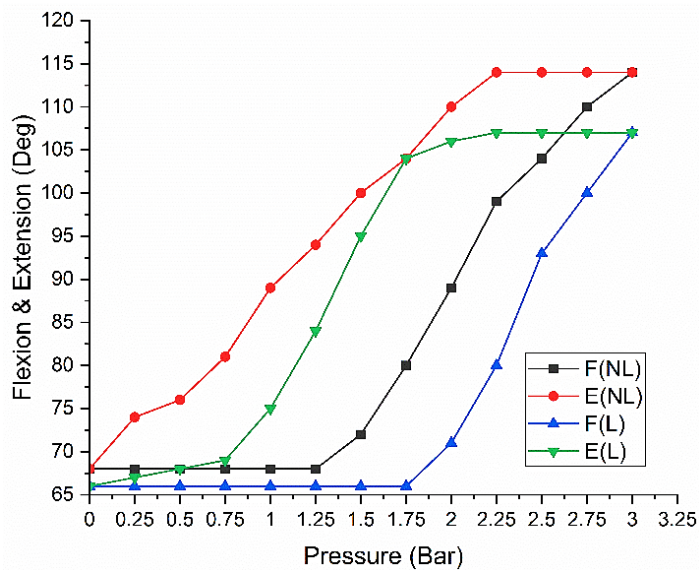


Fig 5.32: F/E Angle vs. Pressure for the exoskeleton of the EXPHYSIO

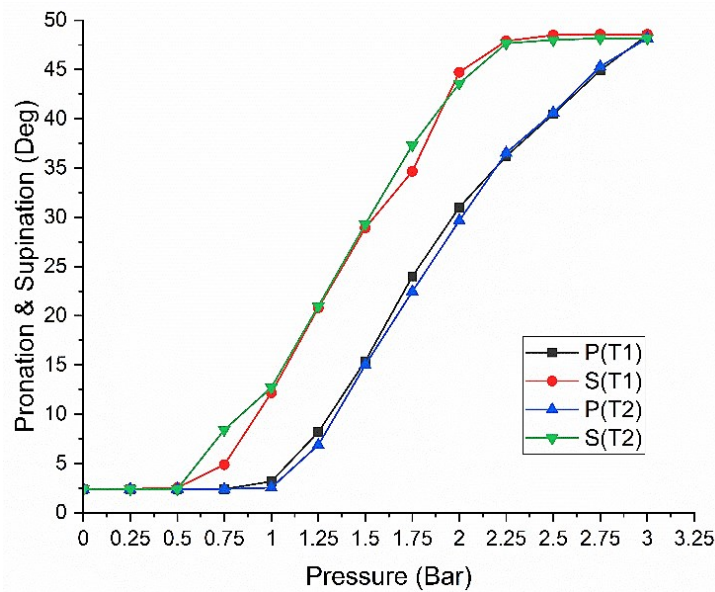


Fig 5.33: P/S Angle vs Pressure for the exoskeleton of the EXPHYSIO

Fig 5.32 depicts the change in flexion (F) and extension (E) angle with variation in input air pressure when the exoskeleton is in the loaded (L) and no-load (NL) state. Fig 5.32 shows that the hysteresis error tends to increase with the addition of load on the exoskeleton. Comparing the loaded state with the no-load state shows a larger pressure requirement for the muscle set to lift the forearm through flexion as the muscle has to overcome the pressure deadband, the load of the structure, and the payload on the exoskeleton. The horizontal portion of the black-coloured line representing the flexion angle in the no-load state is short compared to the blue line, as the muscle only has to overcome the deadband and the weight of the exoskeleton frame. On the other hand, the blue coloured line representing the variation in flexion angle in the loaded state is much longer as it has to generate sufficient force to overcome the pressure deadband, lift the weight of the forearm, the structure, and the payload. The addition of load also results in a slightly lower flexion angle than the exoskeleton with no load. Fig 5.33 shows a pronation angle of almost 50° achieved by the EXPHYSIO. Fig 5.33 also compares two trials (T1 and T2), which indicate a lower repeatability error in the EXPHYSIO actuated by the L12LB PMA. The main aim of this test is to evaluate the behaviour of the muscle set when it is used to actuate the exoskeleton. The test shows that the L12LB muscle can successfully flex and pronate the elbow joint with minimal hysteresis and good repeatability while maintaining its compliant nature.

5.3 Conclusion

The exoskeleton is designed to impart repetitive therapy to the elbow joint through two degrees of freedom. The initial design involved the direct actuator-mounted exoskeleton, wherein the PMA is directly attached to the exoskeleton structure. The key conclusions realized after testing the directly actuated exoskeleton are:

1. The directly actuated exoskeleton has an overall smaller system as most components are attached directly to its frame. Though the system is less complex, the exoskeleton attached to the user itself is bulky.
2. The stainless-steel mounts and arm clamps make the exoskeleton heavy (1.5 kg).
3. As the actuators are directly attached to the exoskeleton, it is challenging to achieve larger values of angular deflection.
4. Though the latex muscles provide balanced compliance and positional accuracy, it is not the right choice for the direct mounted exoskeleton due to its larger length and lower contraction capability. The S12LB muscle with higher contraction percentage and force characteristics will better fit the direct actuator mounted (AM) arrangement.
5. The direct AM exoskeleton is a space-constrained device that can accommodate only one actuator for flexion and extension of the elbow joint. Adding additional degrees of freedom, such as pronation/supination, is not feasible with such a mounting arrangement.
6. Additional force requirement requires the pneumatic muscles to be arranged in parallel, which is not feasible in the direct AM setup.
7. The hinge designed for the direct AM arrangement increases the flexion angle capability to 110° compared to the previously used commercial hinge, whose range of motion was restricted to 90°.
8. Literature shows that previous researchers used two pneumatic muscles to counter the antagonistic nature of the pneumatic muscle. The hinge designed in

this research uses a torsion spring to act in the extension stroke of the muscle (or extension of the elbow), thus allowing the elbow joint to be actuated (in flexion) using only one muscle actuator. This significantly reduces the cost of the setup.

The shortfalls of the direct actuator-mounted exoskeleton prompted an improvement in the design. Therefore, an enhanced exoskeleton system called the EXPHYSIO is developed. The key highlights of the improved exoskeleton design include the following:

1. The exoskeleton of the EXPHYSIO is lighter by 0.5 kg compared to the previous design due to the 3D printed clamps and indirect actuation mechanism via cables.
2. The indirect actuation allows the EXPHYSIO to achieve 20% higher flexion angle compared to the direct AM exoskeleton.
3. The angle sensor at the hinge allows the real-time angular position feedback of elbow joint flexion.
4. The indirect actuation mechanism allows the addition of features such as forearm length adjustment and pronation/supination functionality to the exoskeleton.
5. Unlike previous pronation/supination mechanisms observed in the literature, the current design is able to perform the elbow joint motion without hindering the freedom of the hands and fingers. Therefore, keeping the fingers and hand free to be given other therapy exercises such as strength training or activities of daily living (ADL).
6. The novel cam-type mechanism used for pronation and supination allows the use of linear pneumatic muscle actuators without compromising their compliant nature.
7. The actuator block allows the soft actuator to achieve a smooth linear motion with its linear mechanism.
8. The linear mechanism also allows adding a linear sensor in parallel to the P/S muscle to monitor the forearm pronation in real time.

9. The actuator block provides an enclosure for the soft muscle actuators, thus protecting them from damage or getting tampered.
10. The indirectly actuated arrangement using cables helps keep the muscles at a safe distance from the users, thus reducing the danger of being startled by the sudden rupture of the bladder.
11. Two pneumatic circuits have been designed in the development of the EXPHYSIO. The first circuit with two proportional pressure regulators is improvised in the second design with a single pressure regulator. Both circuits could perform the same exoskeleton motion functionality, but the second circuit is more cost-effective and has additional safety features incorporated by adding the DCVs.
12. The safety features incorporated in the design of the EXPHYSIO are:
 - a. An emergency stop toggle on the control unit.
 - b. Another emergency stop pushbutton on the actuator block.
 - c. The designed hinge prevents the elbow joint from extending beyond the safe limit of 180°.
 - d. In case of a sudden drop in system pressure due to air leakage or the rupture of a PMA, the system automatically halts.
 - e. In case of power loss, the 5/3 DCV is centred and stops the motion of the exoskeleton.

6 SUMMARY AND CONCLUSIONS

This research aims at developing a compliant, modular, and safe exoskeleton robot for physiotherapy applications. The conclusions of this study are discussed in this section.

The literature has shown pneumatic muscle actuators to have a high power-to-weight ratio and good compliance, making them excellent for rehabilitation applications. The drawbacks of the commercial muscle, such as the fixed end-fittings, larger actuator length, smaller force, and contraction capacities, led to the development of an in-house muscle actuator. The in-house muscle is designed with a pair of novel end-fittings, making the muscle construction modular, compact and lightweight.

The preliminary tests on the developed muscle showed high contraction (18%) and force (50%) characteristics compared with the tested commercial muscle. The tests showed the styrene-based S12LB muscle producing a larger force and contraction while occupying a smaller space. The characterization experiments also showed the longer length latex muscle L12LB(long) having a good contraction and force characteristics with balanced compliance and positional accuracy (i.e., lower hysteresis error).

The exoskeleton is built to be modular and a universal fit for most Indian upper extremities. The exoskeleton is designed with an aluminium t-slot frame, and the actuators are directly attached to the exoskeleton frame using stainless steel mounts. The tests on the direct actuator mounted exoskeleton showed the S12LB muscle forming the best actuator for the space constraint application, thus allowing a 38° of elbow flexion. The direct actuator mounted arrangement resulted in space constraints that led to the inability to add the pronation/supination functionality. Therefore, the direct actuator arrangement is restricted to a single degree of freedom (flexion/extension) capability.

The shortfalls of the direct actuator-mounted exoskeleton led to the development of an indirect cable-actuated exoskeleton system called the EXPHYSIO or exoskeleton for physiotherapy. The EXPHYSIO being actuated via cables had the provision to be actuated by the longer L12LB(long) muscle actuator, allowing it to achieve a 46° of elbow flexion. The indirect actuation mechanism also allowed us to add the pronation/supination functionality and the forearm length adjustment mechanism. The

EXPHYSIO is developed with a new hinge design with a compact construction and features such as flexion angle sensing, pneumatic muscle antagonistic compensation, and a safety feature that prevents excess elbow extension. The indirect actuator mechanism allows the pneumatic muscles to be kept at a safe distance from the user, preventing any harm to the user in case of an accidental muscle rupture. The EXPHYSIO is also built with a unique pneumatic circuitry that allows the use of a single proportional pressure regulator to control both degrees of freedom and improves the system's safety, especially in case of a sudden drop in pressure. The last but important feature of the EXPHYSIO is the control unit and related electronics that ease the process of training the physiotherapy routine and controlling the overall device.

6.1 Summary

When actuated with the S12LB muscles, the direct actuator-mounted exoskeleton has been shown to achieve a 38° of elbow flexion. The lack of space in the direct actuator-mounted exoskeleton prevented the addition of the second degree of freedom, thus restricting its capability to only flexion/extension for the elbow joint. It is also inferred that having the actuators too close to the user compromised the safety of the device. The shortfalls of the direct actuator-mounted exoskeleton are rectified in the newly developed EXPHYSIO. The EXPHYSIO is an indirectly actuated exoskeleton with two degrees of freedom (flexion/extension & pronation/supination). The indirect cable mechanism with the longer latex muscles has demonstrated a flexion angle of 46°, which is much greater than the direct actuator-mounted exoskeleton setup. The control unit hardware and software of the EXPHYSIO have been designed to ease the process of controlling and training the device. The main advantage of training the EXPHYSIO is the visual feedback the operator experiences during the training phase, thus allowing for easy and efficient training of the physiotherapy routines. The tests on the EXPHYSIO reveal that the device can successfully impart repetitive therapy to the elbow joint through two degrees of freedom.

7 FUTURE SCOPE

This research deals with the development of a soft compliant pneumatic muscle actuator for the actuation of an elbow exoskeleton. The elbow exoskeleton developed in this research has two functional degrees of freedom, namely flexion/extension and pronation/supination. The developed muscle actuator was experimentally characterised and tested to actuate the exoskeleton through its various degrees of motion. The study is concluded with the effectiveness of the indirectly actuated elbow exoskeleton known as the EXPHYSIO with a few points for future scope listed as follows:

1. Improving the positional accuracy of the developed pneumatic muscle actuator.
2. Adding additional feedback sensors to the system such as EMG and ECG to enhance the systems performance and safety.
3. Designing a shoulder mechanism to allow the actuation of the entire upper limb.
4. Also looking into other materials to construct the exoskeleton in order to improve structural stability, and reduce the weight and size of the overall system.

REFERENCES

- Alahmari, K., and Kakaraparthi, V. (2015). “Common musculoskeletal conditions in Upper limb-Physiotherapy Management.” 96.
- Alia, C., Spalletti, C., Lai, S., Panarese, A., Lamola, G., Bertolucci, F., Vallone, F., Garbo, A. di, Chisari, C., Micera, S., and Caleo, M. (2017). “Neuroplastic Changes Following Brain Ischemia and their Contribution to Stroke Recovery: Novel Approaches in Neurorehabilitation.” *Front Cell Neurosci*, 11, 76.
- Ariga, Y., Pham, H. T. T., Uemura, M., Hirai, H., and Miyazaki, F. (2012). “Novel equilibrium-point control of agonist-antagonist system with pneumatic artificial muscles.” *Proc IEEE Int Conf Robot Autom*, 1470–1475.
- Ball, E., and Garcia, E. (2016a). “Effects of bladder geometry in pneumatic artificial muscles.” *Journal of Medical Devices, Transactions of the ASME*, 10(4).
- Ball, E., and Garcia, E. (2016b). “Effects of bladder geometry in pneumatic artificial muscles.” *Journal of Medical Devices, Transactions of the ASME*, 10(4).
- Ball, S. J., Brown, I. E., and Scott, S. H. (2007). “MEDARM: a rehabilitation robot with 5DOF at the shoulder complex.” *2007 IEEE/ASME international conference on advanced intelligent mechatronics*, IEEE, 1–6.
- Byrd, J. (n.d.). “8 Key Benefits of Automation in Healthcare - Relatient.” <<https://www.relatient.com/automation-in-healthcare/>> (Aug. 16, 2022).
- Caldwell, D. G., Tsagarakis, N., and Medrano-Cerda, G. A. (2000). “Bio-mimetic actuators: polymeric Pseudo Muscular Actuators and pneumatic Muscle Actuators for biological emulation.” *Mechatronics*, 10(4–5), 499–530.
- Carignan, C., Tang, J., Roderick, S., and Naylor, M. (2007). “A Configuration-Space Approach to Controlling a Rehabilitation Arm Exoskeleton.” *2007 IEEE 10th International Conference on Rehabilitation Robotics*, IEEE, 179–187.
- Chakrabarti Debkumar. (1999). *Indian anthropometric dimensions for ergonomic design practice (1997 edition)* | *Open Library*. Ahmedabad: National Institute of Design.

Chakravarthy, S., Aditya, K., and Ghosal, A. (2014). "Experimental characterization and control of miniaturized pneumatic artificial muscle." *Journal of Medical Devices, Transactions of the ASME*, 8(4).

Cheng, H.-S., Ju, M.-S., and Lin, C.-C. K. (2003). "Improving elbow torque output of stroke patients with assistive torque controlled by EMG signals." *J Biomech Eng*, 125(6), 881–6.

"Classification of Stroke." (2018). <<https://www.flintrehab.com/2018/can-the-brain-heal-itself-after-a-stroke/>> (Dec. 12, 2018).

Colombo, R., Pisano, F., Mazzone, A., Delconte, C., Micera, S., Carrozza, M. C., Dario, P., and Minuco, G. (2007). "Design strategies to improve patient motivation during robot-aided rehabilitation." *J Neuroeng Rehabil*, 4, 3.

Coyle, S., Majidi, C., LeDuc, P., and Hsia, K. J. (2018). "Bio-inspired soft robotics: Material selection, actuation, and design." *Extreme Mech Lett*, 22, 51–59.

Daerden, F., and Lefeber, D. (2002). "Pneumatic artificial muscles: Actuators for robotics and automation." *European Journal of Mechanical and Environmental Engineering*, 47(1), 11–21.

Das, G. K. H. S. L., Tondu, B., Forget, F., Manhes, J., Stasse, O., and Soueres, P. (2016). "Controlling a multi-joint arm actuated by Pneumatic muscles with quasi-DDP optimal control." *IEEE International Conference on Intelligent Robots and Systems*, 2016-November, 521–528.

Dhameliya, N. (2022). "ELBOW JOINT - SAMARPAN PHYSIOTHERAPY CLINIC AHMEDABAD." <<https://samarpanphysioclinic.com/elbow-joint/>> (Feb. 23, 2022).

Diani, J., Fayolle, B., and Gilormini, P. (2009). "A review on the Mullins effect." *Eur Polym J*, 45(3), 601–612.

Farah, S., Anderson, D. G., and Langer, R. (2016). "Physical and Mechanical Properties of PLA, and Their Functions in Widespread Applications-A Comprehensive Review." *Adv Drug Deliv Rev*, 107, 367–92.

- Ferraresi, C., Franco, W., and Bertetto, A. M. (2001). "Flexible Pneumatic Actuators: A Comparison between The McKibben and the Straight Fibres Muscles." *Journal of Robotics and Mechatronics*, 13(1), 56–63.
- Fitzsimmons, S. (n.d.). "Anatomy Quiz: Upper Limb - Anatomy and Physiology." <<http://sscaandp.weebly.com/anatomy-quiz-upper-limb.html>> (Feb. 23, 2022).
- Frisoli, A., Bergamasco, M., Carboncini, M. C., and Rossi, B. (2009). "Robotic assisted rehabilitation in Virtual Reality with the L-EXOS." *Stud Health Technol Inform*, 145, 40–54.
- Gadgil, R. (2022). "India - Physiopedia." <<https://www.physio-pedia.com/India>> (Feb. 24, 2022).
- Garrec, P., Friconneau, J. P., Measson, Y., and Perrot, Y. (2008). "ABLE, an innovative transparent exoskeleton for the upper-limb." *2008 IEEE/RSJ International Conference on Intelligent Robots and Systems*, IEEE, 1483–1488.
- Gaylord, R. H. (1958). "Fluid actuated motor system and stroking device."
- Gentry, M. F., and Wereley, N. M. (2009). "Effects of Braid Angle on Pneumatic Artificial Muscle Actuator Performance." *Proceedings of the ASME Conference on Smart Materials, Adaptive Structures and Intelligent Systems, SMASIS2008*, 2, 617–623.
- Ghergich, A. J. (2021). "How Automation Is Transforming Healthcare Jobs." <<https://www.forbes.com/sites/forbestechcouncil/2021/12/21/how-automation-is-transforming-healthcare-jobs/?sh=7bc717b51d5a>> (Aug. 16, 2022).
- Gopura, R. A. R. C., Bandara, D. S. V., Kiguchi, K., and Mann, G. K. I. (2016). "Developments in hardware systems of active upper-limb exoskeleton robots: A review." *Rob Auton Syst*, 75, 203–220.
- Gopura, R. A. R. C., Kiguchi, K., and Li, Y. (2009). "SUEFUL-7: A 7DOF upper-limb exoskeleton robot with muscle-model-oriented EMG-based control." *2009 IEEE/RSJ International Conference on Intelligent Robots and Systems*, IEEE, 1126–1131.

Gordon, K. E., Sawicki, G. S., and Ferris, D. P. (2006). "Mechanical performance of artificial pneumatic muscles to power an ankle-foot orthosis." *J Biomech*, 39(10), 1832–1841.

Hal F Schulte, J. R. P. (1961). *Characteristics of the Braided Fluid Actuator*. Issue 5 of University of Michigan. Medical School. Dept. of Physical Medicine and Rehabilitation. Orthotics Research Project. Technical report.

Hesse, S., Schulte-Tigges, G., Konrad, M., Bardeleben, A., and Werner, C. (2003). "Robot-assisted arm trainer for the passive and active practice of bilateral forearm and wrist movements in hemiparetic subjects." *Arch Phys Med Rehabil*, 84(6), 915–920.

Hidler, J., Nichols, D., Pelliccio, M., and Brady, K. (2015). "Advances in the Understanding and Treatment of Stroke Impairment Using Robotic Devices." <https://doi.org/10.1310/RYT5-62N4-CTVX-8JTE>, 12(2), 22–35.

Hocking, E. G., and Wereley, N. M. (2012). "Analysis of nonlinear elastic behavior in miniature pneumatic artificial muscles." *Smart Mater Struct*, 22(1), 014016.

Hu, X. L., Tong, K. Y., Song, R., Zheng, X. J., Lui, K. H., Leung, W. W. F., Ng, S., and Au-Yeung, S. S. Y. (2009). "Quantitative evaluation of motor functional recovery process in chronic stroke patients during robot-assisted wrist training." *Journal of Electromyography and Kinesiology*, 19(4), 639–650.

Jackson, A., Culmer, P., Makower, S., Levesley, M., Richardson, R., Cozens, A., Williams, M. M., and Bhakta, B. (2007). "Initial patient testing of iPAM - A robotic system for Stroke rehabilitation." *2007 IEEE 10th International Conference on Rehabilitation Robotics, ICORR'07*, 250–256.

Johnson, G. R., Carus, D. A., Parrini, G., Scattareggia Marchese, S., and Valeggi, R. (2001). "The design of a five-degree-of-freedom powered orthosis for the upper limb." *Proc Inst Mech Eng H*, 215(3), 275–284.

"Joints of the Upper Limb: Anatomy." (2017). <<https://www.howtorelief.com/upper-limb-joints/>> (Dec. 12, 2018).

- Jones, O. (2019). “The Elbow Joint - Structure - Movement - TeachMeAnatomy.” <https://teachmeanatomy.info/upper-limb/joints/elbow-joint/> (Feb. 23, 2022).
- Kiguchi, K., Iwami, K., Yasuda, M., Watanabe, K., and Fukuda, T. (2003). “An Exoskeletal Robot for Human Shoulder Joint Motion Assist.” *TRANSACTIONS ON MECHATRONICS*, 8(1).
- Klein, J., Spencer, S. J., Allington, J., Minakata, K., Wolbrecht, E. T., Smith, R., Bobrow, J. E., and Reinkensmeyer, D. J. (2008). “Biomimetic orthosis for the neurorehabilitation of the elbow and shoulder (BONES).” *2008 2nd IEEE RAS & EMBS International Conference on Biomedical Robotics and Biomechanics*, IEEE, 535–541.
- Koizumi, S., Kurumaya, S., Nabae, H., Endo, G., and Suzumori, K. (2018). “Braiding thin McKibben muscles to enhance their contracting abilities.” *IEEE Robot Autom Lett*, 3(4), 3240–3246.
- Kothera, C. S., Jangid, M., Sirohi, J., and Wereley, N. M. (2009). “Experimental characterization and static modeling of McKibben actuators.” *Journal of Mechanical Design, Transactions of the ASME*, 131(9), 0910101–09101010.
- Kousidou, S., Tsagarakis, N. G., Smith, C., and Caldwell, D. G. (2007). “Task-Orientated Biofeedback System for the Rehabilitation of the Upper Limb.” *2007 IEEE 10th International Conference on Rehabilitation Robotics*, IEEE, 376–384.
- Kung, P.-C., Ju, M.-S., and Lin, C.-C. K. (2007). “Design of a forearm rehabilitation robot.” *2007 IEEE 10th International Conference on Rehabilitation Robotics*, IEEE, 228–233.
- Liu, Y., Li, C., Ji, L., Bi, S., Zhang, X., Huo, J., and Ji, R. (2017). “Development and Implementation of an End-Effector Upper Limb Rehabilitation Robot for Hemiplegic Patients with Line and Circle Tracking Training.” *J Healthc Eng*, 2017.
- Lo, H. S., and Xie, S. Q. (2012). “Exoskeleton robots for upper-limb rehabilitation: State of the art and future prospects.” *Med Eng Phys*, 34(3), 261–268.

Looned, R., Webb, J., Xiao, Z., and Menon, C. (2014). “Assisting drinking with an affordable BCI-controlled wearable robot and electrical stimulation: a preliminary investigation.” *J Neuroeng Rehabil*, 11(1), 51.

Lum, P. S., Burgar, C. G., Shor, P. C., Majmundar, M., and Loos, M. van der. (2002). “Robot-assisted movement training compared with conventional therapy techniques for the rehabilitation of upper-limb motor function after stroke.” *Arch Phys Med Rehabil*, 83(7), 952–959.

Maciejasz, P., Eschweiler, J., Gerlach-Hahn, K., Jansen-Troy, A., and Leonhardt, S. (2014). “A survey on robotic devices for upper limb rehabilitation.” *Journal of NeuroEngineering and Rehabilitation 2014 11:1*, 11(1), 1–29.

Mackenzie, C., and Iberall, T. (1994). “Chapter 2. Prehension.” *Advances in Psychology*, 104(C), 15–46.

Mao, Y., and Agrawal, S. K. (2012). “Design of a cable-driven arm exoskeleton (CAREX) for neural rehabilitation.” *IEEE Transactions on Robotics*, 28(4), 922–931.

“Materials data sources.” (1988). *Mater Des*, 9(5), 305.

Meller, M. A., Bryant, M., and Garcia, E. (2014). “Reconsidering the McKibben muscle: Energetics, operating fluid, and bladder material:” <http://dx.doi.org/10.1177/1045389X14549872>, 25(18), 2276–2293.

Morrey, B. F., Llusá-Pérez, M., and Ballesteros-Betancourt, J. R. (2018). “Anatomy of the Elbow Joint.” *Morrey’s the Elbow and its Disorders*, 9–32.

Moubarak, S., Pham, M. T., Pajdla, T., and Redarce, T. (2009). “Design and Modeling of an Upper Extremity Exoskeleton.” Springer, Berlin, Heidelberg, 476–479.

Nef, T., Guidali, M., and Riener, R. (2009). “ARMin III – arm therapy exoskeleton with an ergonomic shoulder actuation.” *Appl Bionics Biomech*, 6(2), 127–142.

Nef, T., Mihelj, M., and Riener, R. (2007). “ARMin: a robot for patient-cooperative arm therapy.” *Med Biol Eng Comput*, 45(9), 887–900.

- Ogneva, I. v., Lebedev, D. v., and Shenkman, B. S. (2010). “Transversal stiffness and young’s modulus of single fibers from rat soleus muscle probed by atomic force microscopy.” *Biophys J*, 98(3), 418–424.
- Oliver-Salazar, M. A., Szwedowicz-Wasik, D., Blanco-Ortega, A., Aguilar-Acevedo, F., and Ruiz-González, R. (2017). “Characterization of pneumatic muscles and their use for the position control of a mechatronic finger.” *Mechatronics*, 42, 25–40.
- Oujamaa, L., Relave, I., Froger, J., Mottet, D., and Pelissier, J. Y. (2009). “Rehabilitation of arm function after stroke. Literature review.” *Ann Phys Rehabil Med*, 52(3), 269–293.
- Perry, J. C., and Rosen, J. (n.d.). “Design of a 7 Degree-of-Freedom Upper-Limb Powered Exoskeleton.” *The First IEEE/RAS-EMBS International Conference on Biomedical Robotics and Biomechatronics, 2006. BioRob 2006.*, IEEE, 805–810.
- Pillsbury, T. E., Kothera, C. S., and Wereley, N. M. (2015). “Effect of bladder wall thickness on miniature pneumatic artificial muscle performance.” *Bioinspir Biomim*, 10(5).
- Plagenhoef, S., Gaynor Evans, F., and Abdelnour, T. (1983). “Anatomical Data for Analyzing Human Motion.” *Res Q Exerc Sport*, 54(2), 169–178.
- Pollock, A., Farmer, S. E., Brady, M. C., Langhorne, P., Mead, G. E., Mehrholz, J., and Wijck, F. van. (2014). “Interventions for improving upper limb function after stroke.” *Cochrane Database Syst Rev*, 2014(11).
- Qian, Z., and Bi, Z. (2015). “Recent Development of Rehabilitation Robots.” *Advances in Mechanical Engineering*, 7(2), 563062.
- Rasedul Islam, M. (2017). “A Brief Review on Robotic Exoskeletons for Upper Extremity Rehabilitation to Find the Gap between Research Porotype and Commercial Type.” *Advances in Robotics & Automation*, 6(3).
- Rech, K. D., Salazar, A. P., Marchese, R. R., Schifino, G., Cimolin, V., and Pagnussat, A. S. (2020). “Fugl-Meyer Assessment Scores Are Related With Kinematic Measures

in People with Chronic Hemiparesis after Stroke.” *Journal of Stroke and Cerebrovascular Diseases*, 29(1), 104463.

Ren, Y., Park, H.-S., and Zhang, L.-Q. (2009). “Developing a whole-arm exoskeleton robot with hand opening and closing mechanism for upper limb stroke rehabilitation.” *2009 IEEE International Conference on Rehabilitation Robotics*, IEEE, 761–765.

Robinson, R. M., Kothera, C. S., and Wereley, N. M. (2014). “Control of a Heavy-Lift Robotic Manipulator with Pneumatic Artificial Muscles.” *Actuators 2014, Vol. 3, Pages 41-65*, 3(2), 41–65.

Robinson, R. M., Wereley, N. M., and Kothera, C. S. (2012). “Control of a heavy-lift robotic manipulator with pneumatic artificial muscles.” *Collection of Technical Papers - AIAA/ASME/ASCE/AHS/ASC Structures, Structural Dynamics and Materials Conference*.

Rocon, E., Belda-Lois, J. M., Ruiz, A. F., Manto, M., Moreno, J. C., and Pons, J. L. (2007). “Design and Validation of a Rehabilitation Robotic Exoskeleton for Tremor Assessment and Suppression.” *IEEE Transactions on Neural Systems and Rehabilitation Engineering*, 15(3), 367–378.

Rosati, G., Gallina, P., and Masiero, S. (2007). “Design, Implementation and Clinical Tests of a Wire-Based Robot for Neurorehabilitation.” *IEEE Transactions on Neural Systems and Rehabilitation Engineering*, 15(4), 560–569.

S. Vancouver Physio Clinic. (n.d.). “What is Physiotherapy? A Physiotherapy Definition - South Vancouver Physiotherapy Clinic.” <<https://southvanphysio.com/what-is-physiotherapy/>> (Aug. 16, 2022).

Sangian, D., Naficy, S., Spinks, G. M., and Tondu, B. (2015). “The effect of geometry and material properties on the performance of a small hydraulic McKibben muscle system.” *Sens Actuators A Phys*, 234, 150–157.

Sharma, K., Mansur, D. I., Khanal, K., and Haque, M. K. (2013). “Variation of Carrying Angle With Age, Sex, Height and Special Reference to Side.” *Kathmandu University Medical Journal*, 11(4), 315–318.

- Shen, Y., Ferguson, P. W., and Rosen, J. (2020). "Upper Limb Exoskeleton Systems—Overview." *Wearable Robotics: Systems and Applications*, 1–22.
- Sicuri, C., Porcellini, G., and Merolla, G. (2014). "Robotics in shoulder rehabilitation." *Muscles Ligaments Tendons J*, 4(2), 207–13.
- Snelson, R., Karchak, A., and Nickel, V. (1961). "Application Of External Power In Upper Extremity Orthotics." *Orthopedic & Prosthetic Appliance Journal*, 345–348.
- Song, A., Pan, L., Xu, G., and Li, H. (2015). "Adaptive motion control of arm rehabilitation robot based on impedance identification." *Robotica*, 33(9), 1795–1812.
- Sugar, T. G., Jiping He, Koeneman, E. J., Koeneman, J. B., Herman, R., Huang, H., Schultz, R. S., Herring, D. E., Wanberg, J., Balasubramanian, S., Swenson, P., and Ward, J. A. (2007). "Design and Control of RUPERT: A Device for Robotic Upper Extremity Repetitive Therapy." *IEEE Transactions on Neural Systems and Rehabilitation Engineering*, 15(3), 336–346.
- Sukal, T. M., Dewald, J. P. A., and Ellis, M. D. (2005). "Use of a Novel Robotic System for Quantification of Upper Limb Work Area Following Stroke." *2005 IEEE Engineering in Medicine and Biology 27th Annual Conference*, IEEE, 5032–5035.
- Sutapun, A., and Sangveraphunsiri, V. (2015). "A 4-DOF Upper Limb Exoskeleton for Stroke Rehabilitation: Kinematics Mechanics and Control." *International Journal of Mechanical Engineering and Robotics Research*, 4(3), 269–272.
- Takosoglu, J. E., Laski, P. A., Blasiak, S., Bracha, G., and Pietrala, D. (2016). "Determining the Static Characteristics of Pneumatic Muscles." *Measurement and Control*, 49(2), 62–71.
- Tiboni, M., Borboni, A., Vèrité, F., Bregoli, C., and Amici, C. (2022). "Sensors and Actuation Technologies in Exoskeletons: A Review." *Sensors (Basel)*, 22(3).
- Tondu, B., Ippolito, S., Guiochet, J., and Daidie, A. (2016). "A Seven-degrees-of-freedom Robot-arm Driven by Pneumatic Artificial Muscles for Humanoid Robots." <http://dx.doi.org/10.1177/0278364905052437>, 24(4), 257–274.

Tondu, B., and Lopez, P. (2000). “Modeling and Control of McKibben Artificial Muscle Robot Actuators.” *IEEE Control Syst*, 20(2), 15–38.

Trivitron Healthcare. (2019). “How Healthcare Industry Helps in Contributing to the Economy.” <https://www.trivitron.com/blog/how-healthcare-industry-helps-in-contributing-to-the-economy/> (Aug. 16, 2022).

Tsagarakis, N. G., and Caldwell, D. G. (2003). “Development and Control of a ‘Soft-Actuated’ Exoskeleton for Use in Physiotherapy and Training.” *Auton Robots*, 15(1), 21–33.

Tsai, B.-C., Wang, W.-W., Hsu, L.-C., Fu, L.-C., and Lai, J.-S. (2010). “An articulated rehabilitation robot for upper limb physiotherapy and training.” *2010 IEEE/RSJ International Conference on Intelligent Robots and Systems*, IEEE, 1470–1475.

Turchetti, G., Vitiello, N., Trieste, L., Romiti, S., Geisler, E., and Micera, S. (2014). “Why effectiveness of robot-mediated neurorehabilitation does not necessarily influence its adoption.” *IEEE Rev Biomed Eng*, 7, 143–153.

Ulutas, B., Erdemir, E., and Kawamura, K. (2008). “Application of a hybrid controller with non-contact impedance to a humanoid robot.” *IEEE 10th International Workshop on Variable Structure Systems, VSS’08*, 378–383.

Vallery, H., Veneman, J., Asseldonk, E. van, Ekkelenkamp, R., Buss, M., and Kooij, H. van der. (2008). “Compliant actuation of rehabilitation robots.” *IEEE Robot Autom Mag*, 15(3), 60–69.

Vocke, R. D., Kothera, C. S., Chaudhuri, A., Woods, B. K. S., and Wereley, N. M. (2012). “Design and testing of a high-specific work actuator using miniature pneumatic artificial muscles.” *J Intell Mater Syst Struct*, (C. S. Kothera and M. Philen, eds.), 23(3), 365–378.

Volder, M. de, Moers, A. J. M., and Reynaerts, D. (2011). “Fabrication and control of miniature McKibben actuators.” *Sens Actuators A Phys*, 166(1), 111–116.

Wakimoto, S., Suzumori, K., and Takeda, J. (2011). “Flexible artificial muscle by bundle of McKibben fiber actuators.” *IEEE/ASME International Conference on Advanced Intelligent Mechatronics, AIM*, 457–462.

Wang, G., Wereley, N. M., and Pillsbury, T. (2015). “Non-linear quasi-static model of pneumatic artificial muscle actuators.” *J Intell Mater Syst Struct*, 26(5), 541–553.

Xiang, C., Giannaccini, M. E., Theodoridis, T., Hao, L., Nefti-Meziani, S., and Davis, S. (2016). “Variable stiffness Mckibben muscles with hydraulic and pneumatic operating modes.” *Advanced Robotics*, 30(13), 889–899.

Xiao, F., Gao, Y., Wang, Y., Zhu, Y., and Zhao, J. (2017). “Design of a wearable cable-driven upper limb exoskeleton based on epicyclic gear trains structure.” *Technology and Health Care*, 25, 3–11.

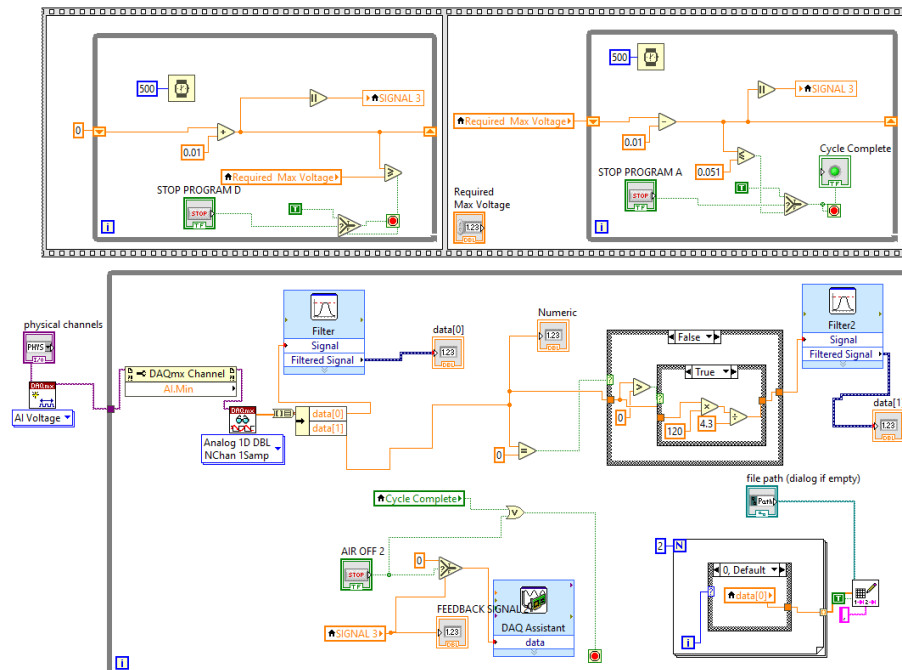
Yashas, M., Rosario Carvalho, A. D. do, Navin Karanth, P., and Desai, V. (2021). “Design and Fabrication of a Test Rig for Performance Analysis of a Pneumatic Muscle Actuator.” Springer, Singapore, 33–45.

ANNEXURE

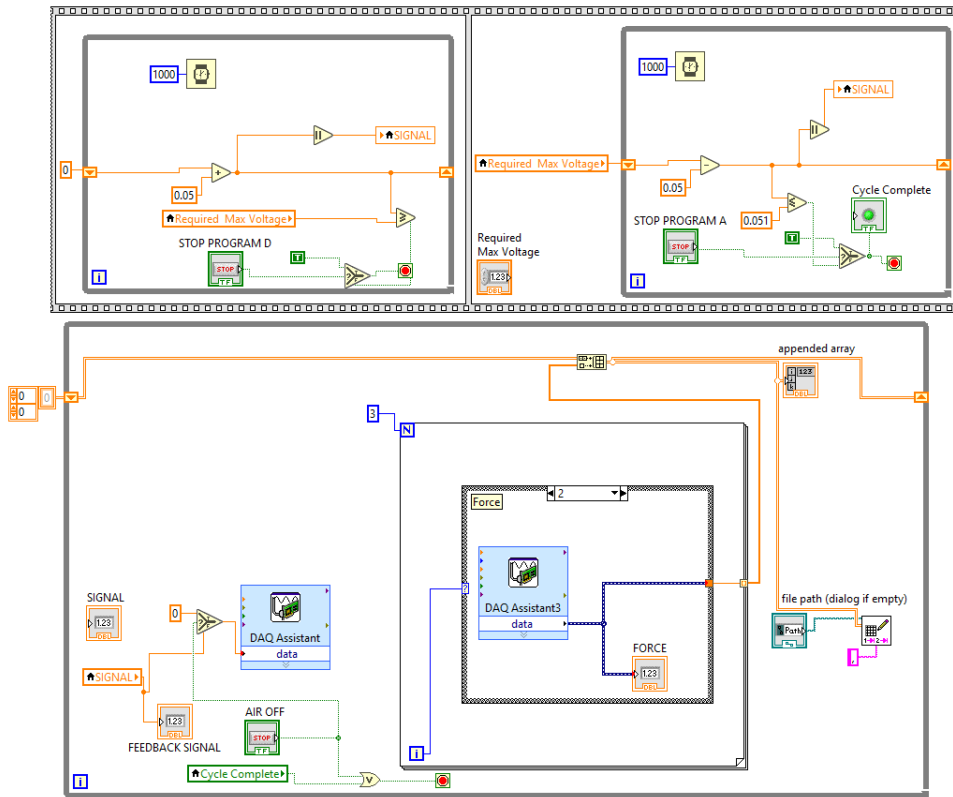
A. PMA Summary from Literature (Hyd: Hydraulic Actuator)

Reference	Diameter	Length	Actuation Pressure	Contraction Percentage	Force
Kothera et al.	12.7 mm	203 mm	4 bar	4.43%	60 N
Hocking et al.	4 mm	40 mm	5.5 bar	8%	140 N
De et al.	1.5 mm	22 mm	10 bar	15%	6 N
Koizumi et al.	8 mm	200 mm	6 bar	37%	1 N
Oliver-Salazar et al.	6.35mm	140 mm	4 bar	22%	100 N
Chakravarthy et al.	1.2 mm	143 mm	8.2 bar	18%	4.2 N
Meller et al.	22.2 mm	173 mm	7 bar (Hyd)	32%	500 N
Ball et al.	5.02 mm	135.8 mm	6.9 bar	30%	78 N
Sangian et al.	6 mm	80 mm	2.5 bar (Hyd)	23%	26 N
Wang et al.	7.78 mm	43.9 mm	5.51 bar	32%	189 N
Tondu et al.	24 mm	230 mm	5 bar	0.40%	45 N

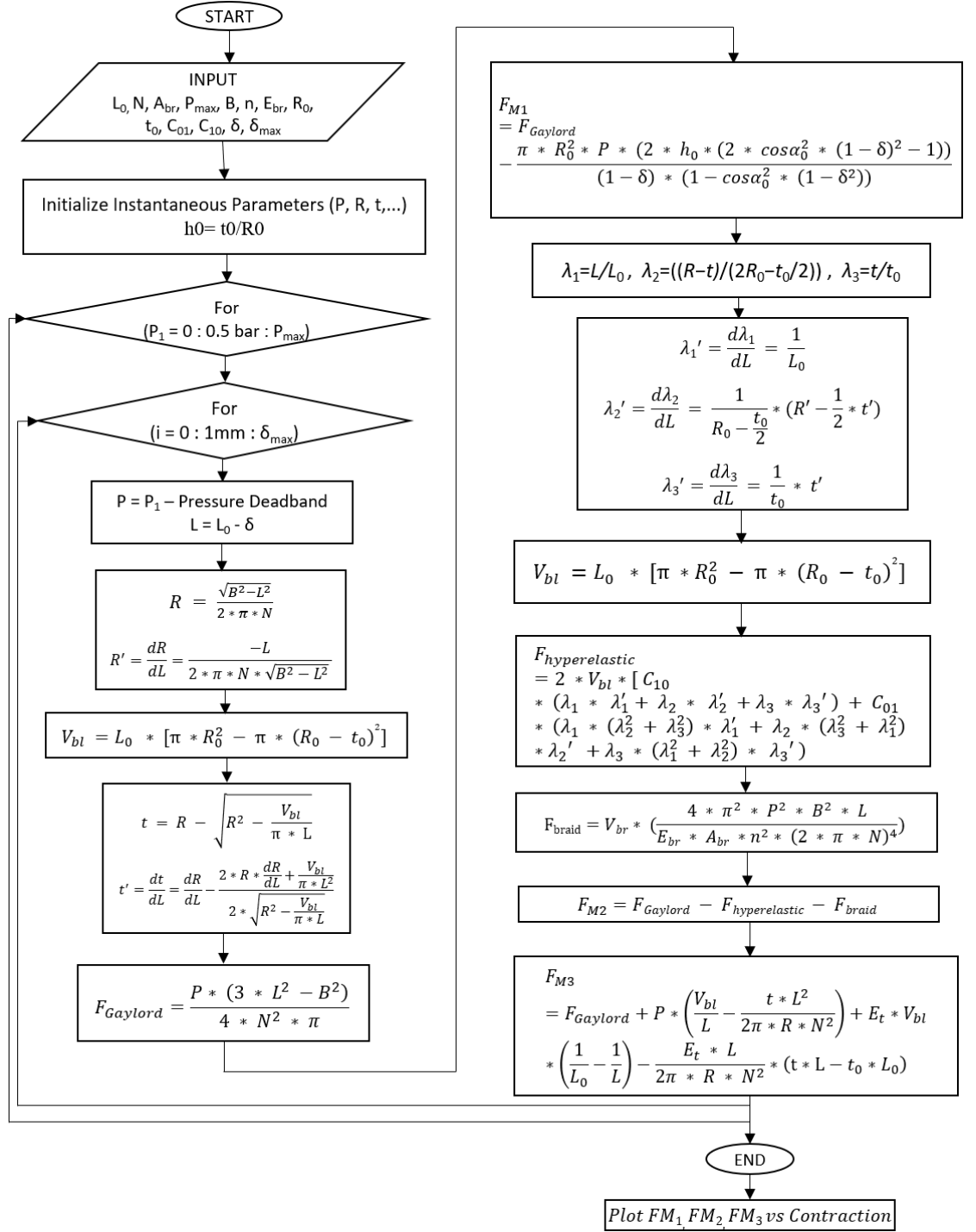
B. LabView Block Diagram for Displacement Setup



C. LabView Block Diagram for Force Setup



D. MATLAB flow chart for muscle model simulation



LIST OF PUBLICATIONS

Sl. No.	Title of the paper	Authors	Name of the Journal/ Conference/ Symposium, Vol., No., Pages	Month & Year of Publication
1	Design and characterization of a pneumatic muscle actuator with novel end-fittings for medical assistive applications	<u>Antonio Dylan Do Rosario Carvalho</u> , Navin Karanth P, Vijay Desai	Sensors and Actuators A: Physical, Volume 331, 2021, 112877, ISSN 0924-4247 (Elsevier, SCI, IF=4.291, Q1)	June 2021 (Published)
2	Characterization of pneumatic muscle actuators and their implementation on an elbow exoskeleton with a novel hinge design	<u>Antonio Dylan Do Rosario Carvalho</u> , Navin Karanth P, Vijay Desai	Sensors and Actuators Reports, Volume 4, 2022, 100109, ISSN 2666-0539, (Elsevier, ESCI, Q1)	June 2022 (Published)
3	Design and Fabrication of a Test Rig for Performance Analysis of a Pneumatic Muscle Actuator	M. Yashas, <u>Antonio Dylan Do Rosario Carvalho</u> , P. Navin Karanth, Vijay Desai	Advances in Industrial Automation and Smart Manufacturing, 2020, pp 33–45, ISBN 978-981-15-4739-3 (Springer, Singapore, SCOPUS)	October 2020 (Published)
4	A Modular System and Apparatus for Pneumatic Muscle Actuation in Medical Rehabilitation Exoskeleton Robots	Navin Karanth P, Vijay Desai, <u>Antonio Dylan Do Rosario Carvalho</u>	Indian Patent (Application No.: 202141004899)	August 2022 (Published)
5	A System for Operating an Exoskeleton with a Novel Pronation Supination Mechanism	Navin Karanth P, Vijay Desai, <u>Antonio Dylan Do Rosario Carvalho</u>	Indian Patent (Application No.: 202241057878)	December 2022 (Published)

BIO-DATA

1. Name : Antonio Dylan Do Rosario Carvalho
2. Father's Name : Antonio Olavo Do Rosario Carvalho
3. Date of Birth : 4th Jan 1992
4. Nationality : Indian
5. Marital Status : Single
6. Address : Department of Mechanical Engineering,
National Institute of Technology Karnataka,
Surathkal, P.O. Srinivasnagar – 575 025
Karnataka, India.
7. Mobile Number : +91 8275645004
8. E-mail id. : carvalho.dylan@gmail.com
9. Educational Qualification :

Qualification	University/Board	Year of Passing
PhD (Mechanical engineering)	National Institute of Technology Karnataka, Surathkal, Mangalore	Pursuing
M. Tech (Robotics)	SRMIST, Kattankulathur	2017
B.E. (Mechanical Engineering)	Goa University, Goa	2014